ECAP-2021

About Temperature Dependence of TARGET C and CTC Calibration

Master's Thesis in Physics

Presented by
Benjamin Andreas Schwab
20.07.2021

Erlangen Centre for Astroparticle Physics
Physikalisches Institut II
Friedrich-Alexander-Universität Erlangen-Nürnberg

Supervisor: Prof. Dr. Stefan Funk

ERLANGEN CENTRE FOR ASTROPARTICLE PHYSICS

cherenkov telescope array

Contents

1. Introduction

Gamma-ray astronomy is a flourishing branch of astroparticle physics to probe the high energy universe from about 100 GeV to 100 TeV. The advantages over other messenger particles as cosmic rays or neutrinos are that they point towards the source and have a reasonable cross section. The downside is certainly that gamma-rays at such high energies can not penetrate the atmosphere, making a direct observation at ground level impossible. A satellite based detection for such high energies is then again uneconomical, since the flux is fairly low and the effective area is limited. Thus specialized Imaging Atmosphere Cherenkov Telescopes (IACTs) are used to measure the Cherenkov emission from the gamma-ray induced extended air shower proportional to the energy of the primary gamma-ray, which also directs to it. As these event are only a few nanoseconds long and very faint, a time resolution of about 1ns is needed to seperate the Cherenkov emission from scattering light of the night sky background. For the future Cherenkov Telescope Array (CTA) and its Small Sized Telescopes (SST), the SST camera is developed, which combines a space and cost efficient Silicon PhotoMultiplier (SiPM) with a 1GSa/s read-out system to acquire a 1ns time resolution. An in-depth study of the calibration method and how it responds to temperature changes will be the object of this thesis as the temperature is not stable in the camera.
With all these efforts of the whole collaboration, we may be finally able to explain the fundamental questions of how cosmic rays are accelerated, if there are axions, what dark matter is, and so on. [1, 2, 3, 4]

1.1. Extended Air Showers

When a gammray penetrates the atmosphere, it interacts with the surrounding nucleis Coulomb field, creating a electron and positron in pair production. The pair then emits Bremsstrahlung in the same Coulomb field, leading to more high energetic gamma-rays. These gamma-rays then get again pair produce into a electron positron pair and so on, cascading into a electromagnetic shower. This is repeated until ionisation and atomic excitation processes are the dominant way of loosing energy for the electrons/positrons.But not all shower are of electromagnetic kind. Most of the showers get induced by cosmic rays, which are way more common than gamma-rays. Due to their hadronic nature they will also produce pions and K mesons while colliding with the nuclei of the atmosphere. These will then decay into gamma-rays, muons and neutrinos. The gamma-rays can then create an electromagnetic subshower, while the neutrinos rarely interact with anything due to their low cross section. The muons then decay into electrons/positrons or are such high energetic that they make it to the ground.
These hadronic showers and the induced muons are the major background for detecting gamma-rays. Fortunately due to the chaotic nature of hadronic showers, they can be distinguished from electromagnetic ones. A example of both can be seen in figure 1. [1, 5]

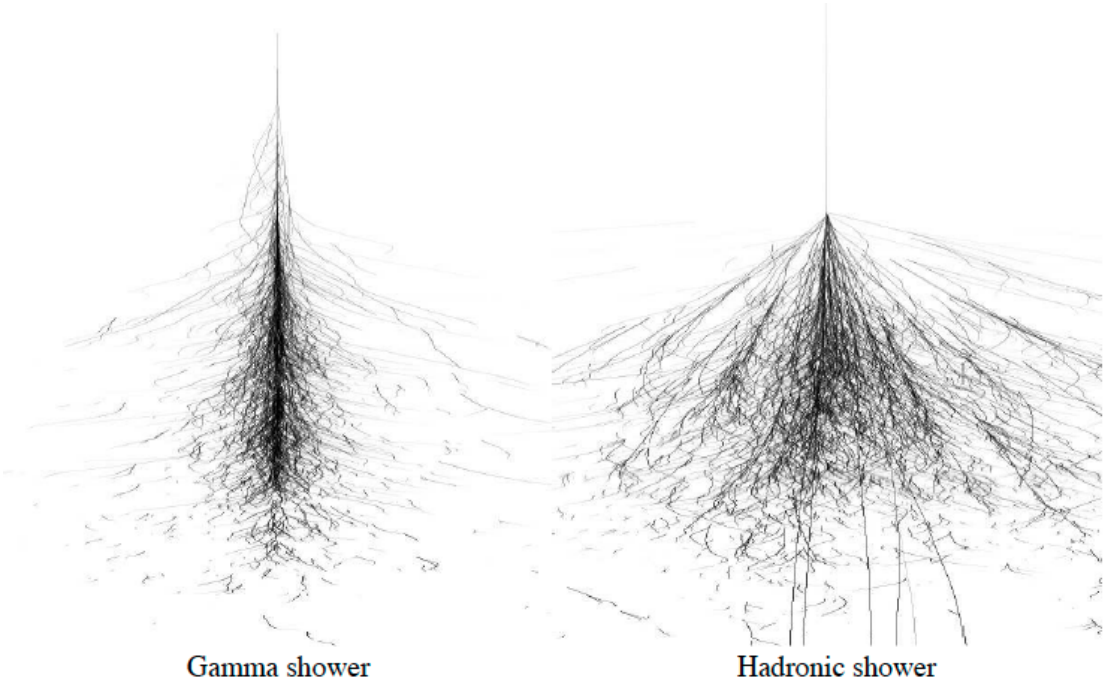

Figure 1: Simulation of the two distinct shower topologies [6]

1.2. Cherenkov Radiation

The Cherenkov effect is the fundamental principle of ground based gamma ray telescopes. Charged particles traveling through dielectric medium induce dipols around them on their trajectory, which then generate a local electromagnetic polarisation field around the particle (see figure 2 left). For velocity below the phase velocity of light in that medium, this happens fully symmetrical around the particle. Therefore no netto field is generated due to destructive interference. However, for $v_{\text{particle}} > c_{\text{phase}}$, the particle moves faster than the polarisation, breaking the symmetry. The polarisation field generated at each point then interferes constructive, creating a shock wave of photons, the Cherenkov cone. This can be nicely illustrated by the Huygens principle in figure 2 on the right, where each circle corresponds to the polarisation fields the particle created along its path. [7] Through simple geometry and by ignoring the energy loss through the Cherenkov photons, one can then determine the opening angle of the Cherenkov cone:

$$\cos(\theta) = \frac{\frac{c}{n(\lambda)} \cdot t}{v \cdot t} = \frac{1}{n(\lambda)\beta} \quad [7] \tag{1}$$

It only depends on the velocity of the particle and the refractive index of the dielectric material, which also depends on the wavelength. In relation to ground based gamma ray astronomy, where optical wavelengths and the atmosphere as dielectric medium are used, the refractive index changes with the pressure and therefore altitude. At 30km, the sparse atmosphere leads to a Cerenkov angle of $\theta = 0.2°$, whilst at sea level it is $\theta = 1.5°$ [5].

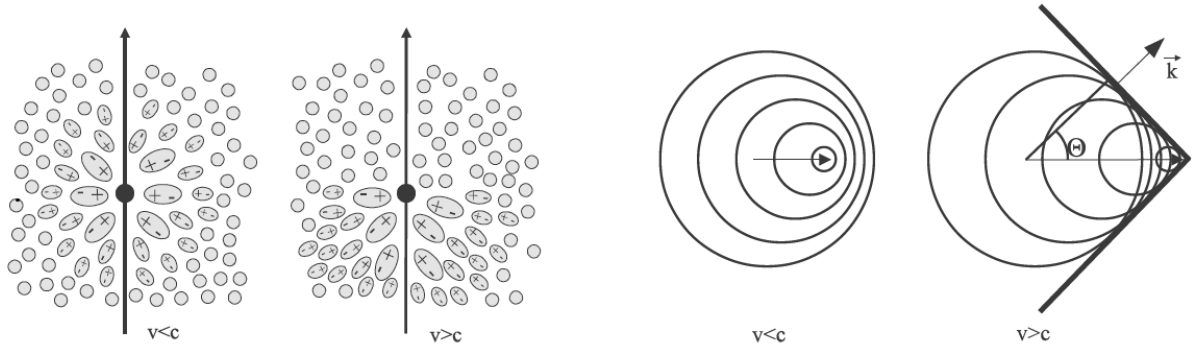

Figure 2: *left:* Induced dipols around the particle for different velocities, *right:* Corresponding illustration through the Huygens principle [5]

One can also take a look at the Cherenkov photon yield

$$\frac{\mathrm{d}^2\mathrm{N}}{\mathrm{d}\lambda\mathrm{dx}} = \frac{2\pi Z^2\alpha}{\lambda^2}\sin(\theta(\lambda)) \quad [7] \tag{2}$$

with α the fine-structure constant and Z the atomic number. Smaller wavelengths are clearly favoured. By integrating over the optical wavelengths, one yields about 500 photons per 1 cm, which is proportional to the energy loss of the particle. Therefore it is possible to do dosimetry with Cherenkov radiation.

1.3. IACTs (Imaging Atmosphere Cherenkov Telescope)

The Cherenkov light pool of such shower must then be collected for an energy reconstruction. A favourable method to accomplish such undertaking are IACTs, which are also able to visualise the direction of the shower and therefore of the primary gamma-ray. The most basic form of IACT is a single optical telescope to image the particle shower by standing in its light pool as seen in figure 3. An electromagnetic shower will then leave a nearly elliptical pattern in the camera, while a hadronic shower is much more diffuse in display and timing due to their unpredictable character. This allows a straight forward discrimination between gamma-rays and potential background.
By the orientation and size of the event, one can then calculate the direction of the primary particle and its corresponding energy. To further improve the angular resolution, multiple optical telescopes are used in arrays. This allows a stereoscopic imaging of the shower, so different projections of the same shower are available. Through intersecting the directions of the projected showers one can then determine the precise direction. Therefore allow arrays of optical telescopes not only a better sensitivity for low gamma ray fluxes, but also a improved angular reconstruction.
Still there are some downsides, as for example, the low duty cycle of about 10%. Only at clear moonless night the IACT can be used as otherwise the photon background would be too high to visualise the faint Cherenkov light pool. [5, 6]

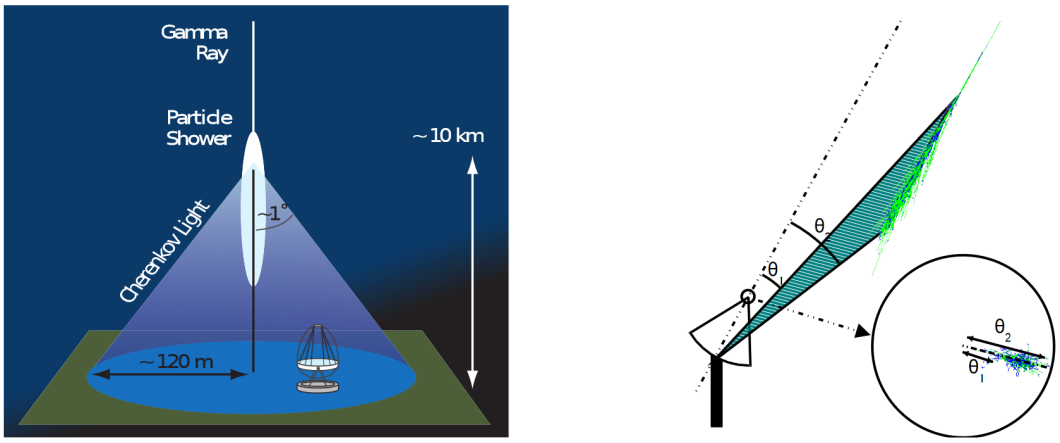

Figure 3: *left:* Working principle of a IACT, *right:* Projection of the shower onto the focal plane of the telescope [5]

1.4. Cherenkov Telescope Array (CTA)

The Cherenkov Telescope Array is the next generation of IACTs to detect gamma rays in an energy range of 20 GeV to 300 TeV [3]. Besides reaching new energy ranges in the high TeV scale and lower GeV scale that were not accessible for IACTs yet, it will also be up to one magnitude more sensitive than current generation experiments as MAGIC, HESS and VERITAS [8]. To achieve a full sky coverage, one site is build in La Palma to cover the northern hemisphere and one in Paranal Chile to cover the southern one. The proposed layouts for both sides can be seen in figure 4. It consists of three different telescope types that are specialised in certain energy ranges of gamma rays. Due the Cherenkov photon intensity depending on the initial energy of the gamma ray, larger photon collecting areas are needed for lower energetic showers. Furthermore follows the flux of primary gamma rays an inverted power law. Thus, a larger area needs to be covered to get an acceptable event rate of high energy showers. The Large-Sized Telescopes (LST) are specialised for energy ranges from 20GeV to 150GeV, where the flux of primary gamma rays is high and the Cherenkov photon intensity is low. Therefore a large photon collecting area is needed. This is accomplished by a parabolic mirror area with a dish size of 23m and a focal length of 28m, leading to a field of view of 4.3°. The camera consist of 265 photomultiplier tubes with a quantum efficiency of 42% to maximise the photon yield. This is optimized for active galaxy nuclei surverys, galactic transient events and gamma-ray bursts. Therefore the telescope will also be able to repositionate itself in about 30 seconds, despite standing 45m tall. There will be four on the northern site.
For the core energy range of 150GeV to 5TeV, two different telescopes are proposed, namely the Medium-Sized Telescope (MST) and the Schwarzschild-Couder Telescope (SCT). Both have a field of view of about 7.6° and are therefore optimized for rapid surveys of gamma ray burst. The MST is a modified Davies-Cotton design with a dish size of 11.5m and a focal length of 16m, while the SCT is a Schwarschild-Couder design

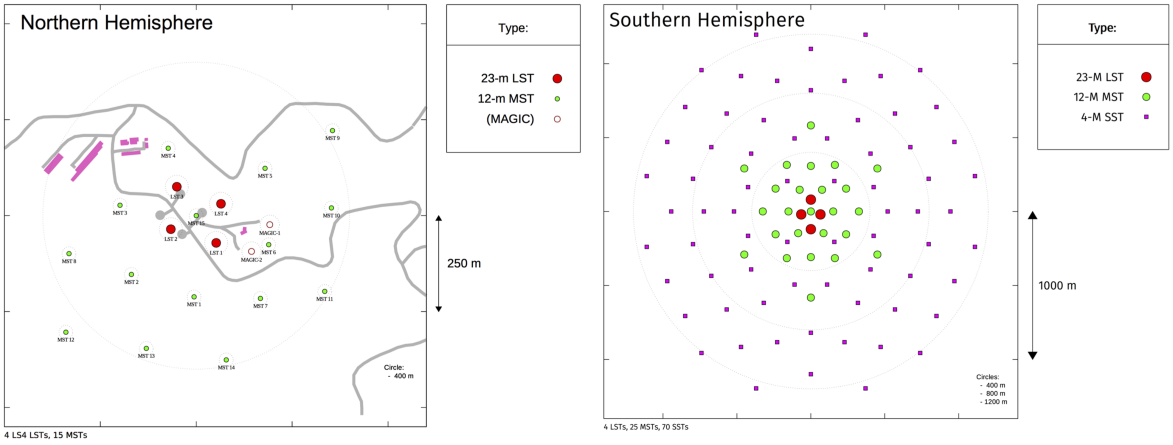

Figure 4: Preliminary layouts for CTA north and south with the initial amount telescopes. Since only a fewer number is financed, the layouts will be modified. [9]

with a primary mirror of 9.7m and a secondary mirror of 5.4m in diameter. While the Davies-Cotton design allows a larger photon collecting area of $88m^2$, the Schwarzschild-Couder design trades a smaller effective area of 41^2 for a smaller point spread function. In combination with the SCT Camera on SiPM basis with its ¿11000 pixel, this leads to a pixel size of only 0.067°, while the MST with its two cameras on PMT basis, the FlashCam and NectarCam, only has one of 0.17°. For the northern site, nine mid sized telescopes are planed and for the southern one 14.
In the energy range of 5TeV to 300TeV , the flux of gamma rays is sparse and the photon yield of showers great. Therefore, 37 Small-Sized-Telescopes (SST) with a effective photon collecting area of $8m^2$ are build on the southern site, spread over several square kilometres, as the primary source of these high energy gamma rays is the galactic plane, which is primarily visible from the southern hemisphere.
Initially three different designs were proposed. Namely the ASTRI-Horn, the GCT and the SST-1M. To keep things less complicated and easy to maintain, the CTA observatory project office singled out in a harmonization process a design based on the ASTRI telescope considering all experiences of the previous designs [10]. With a primary reflector diameter of 4.3 and a secondary of 1.8m, the SST has a focal length of 2.15m and a field of view of 10.5°. Equipped with the SST camera, bared on CHEC-S. [3, 8]

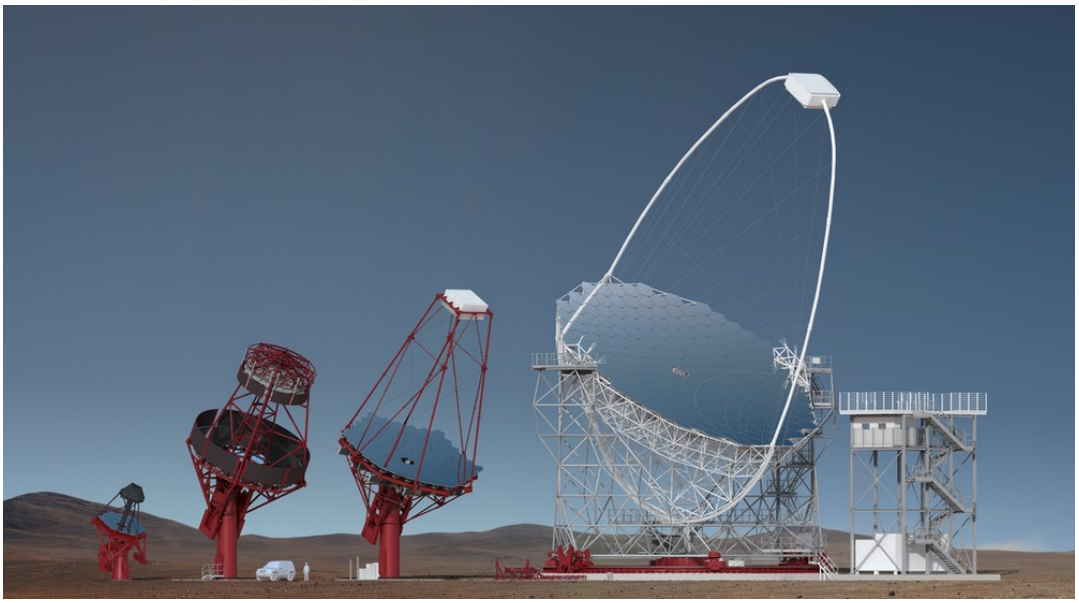

Figure 5: From left to right: the SST, the two mid sized telescopes SCT and MST and on the right the LST [9]

2. SST Cam

The SST cam, formerly known as CHEC-S, is the camera designed for the SST telescope based on the commercial available SiPM Hamamatsu S12642-1616PA-50, providing a cheap and uncomplicated solution for the 70 telescopes. Each SiPM tile consist of 256 pixel with an area of $3\times3\text{mm}^2$. With the above stated optical telescope specs of the SST and the targeted shower events having a minimal width of 0.2°, a pixel size of 6×6 up to $7\times7\text{mm}^2$ is sufficient for an angular pixel size of 0.2°. Therefore four pixels connect to one super pixel, leading to 64 pixel for each SiPM tile. To cover up the whole 10.5° field of view, 32 of such SiPMs are used, leading to a total of 2048 pixels. An exploded view drawing of the whole camera layout can be seen in figure 6.

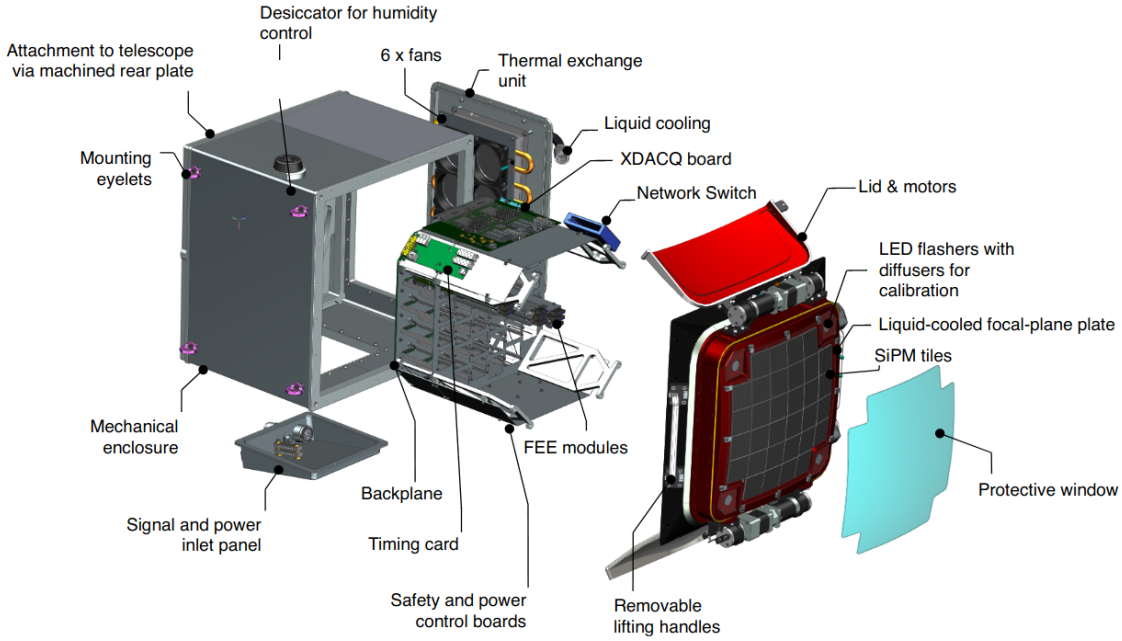

Figure 6: Exploded view drawing of the SST cam [2]

Each SiPM tile is connected to the front end electronic module (FEE), the heart of the SST cam. It is split into several sub boards, each with a specific responsibility. At first, behind the copper heat sink of the SiPM, a preamplifier board is installed to increase the noise immunity before transmitting the signal via ribbon cable to the TARGET module. The TARGET module is named after its key component, the application-specific integrated circuit (ASIC), which originally controlled both, the first level trigger and full waveform read-out. This stands for TeV Array Read-out with GSa/s sampling and Event Trigger and is specially designed to match the requirements of SST. Beside triggering and sampling, the TARGET module also hosts the power supply for the SiPM tile and a signal shaper for each pixel. It can be seen in figure 7. An in-depth description of it

can be found in the following chapter 2.1.
All 32 FEE modules are then connected over a backplane, for power distribution, common clock signal and a trigger on camera level based upon the first level trigger of each module. Also the data lines from the FEE modules connect via the backplane to the XDACQ board, providing a 10 Gbps link, to extract the data out of the camera.
Each FEE gets fitted into the rack and the modular construction of the camera allows a fast swap of components for easy maintenance. [2, 11]

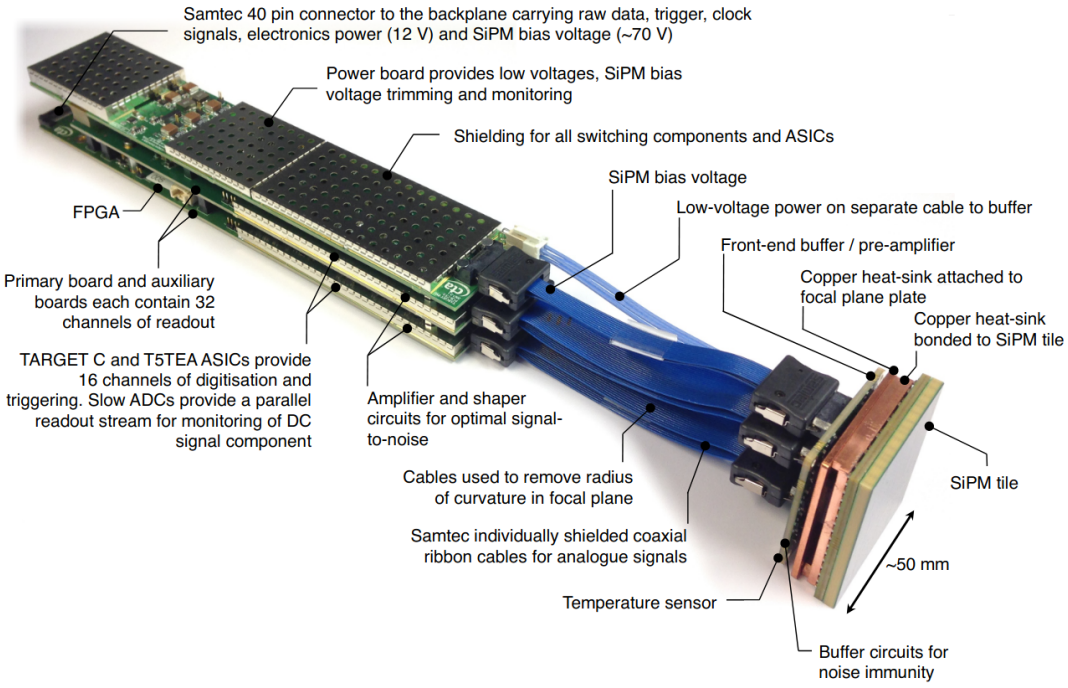

Figure 7: Single FEE module of the SST cam with the SiPM tile attached [2]

2.1. TARGET (TeV Array Read-out with GSa/s sampling and Event Trigger)

The main goal of TARGET is to provide an affordable solution for a read-out system meeting the requirements of a compact IACT such as the SST. This means, a sampling rate of 1 GSa/s to resolve Cherenkov flashes of 5 to 10ns in a night sky background of 125 MHz, a first level trigger based on the sum of 4 pixel to reduce the data volume, a buffer of 16384 samples translating to 16μs for 1 GSa/s to enable an array wide triggering between the telescopes and a high channel count and therefore pixel density at a low cost. Along with the dual mirror optics design of SST, a field of view of 10.5° and high angular resolution can be obtained.
Originally the triggering and sampling was done in one ASIC, but further studies showed that a separate topology leads to less cross talk between digitization and triggering and

an overall better performance of the trigger [4, 12]. Since the TARGET C generation, the ASICs are split into the T5TEA trigger ASICs and the TARGET C sampling ASICs. Each ASIC handles 16 channels parallel, leading to four pairs of ASICs per TARGET module to handle the 64 pixel per SiPM.
In this thesis, a TARGET module of generation C (SN0037) and several TARGET ASICs of the CTC generation on a separate evaluationboard (SN0001, SN0002 and SN0003) are tested (see chapter 2.1.4). [4, 12, 13]

2.1.1. Shaper

The shaper is not part of the TARGET ASICs but part of the TARGET module and therefore stands in symbiotic relation with the ASICs. Additionally have simulations shown, that a pulse width from 5 to 10 ns is small enough to avoid a pile up of different events and long enough to digitize with sufficient signal to noise ratio [2]. For the TARGET C module, the preamplified pulse from the SiPM has a natural width of about 23 ns (FWHM). Therefore the signal gets shaped by a pole-zero shaper, which is a differentiator with an additional parallel resistor to avoid an undershoot of the shortened pulse by pole-zero-cancellation. For the TARGET C generation of preamplifier and shaper this nonetheless leads to an undershoot and needs to optimization. As this does not constrain the significance of this work, the undershoot can be ignored.

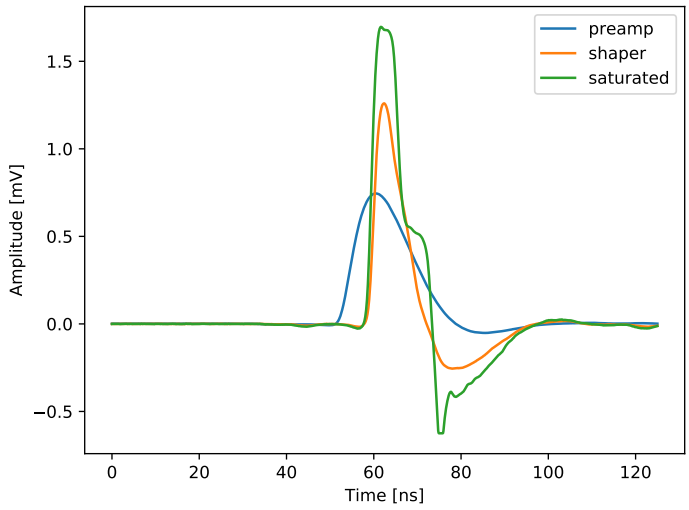

Figure 8: Generic SiPM pulse shapes after certain stages of processing. For comparability the preamplified pulse is inverted

Furthermore the Hamamatsu S12642-1616PA-50 SiPMs get replaced for the next gen CTC modules as they show less optical cross talk, but have a larger tail [14]. Due to the different pulse characteristics of these, a new preamp and shaping circuit must be developed, making an optimization of the TARGET C shaper obsolete.

After being shaped, the signal gets buffered again, inverted and then split up and lead to the (C)T5TEA trigger ASIC and to the (C)TC sampling ASIC. Due to the limited supply voltage of the buffer, the shaper circuit begins to saturate at an input amplitude of about 1.2V. An example for the preamplified, shaped and saturated pulse can be seen in figure 8. For a more detailed insight of the pulse shape see chapter 3.3.2.

2.1.2. (C)T5TEA

To the 1GSa/s sampling rate of TARGET C comes a digitisation time of about 100μs. Therefore a low level trigger is needed which determines if a signal is worthy to be read-out and digitized. This is realized in the (C)T5TEA, whose main purpose is triggering. The trigger signal is an analog sum of four channels of next neighbour pixel. If the sum exceeds the trigger threshold, a signal gets sent to the FPGA, which then instructs the sampling ASIC to read-out its storage cells at the time of the triggering. The trigger can be fine tuned by the parameters Vped_ChNR, PMTref4_TrGp and TRG_Thres_TrGp [15]. Vped_ChNR controls the baseline of the signal per channel and is set on 800 mV for the TARGET C and 700 mV for the CTC for normal data taking. PMTref4_TrGp sets the reference voltage of the summing amplifier for the next neighbour pixel trigger groups and therefore the level after the summation. TRG_Thres_TrGp is, as the name suggest, the trigger threshold. A schematic triggering with its parameters can be seen in figure 9.
The offset voltages (Vped_ChNR and PMTref4_TrGp) are created internally in the (C)T5TEA by a 12-bit R2R network DAC for each channel, which will be later characterised by the VPed transfer function (see chapter 3.2.2). Though the Vped_ChNR can not only be used to manipulate the trigger. As the set Vped DC voltages are also applied to the sampling path, it can be used to characterise the sampling ASIC. [11, 12, 13, 14]

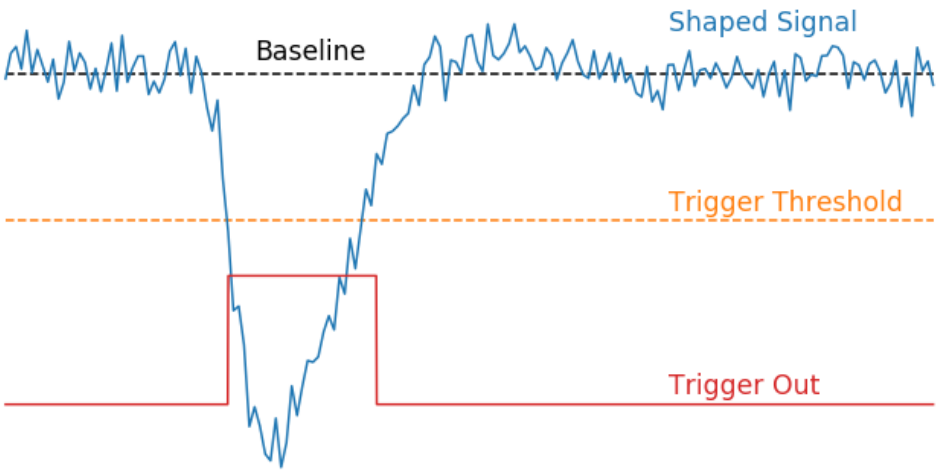

Figure 9: Schematic of a triggering process

2.1.3. (C)TARGET C

The TARGET C ASIC, or for the next gen CTC, is the centrepiece of the TARGET module. Its task is to continuously sample the incoming signals and to digitize them on command. For the sampling, two separately capacity arrays are used for each of the 16 channel. The split into a small sampling array and larger storage array was to reduce the total input capacity of the cells were the unsampled signal is tapped into. A to high capacity easily limits the maximal bandwidth of the ASIC.
The first one is the sampling array consisting of two blocks of 32 cells (capacities). It operates in ping pong fashion to allow a dead time free sampling. While one block is sampling, the other one is read-out, transferring the sampled signal to the next capacity array, the storage array.

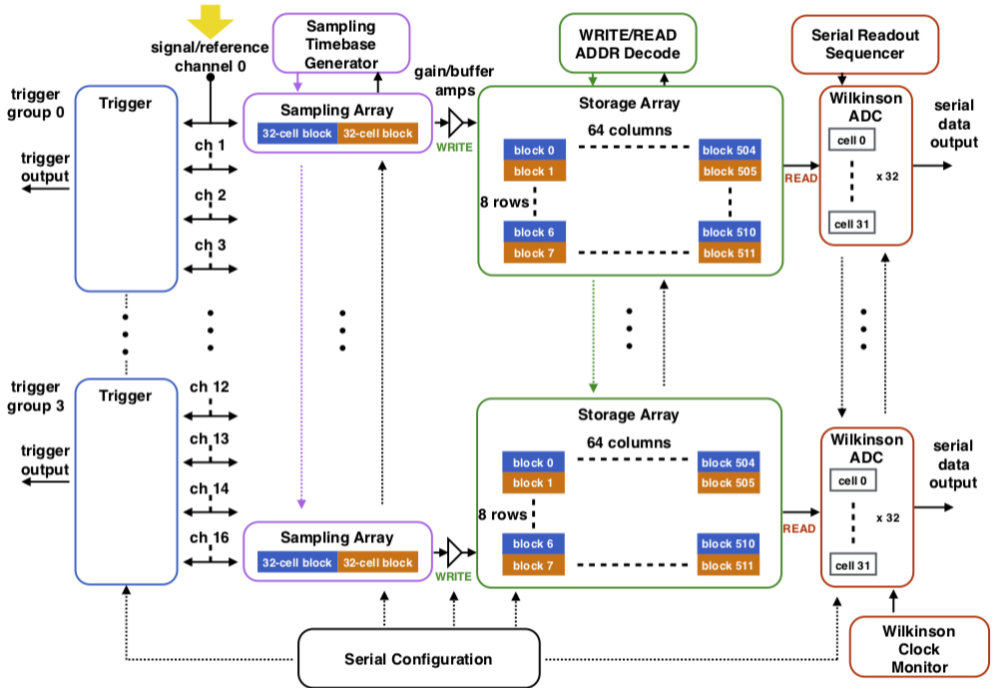

Figure 10: Operation principle of TARGET 7. Conceptional, TARGET C and CTC operate the same way [4]

The storage array then consists of 512 blocks of 32 cells, leading to a total amount of 16384 cells. It continuously gets overwritten by the sampling array until a read-out instruction from the FPGA enters. Then the requested blocks get read-out by the Wilkinson ADC, while the rest continuous with being written over.
A Wilkinson ADC is a combination of a comparator and a 12 bit counter. The voltage of the to read-out cell gets applied to the one input of the comparator and a ramping voltages starts at the other input, while a 12-bit register starts counting until the ramp voltage attains the voltage of the cell. The count of the 12-bit register is then the digitized voltage value of the cell.
Each channel has Wilkinson ADCs for a whole block of cells. The read-out of a full

waveform of 128 cells last for about 100μs, depending on the Wilkinson ramp parameters.
To adjust the digitisation process of the Wilkinson ADC, the frequency of 12-bit counter can be changed by the Wilkinson clock or the slope of the voltage ramp can be adapted by changing the charging current of the Wilkinson capacity generating it. This is accomplished by the Isel parameter.
A sketch of the operation principle of the sampling ASIC can be seen in figure 10.
An additional "feature" of the sampling ASIC is that each 32th cell has an innately higher capacity, reducing the cached voltage for these cells. Calling it a feature is a bit euphemistic as this is indeed unwanted and must be recalibrated. This is conducted by the pedestal correction among further things (see chapter 3.2.3). [11, 12, 13, 14]

2.1.4. CTC Evaluationboard

Since the whole TARGET module is a relative complex environment to test the characteristics of a single ASIC, a separate board is used for the next gen CTC ASICs. It consists of one pair of triggering and sampling ASIC, a FPGA module and the crucial set up to run them, including a multimode optical fiber socket for data transmission and communication. Each of the 16 channels has its own input MMCX socket for individual input. There also is a trigger input MMCX socket for external triggering. To monitor the temperature, a PT100 is placed in between the thermal pad (13 $\frac{\mathrm{W}}{\mathrm{mK}}$, 5mm thick) on top of the CTC and its heat sink, where a notch is milled, to guarantee maximal contact between them. The board can be seen in figure 11 with all important features labeled.

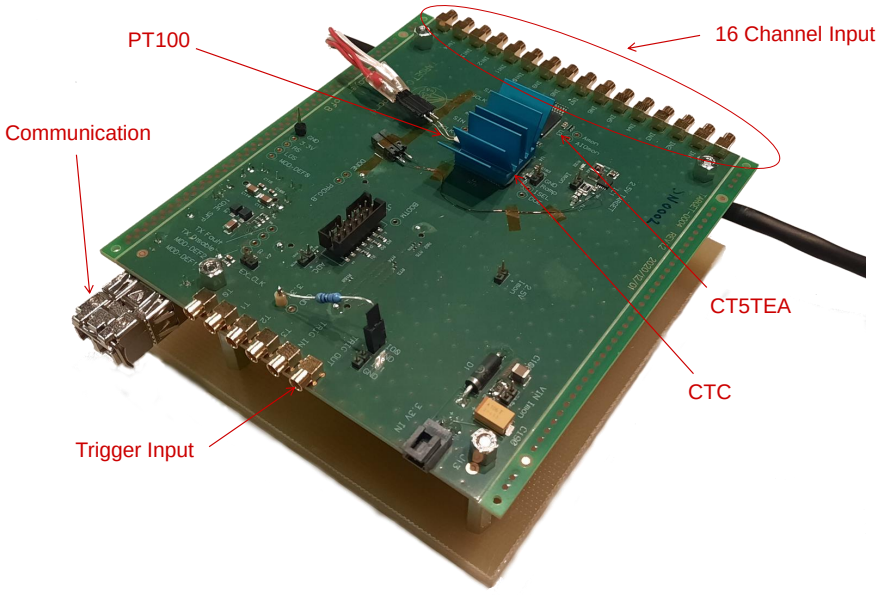

Figure 11: CTC evaluationboard labelled with the major used features

3. Calibration

The energy reconstruction of a shower in IACTs, and therefore SST, is based on the measured Cherenkov photon number. As the photons hit the SiPM, certain amplitudes are created corresponding to the given inputs. Hence, the whole energy reconstruction depends upon the charge resolution of each TARGET module or, to be more precise, of each pixel/channel. A calibration is thus indispensable to ensure that the measured amplitude corresponding to the photon pulse is rightfully sampled and digitized.

One method to calibrate the TARGET module is by creating AC transfer functions, where a pulse in shape of a typical output of the SiPM with different amplitudes is feed onto the board. A measured ADC value is then assigned to the input amplitude. This method was tested in-depth by Johannes Schäfer [15]. The greatest advantage of this method is that the module as a whole is calibrated and therefore the shaper and the TARGET C ASIC get calibrated in one step. But it has shown, that these transfer functions are temperature dependent, leading to deviations of up to 60 ADC counts for a temperature difference of 30 °C. With the temperature gradient in the camera of up 20 °C from on corner of the camera to the other and the limitation, that each module must then be calibrated at several temperatures, these transfer functions alone are quite cumbersome.
Hence another approach is proposed, where the AC transfer function is split into a DC transfer function to assign the ADC values to input voltages and a AC correction to take the AC effects and the gain of the shapers into account. The underlying idea is that the observed temperature dependency is assumed to be an effect of the storage cells and that the AC effects should be temperature independent.
The advantage of this method is, that the DC voltages, which are needed for the transfer function, are generated internally on the TARGET module by the DACs of the sampling ASIC (C)T5TEA. Therefore it is possible to aquire a DC transfer function calibration while the camera is operating, responding to changes in temperature. Although these DACs have to be additionally calibrated in form of a so called VPed transfer function, making this way of module calibration way more elaborate. But as only two calibration on the bench are assumed and the rest can be done on the fly while the camera is operating, this method is worth to be tested.

3.1. Temperature Chamber

To achieve a temperature stable environment for calibrating, the temperature chamber TestEquity 1007C is used, which has a temperature range of -73 °C to +175 °C with a stability of ±0.5 °C and a spatial deviation of ±1 °C according to the data sheet [16]. To counteract the spatial deviation, a extra fan is used to support the air flow ensuring a homogeneous distribution of equal tempered air.
Unfortunately, the valve of the cooling water is not correctly working, so that the cooling starts too late and when it cools, it cools for a too long time. This leads to a regulation loop of over cooling and heating for temperatures lower than the room temperature with

a periodicity of 38.4s and a higher deviation than the indicated one.
The temperature oscillation can clearly be observed in figure 12 (blue line) for the lower temperatures of 18 °C and 23 °C while for 43 °C the temperature remains stable as there is no active cooling needed for such high temperatures.
Exemplary the temperature distribution for set 18 °C can be seen in figure 13 on the left. It is a widespread grouping with a mean of 18.02 °C as set, but most of the time the chamber will have the temperature of of 18.47 °C, which should be considered for later measurements.

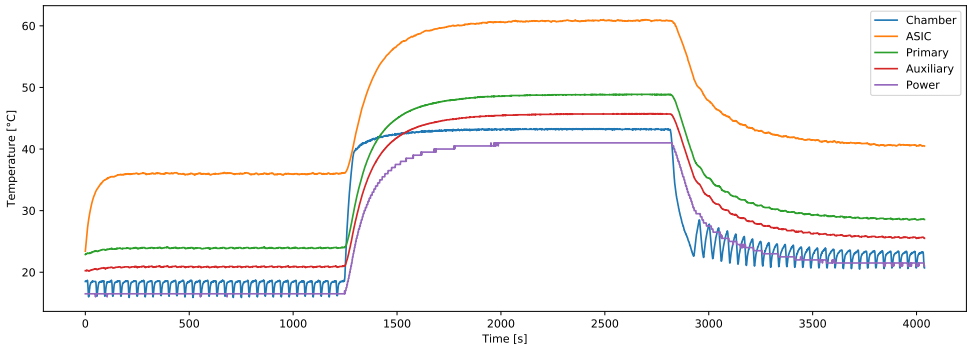

Figure 12: Time series of the temperatures of the chamber and each temperature sensor on the TARGET module, while the TARGET module is initialised

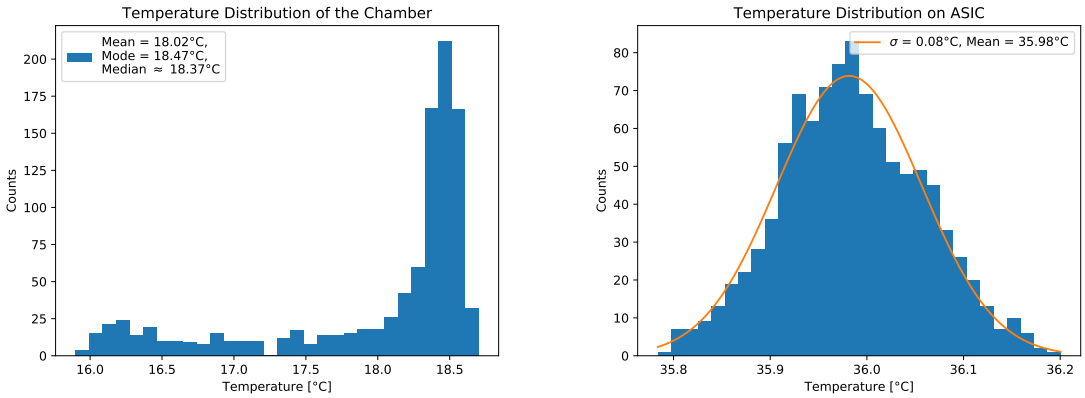

Figure 13: *left:* Temperature distribution of the chamber, ascertain the temperature spikes and a mode differing from the mean, *right:* Temperature distribution of the ASIC, which is strictly not a Gaussian distribution as the ASIC temperature correlates with the chamber temperature

But the more important question is, whether the temperature oscillation affects the temperature on the board or to be more specific, the ASIC, as temperature dependent effects on the ASIC calibration shall be investigated. Additionally to the temperature

time series of the chamber in figure 12, the corresponding temperatures on the primary-, auxiliary-, power-board and the ASIC of the TARGET C module can be seen. The temperature sensors are mounted on each board, whilst the temperature sensor on the ASIC was top mounted onto the heat sink with a thermal pad of $1.8\frac{\mathrm{W\cdot K}}{\mathrm{m}}$. The thermal distribution of the ASIC can be seen in figure 13 on the right. While the chamber oscillates 4 °C up and down, the temperature of the ASIC remains nearly constant with a standard deviation of 0.08 °C. Although the temperature of the ASIC still corresponds to the temperature changes of the chamber. But as the cooling spikes happen so fast, the ASIC has no time to catch up with the chamber temperature. Therefore, the temperature chamber is sufficient for the in this thesis proposed investigation. The same applies to the CTC evaluationboard.
Before doing measurements with the TARGET module or a CTC evaluationboard on a certain temperature, the chamber needs at least ten minutes of heating/cooling before reaching thermal equilibrium (see figure 12). Nevertheless, this time span is stretched to one hour, not allowing any margins. Furthermore TARGET has to be initialized for at least ten minutes before measuring as it consumes power and therefore heats itself up. The baseline of a freshly initialized module and a warmed up module can differ up to 10 mV.

3.2. DC Calibration

3.2.1. Set up

All DC calibrations have in common, that the DC voltages that are used for the calibration are generated internally on the (C)T5TEA and therefore no external input voltages are needed. As the back plane of the SST cam for a single TARGET C module is to cumbersome to use, a stand alone adapter (see figure 14) is provided to power and to communicate with the module. It maintains a multimode optical fiber socket for data transfer and several SMA sockets for trigger in- and output and SiPM power in.

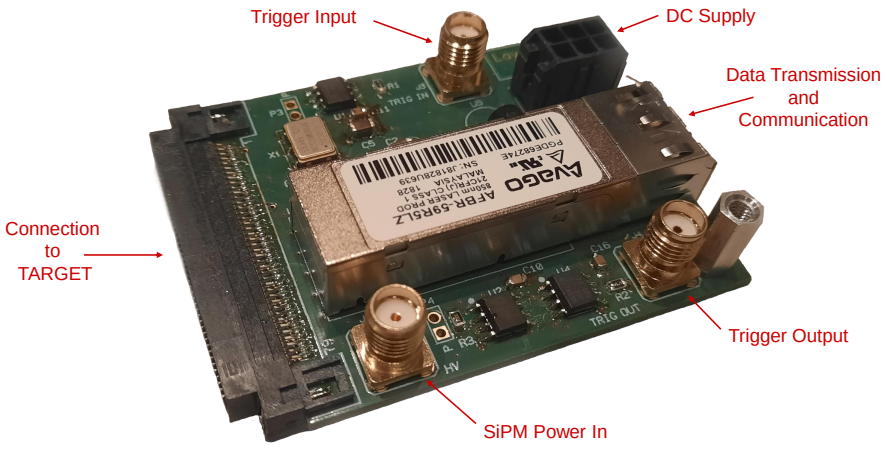

Figure 14: Stand alone adapter for the TARGET C module with labeled features

Since the (C)T5TEA trigger works with a threshold and only DC signals are used, it would either trigger uncontrollably all the time or not at all. Hence an external trigger is fed into the board via the TRIG IN socket. This trigger is hosted by a function generator, generating a rectangular pulse of 25ns length and 3.3V height at a period of 330μs. So every 330μs the four to five blocks of storage cells containing the event get digitized and read-out.
A schematic of the whole set up on the basis of the TARGET C module can be seen in figure 15. It also includes all major components of the module and how they communicate with each other.

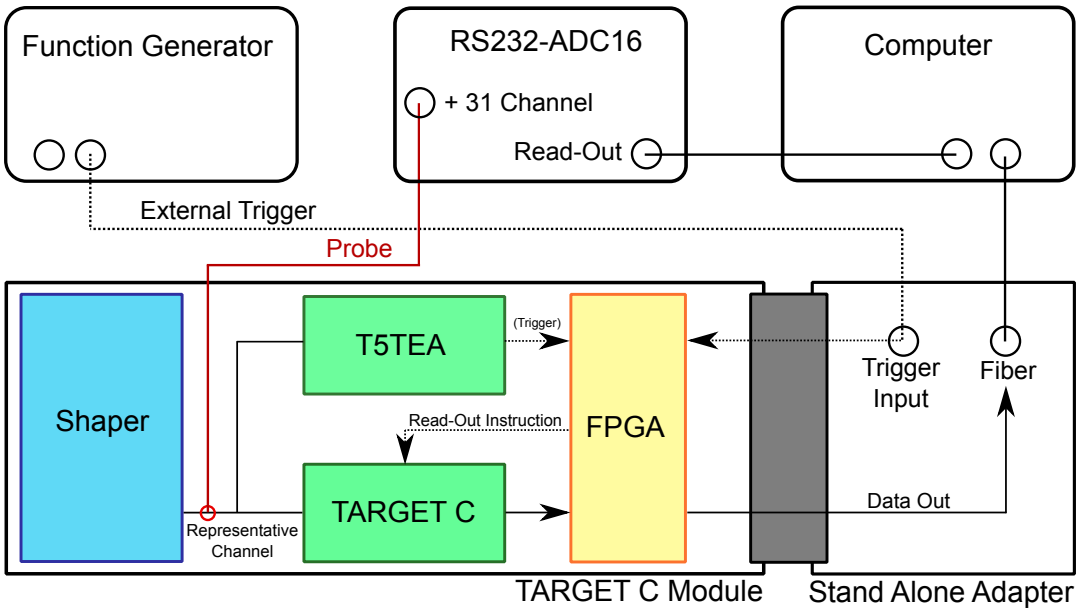

Figure 15: Schematic of the used set up for all DC calibrations including the ADC and probes for the Vped transfer functions

For the Vped transfer functions, the output of each DAC of the (C)T5TEA must be read-out independently, which can be done via the test points in front of the sampling ASIC. In case of the CTC evaluationboard, each channel gets probed this way and measured with a multimeter. To fasten things up for the TARGET C module and its 64 channel, an adapter probing 32 channel at once was developed. Instead of using 32 multimeter, four 16 bit ADC RS232-ADC16 are used, each hosting the capacity to measure eight channels at once. The test probes were hand wired onto the DSUB-25 sockets and the ADCs connected to the computer via USB. With a by the manufacturer provided C library the then digitized signals can be read-out and accessed. The already on the TARGET module mounted connector and the 32 channel probe can be seen in figure 16. Unfortunately, the pins for channel 5, 14 21, 30 and thus also 37, 46, 53, 62 are broken. Therefore no Vped transfer function for these channel were made, which is still sufficient for a statistical characterisation of the board.

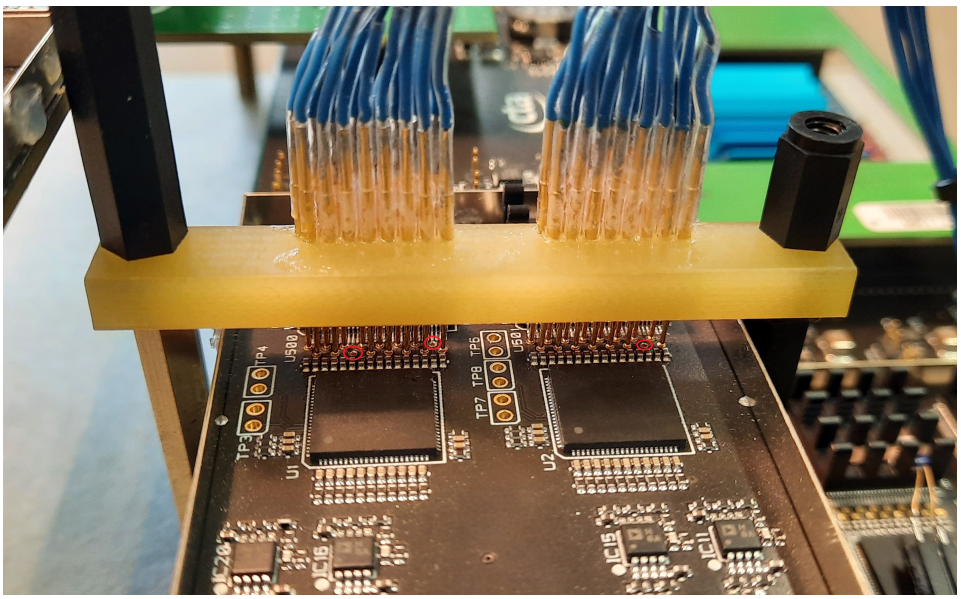

Figure 16: Custom spring loaded test pins for probing 32 channel at once with the missing pins marked

3.2.2. VPed Transfer Function

As described in chapter 2.1.2, the T5TEA produces the needed pedestal voltages through DACs. To set a certain voltages, the corresponding DAC count has to be determined by a transfer function at first. In addition are there production tolerances in the DACs. To have the same pedestal on each channel, different DAC counts have to be set on each channel. Another advantage of the fully characterized T5TEA DACs is that it is therefore possible to create a nearly arbitrary DC voltage on the sampling path, implementing the option to do an internally DC transfer function. This allows a calibration of the TARGET C while the camera is mounted and operating.
For the transfer function, the possible DAC counts get set and measured with the previously introduced external ADCs. The VPed transfer function of the TARGET C module SN0037 and all of its 64 channels can exemplary be seen in figure 17 (excluding the broken ones).
Due to the characteristics of a R2R network DAC, jumps in the transfer function happen when a large amount of bits flip. This can exemplary be seen at 2048 ADC counts as the binary transfers from 011111111111 to 100000000000. The more bits are on 1, the more resistors are introduced to the network. As resistors have tolerances, they stack up the more bits are on 1. By changing the bit string from 011111111111 to 100000000000, all these extra resistance fade at the same time, leading to a different voltage than the previous. To prevent double allocation of voltages if a voltage drops lower than the previous ones, these bits and voltages get sorted out and mask as -1. For clarity these -1 are set to the previously DAC count in the seen figure 17. Whereas jumps to higher voltages leave unwanted gaps in the voltage range. Therefore, for the CT5TEA generation, the R2R network DAC were tweaked so that only jumps to a smaller voltage

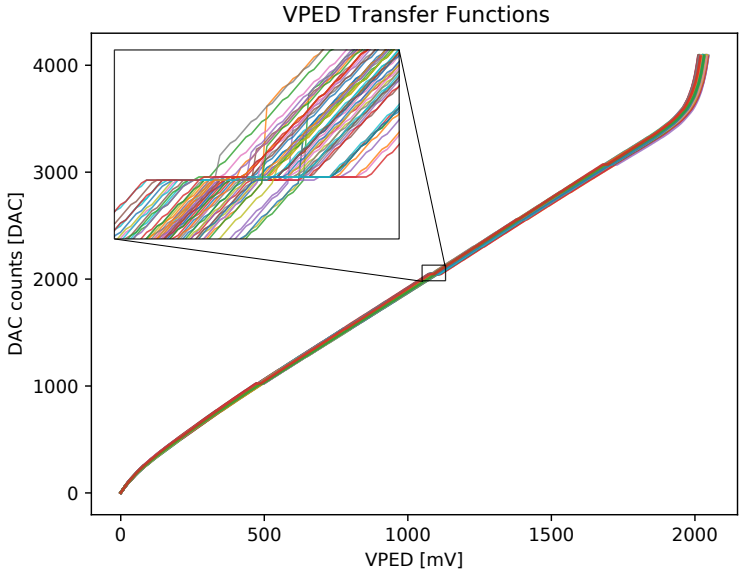

Figure 17: VPed transfer function of TARGET C module SN0037 over all available channels

are possible, allowing a continuous voltage span without missing voltage values.
Because of the CMOS switching of the R2R DACs, voltages below about 250 mV are not accessible, as the CMOS has not reached its operation point yet. The non linearity at small voltages is a attribute to this behaviour. Even with a supply voltage of 2.5V it is not possible to access voltages above about 2.3V as the OTA (Operational Transconductance Amplifier) after the R2R network saturates. This can theoretically be tweaked with the VBias parameter, but as more components of the TARGET module depend on it, is an adjustment difficult without further studies.

3.2.3. Pedestal Calibration

The pedestal calibration is the easiest calibration of storage cells possible to get rid of the cell to cell variations. By performing a null measurement with the TARGET module, each storage cell measures the set pedestal voltage. This value can then be subtracted from future measurement, not only considering the individual offset of each cell, but also setting the baseline to 0 ADC counts.
Additionally, one must contest in which block of the waveform the cell is located, as the ramp capacity of the Wilkinson ADC needs about 100 μs to restore the default voltage value. Therefore the ramp starts for the later blocks at a higher voltage value than in the first one, leading to less ADC counts for the same cell voltage. For this reason, each cell has five different pedestal values, one for each block it can appear in the waveform. An example of pedestal correction can be seen in figure 18, where a pulse of amplitude 23.95 mV (for details see chapter 3.3) is measured with the TARGET module, on the left as it is read-out without any calibration and on the right with a pedestal calibration.

The variance between the cells is so high that the pulse is nearly unrecognisable without a proper calibration. Also the 32th cells are cleary visible and the baseline is not around 0 ADC counts. With the calibration, the baseline noise goes from about 23.3 ADC counts, ignoring the 32th cells for convenience, to 1.1 ADC counts. For higher amplitudes (as seen in figure 19), the pulse is apparent, but the signal to noise ratio can still be significantly improved by a pedestal calibration.

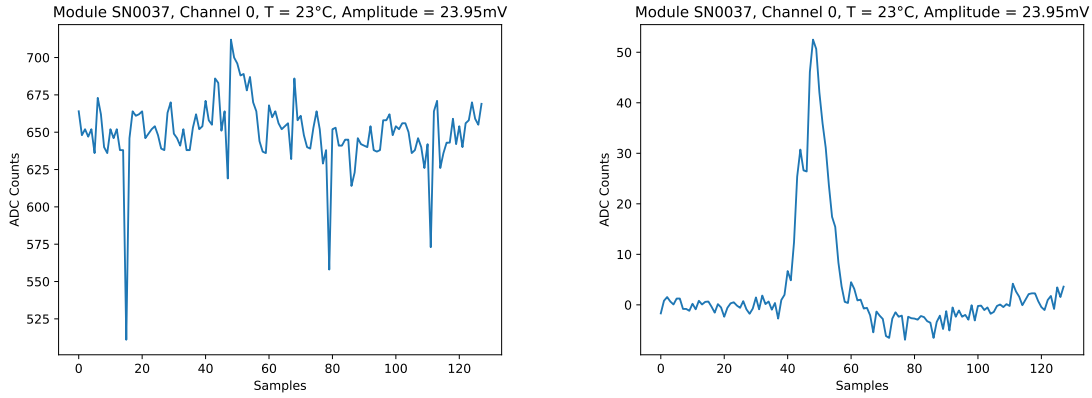

Figure 18: Standardized SiPM pulse with amplitude 23.95 mV measured with the TARGET module SN0037, *left:* Without pedestal calibration, *right:* With pedestal calibraton

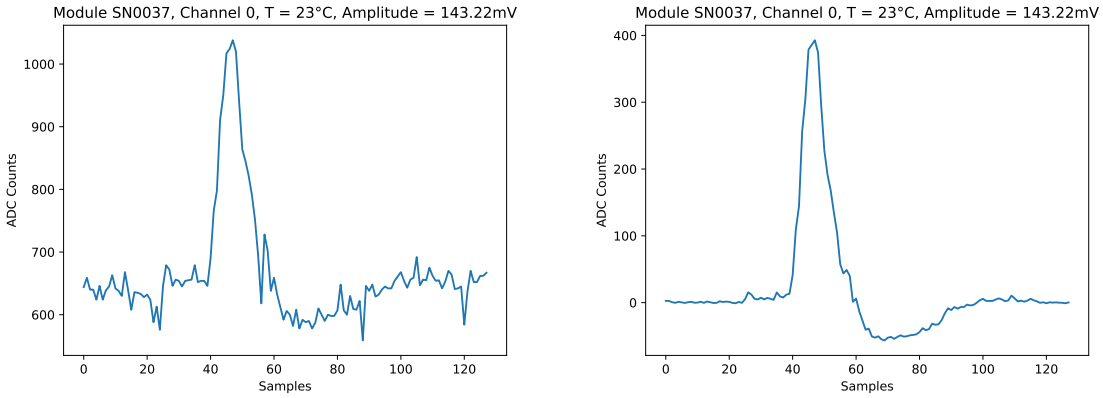

Figure 19: Standardized SiPM pulse with amplitude 143.22 mV measured with the TARGET module SN0037, *left:* Without pedestal calibration, *right:* With pedestal calibraton

To have a sufficient statistic and to additionally counter the fluctuations of the temperature chamber with a periodicity of 38s, 300s worth of pedestal data is taken at a rate of 1kHz. This leads to 300.000 events with 128 samples, so 9375 values per storage cell are taken, assuming an uniform probability. With a mean standard deviation per each storage cell of $\sigma_{\mathrm{ADC}} = 1.1$ ADC counts, the error gets reduced to $\sigma_{\mathrm{mean}} = \frac{\sigma_{\mathrm{ADC}}}{\sqrt{9375}} = 0.01$ ADC counts.

3.2.4. DC Transfer Function

After discarding the cell to cell offset variance with the pedestal calibration, the output of the TARGET ASIC is still in ADC counts. In order to be able to measure the voltage amplitude of an arbitrary signal, these ADC values must be again translated. This gets realised by the so called DC transfer function, where a span of DC voltages are set on the TARGET C and the corresponding ADC value of each storage cell is measured. These DC voltages can either be tapped in externally by a voltage supply or internally from the (C)T5TEA. Due to the flexibility of an internal method without further necessary devices and the possibility to do the DC calibration while the camera operates, it is the chosen approach.
For the data of the DC transfer function about 40 different DC voltages are used, starting at the lowest accessible voltage of the (C)T5TEA and increasing by steps of 50 mV to the end of the Vped transfer function. For each of these DC voltages 80s of data are taken at a rate of 2.5kHz leading to 200000 events and therefore 6250 events per storage cells per DC voltage. A example can be seen in figure 20.

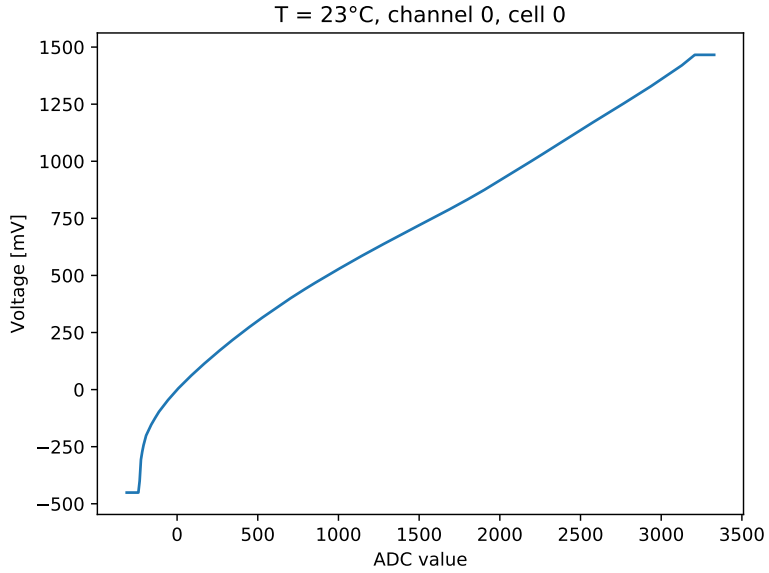

Figure 20: Example DC transfer function of SN0037, channel 0, cell 0

In principle, the DC transfer function is just a set of pedestal calibrations at different Vped levels, put together in a lookup table. Due to how the calibration of the TARGET module evolved, the pedestal calibration still forms the basis for every other calibration and is therefore separated.
The shape of the transfer function is determined by the ASIC itself but can be controlled by different parameters. As fix point, the zero ADC counts corresponds to 0 mV. As the applied DC voltages are produced by the T5TEA, only values between about 250 mV and about 2250 mV are possible, depending on the ASIC. The maximal value for each module can be extracted from the corresponding Vped transfer functions. Since the

module is run on a pedestal, the virtual zero, this value must be subtracted for each channel. At the moment the standard pedestal is set to 802 mV corresponding to a DC transfer function range of -451 mV to 1461 mV for the TARGET C module and a pedestal of 700 mV for the CTC evaluationboard and a range of about -451 mV to 1361 mV all depending on the module. By changing the pedestal, the voltage range can thus be shifted up- and downwards. Therefore, the maximal voltage of the DC transfer function is limited by the maximal setable pedestal voltage of the (C)T5TEA and the position of the pedestal calibration.
As the shapers saturate at first at about 1750 mV output amplitude (see chapter 4.3.3) and negative amplitudes are not needed, it seems strange to set the voltage range of the DC transfer function from -451 mV to 1461 mV on the first glimpse. But due to the non linearities at the beginning of the transfer function, a small ADC value difference makes a big voltage difference. This is unintentional for small amplitudes as it would blow up the relative error. Hence the negative amplitudes are more of a buffer to get a reasonable slope and linearity at small amplitudes.
Still, this diminishes the potential dynamical voltage range of the ASIC. But if one looks closer at the example DC transfer function in figure 20, one sees that not the whole ADC range is used. Through extrapolation it is possible to expand the DC transfer function up to wanted 1750 mV. Even if this is non linear, it could be a good enough approximation for the high amplitudes. However, this was not realised in this thesis.
Another way to influence the shape of the DC transfer function directly and therefore the behavior of the single storage cells is by adjusting the digitisation process of a storage cell by the Wilkinson ADC by changing its ramp slope (Isel) or clock frequency. By decreasing the slope of the Wilkinson ramp, the associated Wilkinson clock has more time to count until the ramp matches the voltage of the storage cell. Therefore the corresponding ADC value of a voltage gets bigger. The Wilkinson ADC is hence more sensitive to small voltage changes. But as the clock has a finite 12 bit counter, the maximal displayable voltage drops. This can be counteracted by changing the frequency of the Wilkinson clock. Thus it needs a balance between sensitivity and possible voltage range. For TARGET C a dual edge clocking frequency of 250 MHz is used with an Isel of 2300 DAC counts and for CTC a single clocking frequency of 104 MHz and a Isel of 2550 DAC counts are used. It was later found that the parameters for CTC are not optimized and can be improved, since a 104 MHz clocking is rather slow. Nevertheless, the analysis of the DC transfer functions is still valid if not stated differently.
An example for DC transfer functions with different ramp slopes (Isels) can be seen in figure 21 on the left for the CTC evaluationboard SN0001 at a 208 MHz clock frequency. For greatly inclined slopes only a fraction of the 4096 counts are used leading to a worse resolution over the same voltage range as the voltage range is limited due to the (C)T5TEA. A too steep slope, as the selected Isel of 2550 DAC counts, indeed uses nearly the whole range of 4096 counts, but rises too quick to capture voltages above 1V and has also unwanted non linearities on top of it, making it unsuitable for TARGET. The corresponding used ADC range to each Isel can be seen on the right of figure 21. A high occupation is desired for better resolution, but still some ADC range is needed for the continual range extrapolation.

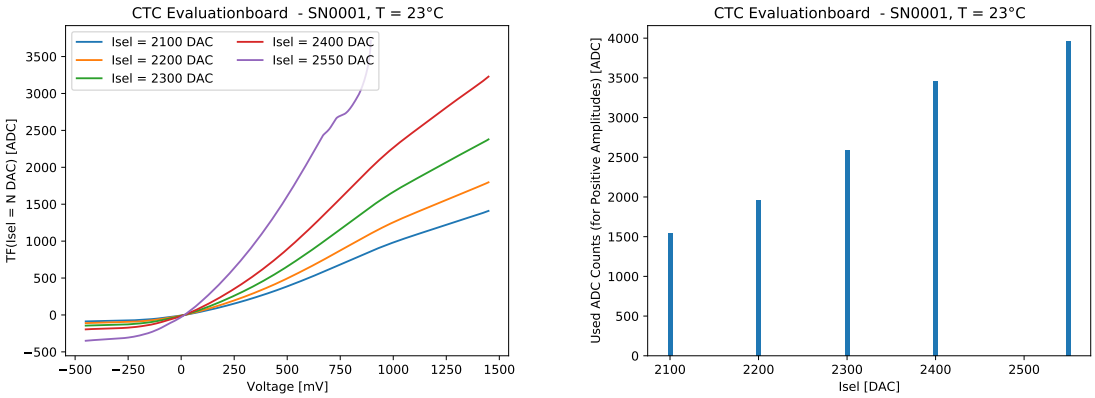

Figure 21: *left:* Mean DC transfer function of the CTC evaluationbard SN0001 at a Wilkinson clocking frequency of 208 MHz and 23 °C, *right:* Corresponding used ADC range

3.3. AC Correction

There are two main motivations for the AC correction. The first one is that the transfer function of the whole TARGET module at this point is still unknown, as the shapers in front of the sampling ASIC have an unknown gain factor. This can exemplary be seen in figure 22, where the measured mean maximal amplitude of a SiPM pulse of 54.21 mV amplitude is plotted for the first 640 storage cells. The amplitude and cell location of the maximum got extracted as described in chapter 3.3.2. The black line is the original amplitude of the pulse the cells should measure. How the offset changes per amplitude can be seen in figure 23 on the right. It decreases until the cells saturate and then the input amplitude advances while the measured one is stuck on the saturated value. Therefore the input amplitudes above about 1V drop out of the dynamical range of the TARGET C module. Around 800 mV only a section of cells saturates, which can still be corrected.

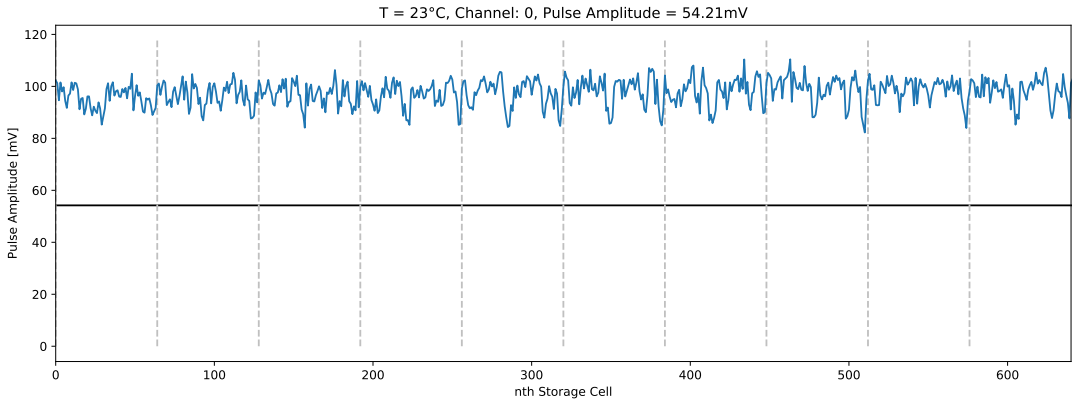

Figure 22: Storage cell response to a 54.21 mV SiPM pulse of the first 640 storage cells of the TARGET C module SN0037

The second motivation for the AC correction is the variation, which magnitude grows with amplitude as seen in figure 23 on the left. The standard deviation of all cells is always above about 2% for all amplitudes. As the TARGET C sampling ASICs of module SN0037 saturates around 1461 mV due to the finite DC transfer function, the standard deviation drops again as the measured amplitudes can not exceed this value. This variation also has a periodicity of 64 storage cells, as highlighted in figure 22 with the dashed lines. Therefore the noise must be a contribution from the 64 sampling cells, which have some individual deviations just as the storage cell. But more important is that they have a non linear response to different amplitudes.
These effects are called AC effects and can only occur at the sampling cells, as they are frequency dependent and all information besides the voltage value measured by the sampling cell is lost. Therefore is this calibration step called AC correction.

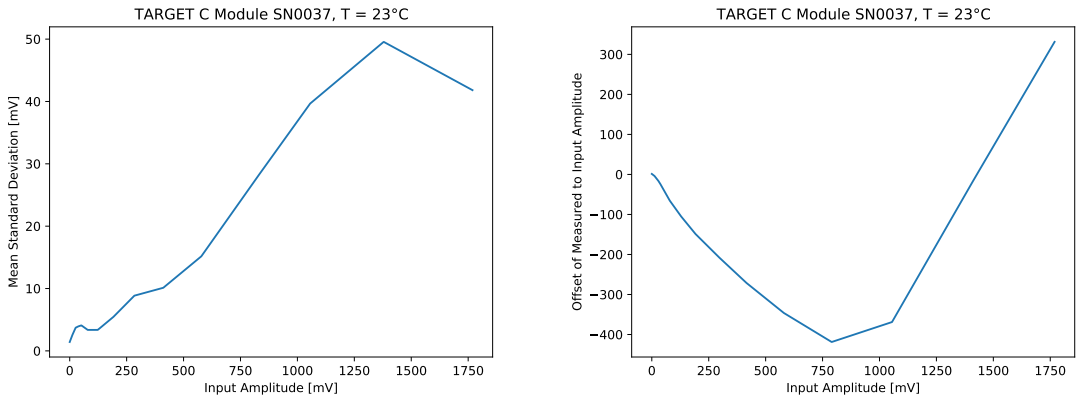

Figure 23: *left:* Mean standard deviation growth of 12 channels of the 48 of the TARGET C module SN0037 over different set amplitudes, *rigth:* Offset between input and measured amplitude of the same module

3.3.1. Set up

For the AC correction of the TARGET C module, the communication, the read-out and the external triggering via the stand alone adapter stays the same as for the DC calibrations (see chapter 3.2.1). Same goes for the evaluationboard of the CTC generation. Additionally to the external trigger signal, the function generator now also creates the for calibration needed AC pulses. Herefore the Keysight 33622a is used which can load arbitrary waveform with 1GSa/s. For detailed review of the pulse shape, see chapter 3.3.2. These pulses must then be equally distributed to the 64 channels of the TARGET C module or the 16 channels of the CTC evaluationboard. Therefore Adrian Zink developed an active splitterboard consisting of 1:16 splitting circuits. For the full description and characterisation of the splitterboard, see chapter 3.3.3. A schematic of the used set up for all necessary measurements for the AC correction can be seen in figure 24. The oscilloscope is only needed for the individual characterisation of the splitterboard or shapers. For the AC correction itself only the corresponding transfer functions of them are important.

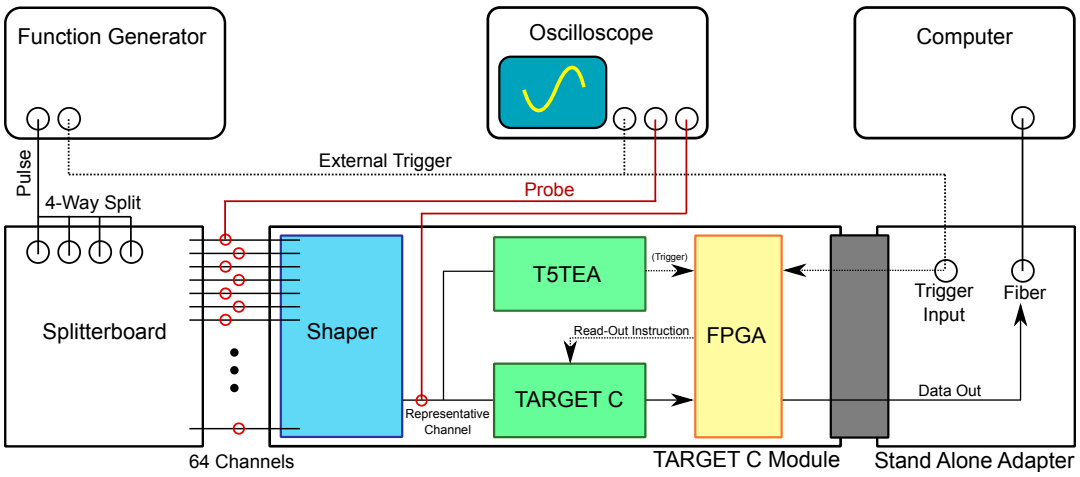

Figure 24: Schematic of the used set up for all DC calibrations including the ADC and probes for the Vped transfer functions

3.3.2. Pulse Form and Extraction

To simulate the occurring AC effects on the TARGET module, a standardized pulse of the SiPM is needed, which also undergoes the preamplifier. For this purpose, Steve Leach of the University of Leicester measured the corresponding output of a Hamamatsu SiPM and its preamplifier for a photon pulse. The mean of 100.000 such waveforms is then used as the standardized pulse. It consists of 352 data points, representing a 175ns long waveform. The pulse can be seen in figure 25 on the left and has a FWHM of 23.65ns and an amplitude of -5.96 mV. Interesting to note is that the edge steepness of a SiPM pulse decreases through the limited bandwidth of the preamplifier. Also is the undershot a product of the preamplifier.
This pulse can then be scaled to one of arbitrary amplitude and write in a signal generator. For the CTC on the evaluationboard, things get a little bit simpler, as there are no shapers in front of the ASIC and a general response of the AC effects is desired. Therefore a Gaussian pulse is used, with a FWHM of 10ns, corresponding to the FWHM of the SiPM pulse (with preamplification) after the shaper.
For the pulse extraction of the with TARGET digitised waveform, the bin (cell) with the maximum amplitude of the pulse is wanted. Due to the noise on the waveform this is inconclusively not the cell with the maximum amplitude per se. This can exemplary be seen in figure 25 on the right, where the neighbouring bins of the actual pulse maxima bin have a higher amplitude due to the noise. To compensate for this behaviour, a Gaussian filter is used to smoothen the waveform, revealing the true position of the maxima. The advantage of the Gaussian filter to other filters is that there is no frequency dependent group delay, so the pulse maxima stays at the same place.
The only characterizing parameter of the Gaussian filter is its standard deviation. It gives the range around the to smoothen data point in which the data points are used to calculate the filtered waveform. The higher it is set, the more distant data points influence the smoothing of the to smoothen data point. A too high standard deviation

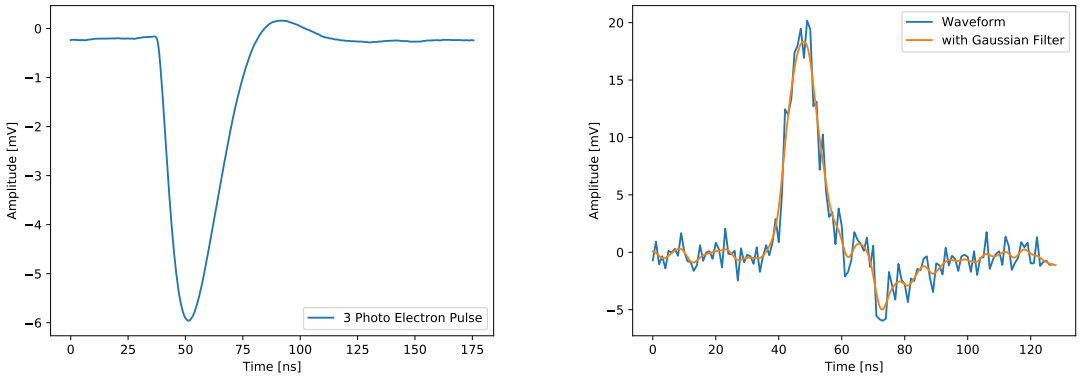

Figure 25: *left:*, Standardised preamplified SiPM pulse, *right:* Read-out and filtered pulse

can therefore lead to a distortion of the waveform. Additionally, the pulse peak is only a few nanoseconds and therefore bins wide. To make the filter finer adjustable, the waveform also gets resampled before filtering, increasing the data points to a tenfold.
For the SiPM pulse, a standard deviation of 15 lead to the best results for the resampled waveform (1.5 if not). An example can also be seen in figure 25. The maximal amplitude is in bin 49 with 20.18 mV, while the maxima of the peak is in bin 48 with an amplitude of 16.93 mV.

3.3.3. Splitterboard

The splitterboard used for the TARGET C AC correction transfer functions, called CHEC-0002, actually consists of two boards, each with two 1:16 splitter and their two SMA input socket. Therefore, the signal is already coaxially split in four signals, leading to a amplitude loss of 1/2. Each channel consists of an non inverting amplifier and can be activated or deactivated by an Arduino, if only certain channels are needed. But by switching certain channels off, a high terminal resistance at the end of the switched off channels is introduced to the circuit, leading to reflections and therefore to unwanted crosstalk. For calibration measurements are therefore all channels enabled. Then the signal gets passed on to the TARGET module via standard ribbon cable.
For the CTC evaluationboard, an upgraded and for the evaluationboard specialized version of the CHEC-0002 is used. Here, the Arduino and splitting circuit are placed on separated PCBs to reduce possible noise crosstalk. As the evaluationboard only consists of 16 channels, the splitterboard only has one 1:16 splitter. Without the coaxial four-way split in front of the splitterboard, there is a nearly 1:1 amplitude transmission between the function generator and the CTC ASIC. As the evalution board has an individual SMA socket for each channel (see figure 11), the splitterboard only has one for each channel.
In the further discussion of the splitterboards, the one for the TARGET C module gets referred as CHEC-0002 while the one for the CTC evaluationboard gets referred as

SSTCAM-0002. Both can be seen in figure 26.

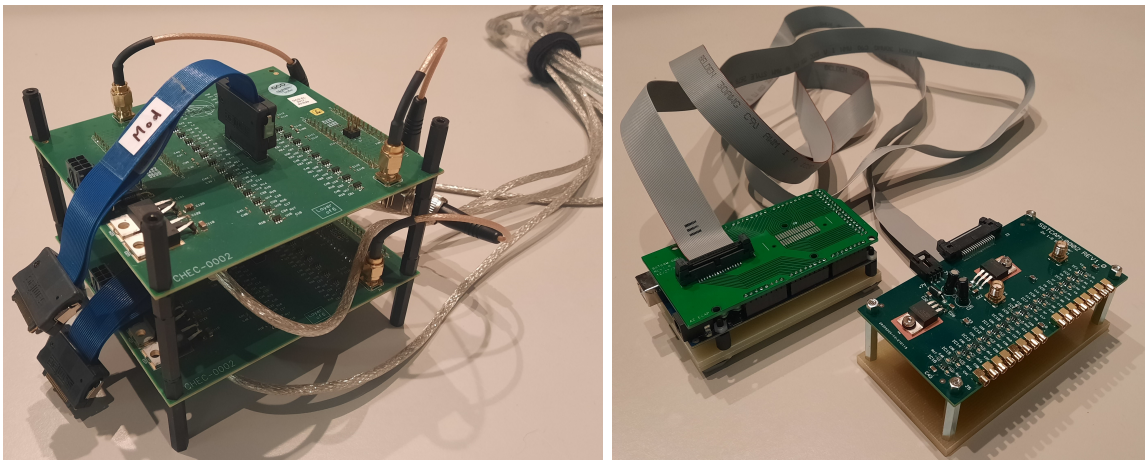

Figure 26: *left:* CHEC-0002 with the coaxial four-way split already plugged in the four SMA sockets and a plugged in ribbon cables for data transmission to the TARGET module. The Arduinos are hidden underneath the two boards, where the silver USB cables connect to them. *right:* SSTCAM-0002 with its external Arduino on the left. Each channel with its own MMCX socket.

To characterise each splitterboard, transfer functions for 16 channels (0 to 64 in steps of 4 for the CHEC-0002) were created by applying the reference voltage pulse from 0V to 5V and measuring the output waveform of the splitterboard with the oscilloscope Tektronix MSO54. For each amplitude a average waveform of 500 pulse is created and read-out by the oscilloscope. To estimate the error of the oscilloscope, a reference transfer function was made, were the waveforms were read-out independently and the statistics were calculated externally. This resulted in an relative error always smaller than 0.2%, converging to zero for larger amplitudes. For more details see appendix A.
As the CHEC-0002 only has a ribbon cable socket for the output, a helper board must be used to convert the ribbon cable socket to a SMA socket. As it is only a socket converter, there are no temperature effect assumed.
The mean transfer function for CHEC-0002 can be seen in figure 27 and for SSTCAM-0002 in figure 28, both on the left, both with a linear corresponse. Due to the fourway split upfront of the CHEC-0002, only maximum amplitudes of 1750 mV are reached, while SSTCAM-0002 reaches the maximum of 2000 mV. After that, the non-inverting op-amp IC OPA693 saturates. Therefore only the range linear of response is used. Since electric components have tolerances, each channel will have a slightly different transfer function as seen in the figures 27 and 28 on the right, where each individual transfer function is subtracted from the mean one. The standard deviation of the mean transfer function can also be seen as the grey area beneath and grows linearly with set amplitude until saturation is reached. From on there, every Op Amp saturates a little bit different, leading to minor differences between the channels.

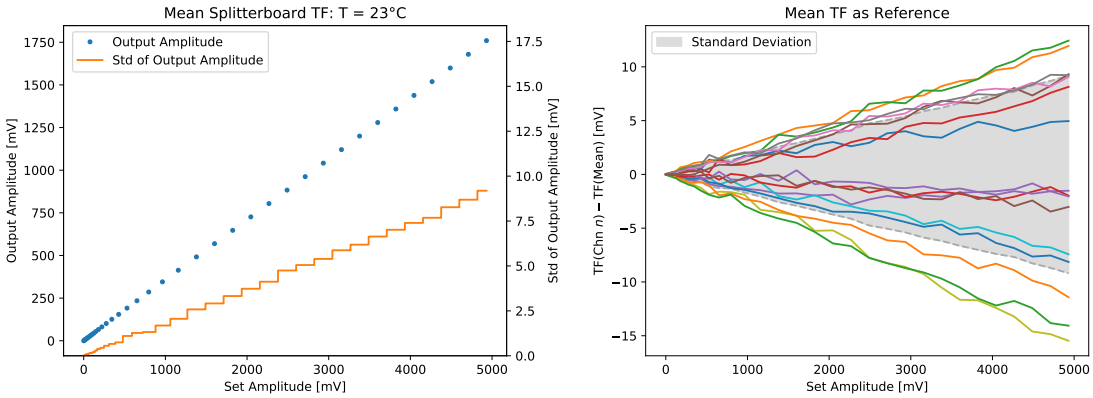

Figure 27: CHEC-0002: *left:* Mean splitterboard transfer function at T = 23 °C with the corresponding standard deviation, *right:* Single channel transfer functions, mean transfer function subtracted

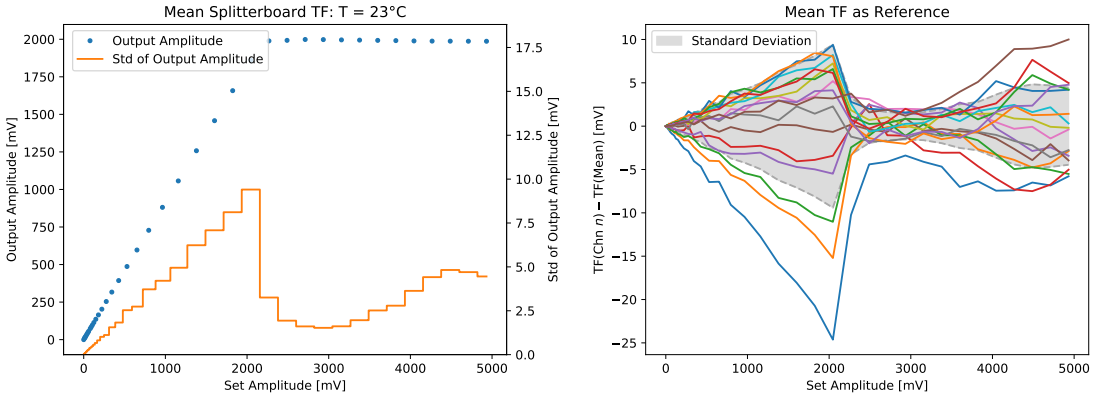

Figure 28: SSTCAM-0002: *left:* Mean splitterboard transfer function at T = 23 °C with the corresponding standard deviation, *right:* Single channel transfer function, mean transfer function subtracted

The cause for these deviation in the linear range could be tracked down to the follow up resistor after the non-inverting op-amp IC, by switching the resistor of channel 4 and 48. By using resistors with a smaller tolerance, this deviation could be lessened. For more details see appendix B.
As the relative standard deviation for the CHEC-0002 never exceeds the 0.5% mark, the mean transfer function (see figure 27 left) can be used for further calculations as there are only 16 channels characterised for the 64 ones. Still, if only the measured 16 channels are used, the single channel transfer functions are used. Contrarily for the SSTCAM-0002 there are transfer functions for all channels, so each channel can use its individual transfer function.

3.3.4. AC Correction Transfer Function

Now that the accurate input for the TARGET module/CTC evaluationboard is determined, the AC correction can be tackled. Only the known dynamic range of TARGET determined by the DC transfer function of 0V to about 1.45V (dependent on the ASIC) has to be scanned. Due to convenience, the whole possible range of the given splitterboard is used. The pulses get fed onto the TARGET ASIC with a rate of 2.6kHz for 5s, so 15.000 events are written down to the disk.

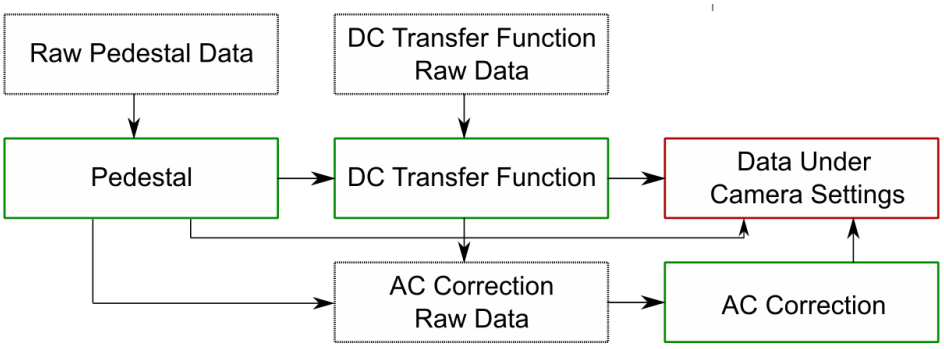

Figure 29: Raw data (dashed) and calibration steps (green) needed in order to produce a AC correction. Camera data (red) needs all three calibration steps

Then the data gets pedestal corrected and the DC transfer function is applied. A schematic of all the calibration data that goes into the AC correction be seen in figure 29. After this, the amplitude of the given pulses is extracted with the above mention method for each channel (see chapter 3.3.2). This leads to about 230 extracted amplitudes per sampling cell. Combined with the transfer function of the splitterboard providing the correct input amplitude to the board, one generates a AC correction transfer function with the measured amplitudes per channel and sampling cell.
An exemplary AC correction transfer function of the TARGET C module can be seen in figure 30. One would assume that the transfer function would saturate at an input amplitude of 1.5V when the DC transfer function ends. But due to the shapers infront of the sampling ASICs on the TARGET C module, this dynamical range shrinks as the shapers have a gain of about 1.5.
One additional feature of the AC correction is that for small amplitude more data points are taken. This is due to how these transfer functions are used as interpolations to get access to all amplitudes in the range. As for lower amplitudes, the relative error easily explodes, while for large amplitudes an offset in the same magnitude is arguable. Therefore the transfer function must be more precise for small amplitudes.
To illustrate the benefits of a AC correction, a data set of different amplitudes was taken, DC calibrated and then the amplitude AC corrected. This data set was taken in the same run, guaranteeing the same temperature on the board, and with a rate of 600Hz, the forseen trigger rate of the SST-Cam. The pulse maxima get extracted as in chapter 3.3.2 and then corrected by the AC correction transfer function.
As the AC correction is a sampling cell correction, it is sufficient to only look at these,

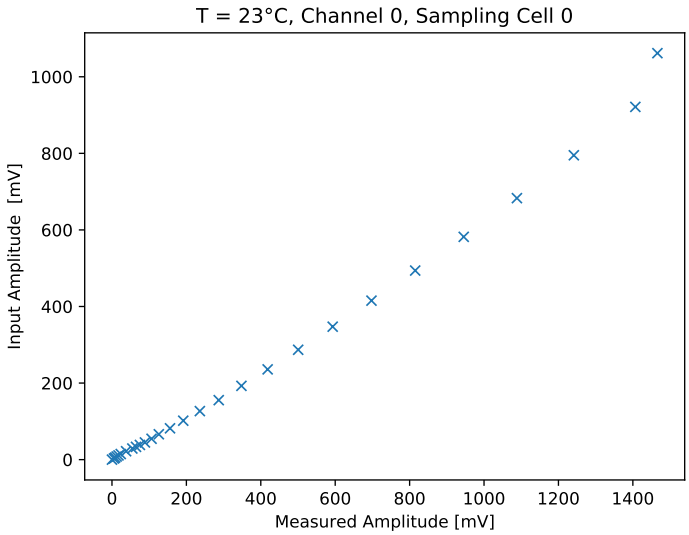

Figure 30: Raw AC correction transfer function of the TARGET C module SN0037 at 23 °C

as the storage cells are already adjusted by the DC transfer function and pedestal. An example can be seen in figure 31.
The offset due to the shapers is corrected and the noise on top is also reduced to a minimum. This was done for multiple amplitudes in the dynamic range of the ASIC for the TARGET C module SN0037. An overview of these can be seen in figure 32 on the

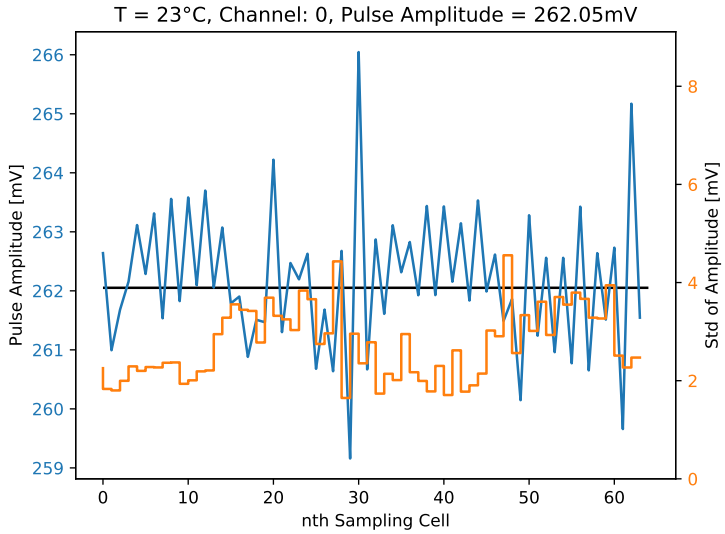

Figure 31: Sampling cell response to a 262.05 mV SiPM pulse of the TARGET C module SN0037 23 °C

left, giving the offset to the input amplitude and on the right addressing the deviation between the sampling cells. In comparison with the figures 23 in the motivation chapter of the AC correction 3.3, both could be significantly dropped, showing the potential of this calibration method.
But it must be noted that these analyses were done for the 12 channels for which a individual splitterboard transfer function exists and that the data was taken in the same run as the AC correction. The temperature dependency at this point is still unknown and will be tackled in chapter 4.3. Also not the whole possible dynamical range of the sampling ASIC is used yet.

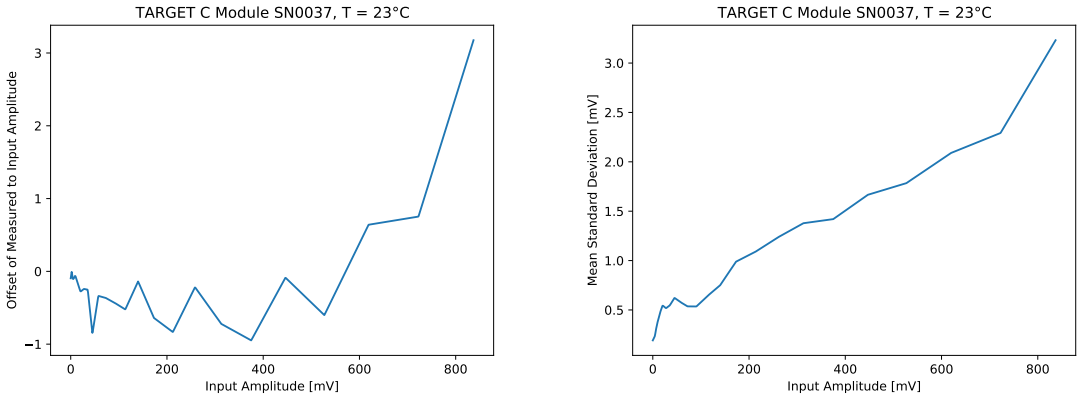

Figure 32: *left:* Mean standard deviation per input amplitude for 12 channel of the TARGET C module SN0037 with AC correction, *right:* Offset between input and measured amplitude of the same module with AC correction

4. Temperature Dependencies

The in chapter 3.2 introduced calibrations are now performed at different temperatures to investigate the temperature dependent effects of them. A in-depth analysis of the temperature dependency of the pedestal calibration is left out as it is already well known [14] and it is easy to readjust the pedestal in the camera dependent on the temperature.
As specific components of the TARGET module are the source for these effects, it would be appropriate to measure the temperature of these. But as this study shall also be comparable with operating modules, only the three sensors on the board are used. For the CTC evaluationboard, where the primary goal is to directly and independently survey the CTC, a external RTD on top of it is used.
To find a common baseline between all these different temperature measurements, the temperature of the chamber is given, if not stated differently. Nevertheless, the placement of the set up and cooling fan between runs does change the temperature on the board and ASICs. Translation plots between the chamber temperature and the sensors of each individual module can be looked up in appendix C.1.

4.1. VPed Transfer Function

It already became apparent from previous works, that the changes in Vped transfer function for TARGET C are smaller than 0.5% for a temperature span of 20-50 °C [17]. This also has to be now confirmed for CTC. Nevertheless,the TARGET C module SN0037 was also probed for in house comparability. As no surprises are assumed, only the temperature dependence of channel 0 was looked at, to be able to use a multimeter instead of the eight channel ADCs.

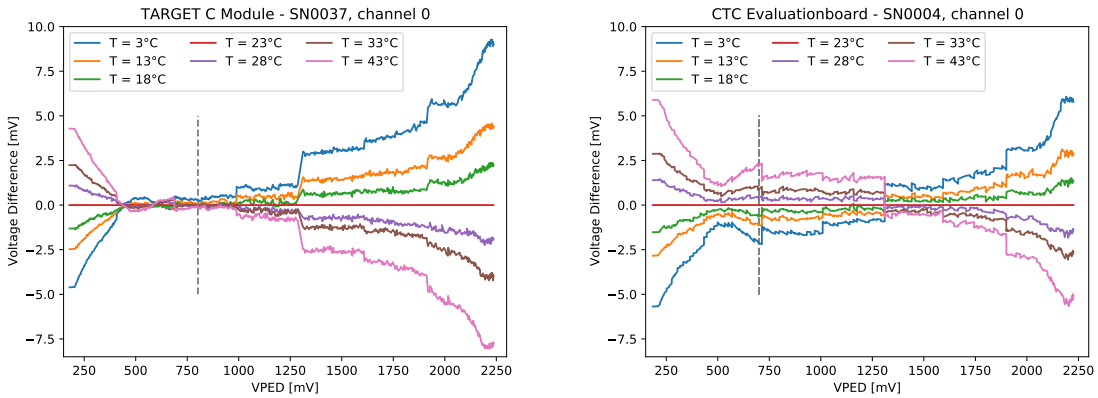

Figure 33: Temperature dependent change in Vped transfer function for channel 0. The grey dashed line marks the pedestal voltage that will be used for standard data taking. *left:* TARGET module SN0037, *right:* CTC Evaluationboard SN0004

In figure 33 one can see the Vped transfer function of each temperature subtracted from the reference at 23 °C for channel 0 of TARGET C module SN0037 on the left and of

CTC evaluationboard SN0004 on the right. Both have similar characteristics and are therefore described simultaneously.
Apparent is that at both ends of the transfer function, the difference grows heavily, linear for the start and exponentially towards the end. For the low voltages it also exceeds the targeted relative deviation of 0.5% with up to 3%. This has to do with the CMOS switching of the R2R DAC which work point is temperature dependent. For higher temperatures, the work point is already reached at lower voltages. Hence, the Vped transfer functions have a higher Vped voltage for the same DAC count, leading to the observed spread at the beginning of the transfer function in figure 33. But as the pedestal, which sets the virtual null for the running TARGET module, is always bigger than 500 mV and negative voltages are not used, this area remains meaningless.
Still one must be concerned about the deviation around the set pedestal as the relative error will explode if it is set to zero. Nethertheless, a deviation of 1 mV around the virtual zero in a temperature range of $\pm 10°C$ is still fully in the scope of error budget, which is the case for both TARGET generations.
The other "divergence" at the end of it is where the non-linearity of the T5TEA comes into effect. For higher temperatures the ASIC goes sooner into the non-linearity than for lower ones. Therefore the voltage difference between the transfer functions grows due to the shape mismatch. But as the Vped voltage are high when this occurs, the relative error stays always 0.5%.
Another aspect of difference between the transfer functions are the jumps. This increase happens always after a big chunk of bits is flipped in the DAC and a new resistor of the R2R network is switched on as described in chapter 3.2.2. The most noticeable one can be seen around 1300 mV, responding to the 011111111111 to 100000000000 bit flip.
Through the design of a R2R network, resistor deviations of resistors, which are responsible for the higher voltages, have a higher impact on the output voltage. Therefore the growing temperature dependent deviations for higher amplitudes. Also, as more resistors are switched on in the R2R network, the more temperature dependent components contribute to the overall temperature dependency of the ASIC.

4.2. DC Transfer Function

While studying the changes in DC transfer functions due to thermal changes, it became apparent that the process of DC transfer function data taking itself affects the temperature on the ASIC. As the effect of initialising the module and triggering is already discussed in chapter 3.1, the only open parameter changing while taking data, is the set pedestal voltage. For each set pedestal 80 seconds worth of data were taken and the temperature got monitored every five seconds. For the RTD set up see also chapter 3.1.
A dependency between the temperature of the ASIC and the set pedestal can be seen in figure 34 for the TARGET C module and for the CTC on the evaluationboard SN0002. For each measured pedestal, the mean temperature point is displayed consisting of 20 individual measurements. The vast drop in temperature for low pedestal voltages is an artefact due to the warm up routine of the board, where it is initialised and triggering on a pedestal of 800 mV for five minutes. Looking at the temperature difference of the

set pedestal voltages 800 mV and 300 mV, the ASIC is obviously not in thermal equilibrium for the data taken at 250 mV. As voltages below 800 mV (for normal data taking) are accounted for negative amplitudes, this does not diminish the accuracy of the DC transfer function, as these are not used.

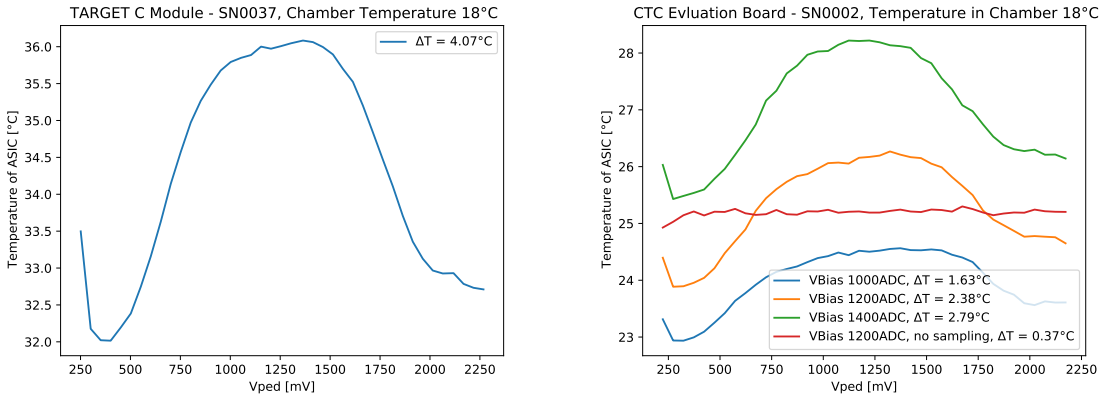

Figure 34: Temperature difference on the ASIC due to the set pedestal. *Left:* TARGET C module SN0037, *right:* CTC evaluationboard SN0002

More concerning is the temperature span of 4.07 °C for the TARGET C module and 2.38 °C for the CTC evaluationboard SN0002 (standard VBias of 1200 ADC counts) for different pedestal voltages. The temperature difference for different set pedestals could be tracked down to the VBias parameter, which is the supply voltage for the Fast OTA (Operational Transcondactance Amplifier) buffering the signal between the sampling and storage cells. The standard setting is 1200 ADC counts. By lowering the value, the OTA gets less power and therefore dissipates less heat. A decrease in the overall temperature is observed as a smaller temperature difference for different pedestal voltages. The opposite applies for a higher VBias. As an additional check, the sampling and therefore the OTA got turned off and the temperature dependency of the pedestals vanished. This can be seen as the red line in figure 34. A temperature dependent influence from the digitisation process, triggering or from the occurrence of AC pulses could not be observed.
Additionally, the 2 °C temperature difference in ΔT between the two generations of ASICs is misleading, as for the TARGET C a standard cross cut heat sink with a heat glue of thermal conductivity $1.8\frac{W \cdot K}{m}$ and 5mm thickness is used, while the CTC got a bigger extruded heat sink with a thermal glue of thermal conductivity $13\frac{W \cdot K}{m}$ and 5mm thickness. Through testing different heat sinks and thermal pads at the CTC ASIC, the temperature difference due to the different pedestal voltages could be dropped from about 4.0 °C to 2.4 °C. The drawback of the momentary used heat sink for SN0002 is that it is to big for the TARGET module and must therefore be replaced with a smaller one for camera operation. For SN0001 and SN0004 a fitting one is used. The plots can be seen in appendix C.2.
To appraise the error due to the temperature difference, a second DC transfer data set

was recorded, where the temperature of the CTC ASIC is kept constant. This was archived by real time monitoring of the ASIC temperature and manually adjusting the chamber temperature before each pedestal voltage measurement. As this was merely challenging, only ten different pedestal voltages were used from 218 mV to 2018 mV in steps of 200 mV. With a mean temperature of 25.50 °C and a standard deviation of 0.08 °C across all set pedestals, the temperature spread of the ASIC is not bigger than the in figure 13 measured deviation for a mean ASIC temperature of 35.98 °C with a constant pedestal of 800 mV. Also the temperature of 25.50 °C was not randomly chosen but consciously selected to sit right in the middle of the temperature span, reducing the maximal deviation in one direction.

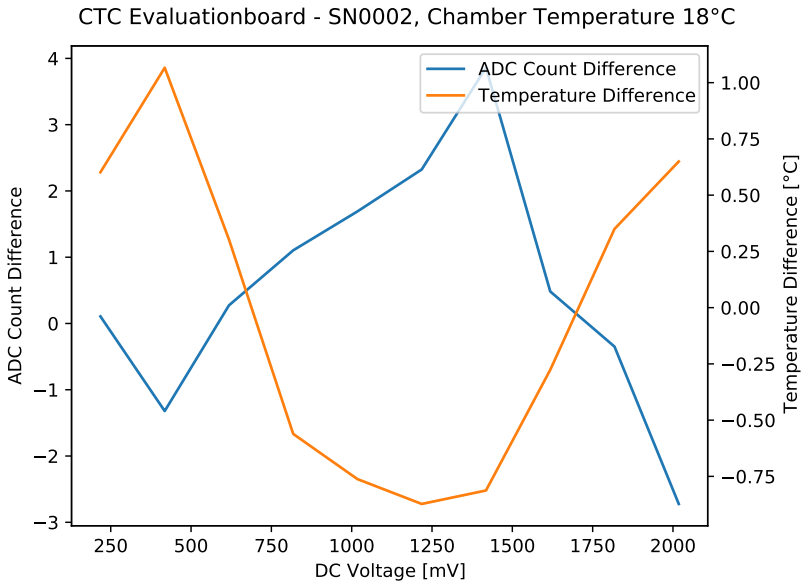

Figure 35: Differences in ADC counts and temperature between standard measurement and fixed temperature measurement

In order to compare both data sets, the raw waveform data of the different pedestal measurements are used. For this purpose the mean ADC count of each DC waveform is taken excluding the 32th cells. In figure 35 in blue, the mean ADC count for certain pedestal voltages of the temperature stabilized data set was subtracted by the data set without thermal equalisation. The difference between the two data set is marginal, peaking in a ADC count difference of about ±3 ADC counts, which can be neglected. Additionally, one can see the temperature difference between the data sets is anti-correlating with the ADC count difference, double checking that the temperature difference is the dominant effect.

Now that it is ensured that the process of taking DC transfer function data is temperature stable in the given requirements, DC transfer functions at different temperatures were taken. As it is tedious to compare all DC transfer functions of all channels with their

4096 storage cells and only comparing few channels and cells is not sufficient for a full characterisation, mean transfer functions of all channels and their respectively 4096 storage cells are used for evaluation. To showcase the difference in the transfer functions due to different temperatures, they were subtracted by a reference transfer function at 23 °C room temperature. This can be seen in figure 36 for the TARGET C on the left and for the CTC evaluationboard SN0001 on the right, for all positive amplitudes.

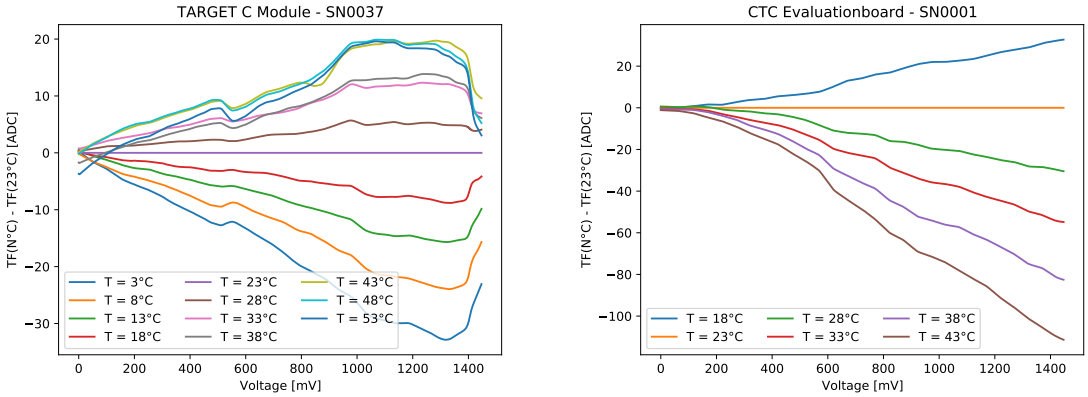

Figure 36: Temperature induced differences of the DC transfer functions. *left:* TARGET C module, *right:* CTC evaluationboard SN0001

A complete data set from 3 °C to 53 °C is aquired for TARGET C and for the CTC only the relevant temperatures which can occur in the camera are conducted.
For TARGET C the differences span from -30 to +20 ADC counts for all temperatures. Considering only the relevant temperatures of 18 °C up to 43 °C, it only spans from -10 to +20 ADC counts. Apparently the ADC count different saturates at 43 °C. Perhaps the temperature characteristic of the ASIC is changing here and a further increase of temperature could then lead to a decrease in ADC counts. But as temperatures above 43 °C are not admissible and measurements above 53 °C are left out, this only remains a speculation.
Comparing that to the CTC evaluationboard SN0001, the temperature induced differences are amped up to -100 to +20 ADC counts. The new generation of sampling ASIC is therefore way more temperature sensitive than its predecessor, making a temperature dependent correction even more indispensable. Interesting is also that the temperature dependency of the CTC is inverted in comparison to the TARGET C. Higher temperatures lead to lower ADC counts instead of higher ones in reference to the 23 °C transfer function. Also it is apparent that the ADC count difference grows with the voltage. In case of the TARGET C this growth stops around 1000 mV.
One significant difference between the DC transfer functions of the TARGET C and CTC are the different ramp parameters in the Wilkinson ADCs. For TARGET C a dual edge clocking of 250 MHz is used, while for the CTC one at 104 MHz is chosen for the three evaluationboards. In the work of Johannes Schäfer [15] it was already proven, that a significant portion of the temperature dependency of the transfer functions is

due to the changes in the Wilkinson ramp. With a slower and therefore longer ramping voltage/time, temperature induced slope differences play a bigger role. Dependent on different parameter scans and analysis, a clocking frequency of 208 MHz is chosen for future operations. Therefore a fitting Isel parameter must be found, to guarantee a stable performance of CTC in the given requirements.

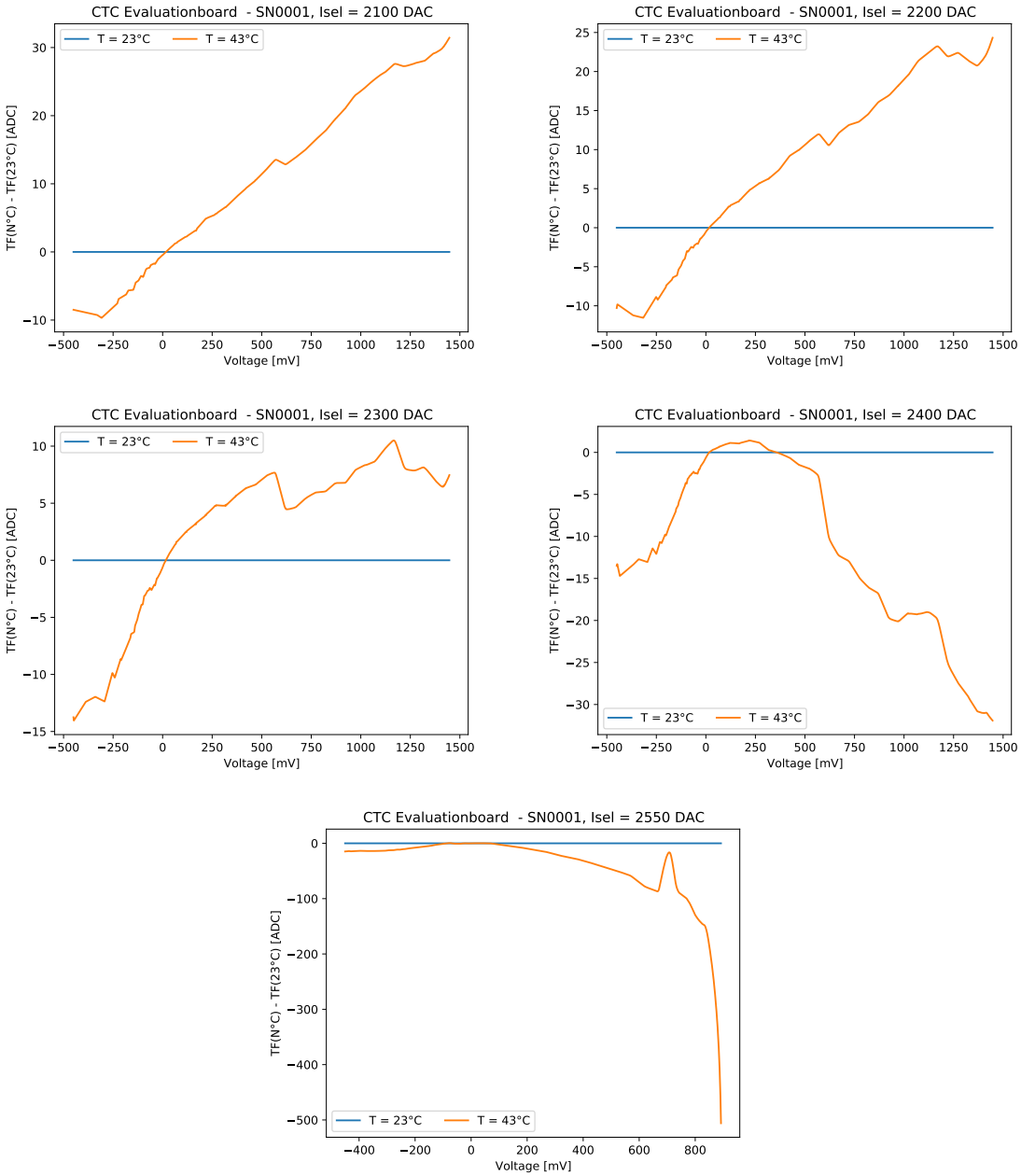

Figure 37: CTC evaluationboard SN0001 with a Wilkinson clock of 208 MHz

In chapter 3.2.4, a scan over different Isels for a clock of 208 MHz has already been done, favouring an Isel of 2400 DAC counts. With these parameters, the DC transfer functions

ranges across the whole dynamical voltage range while using most of the available ADC range without strong non linearities as with a Isel of 2550 DAC counts. Now the question is, how the temperature dependency of the DC transfer function behaves for different parameters and if there is an optimal Isel parameter for the 208 MHz clock frequency where the temperature dependency is minimal.
As a full temperature characterisation across six temperatures for five different Isel is quite elaborate, only DC transfer functions at 23 °C and 43 °C are taken for each Isel. But since the temperature induced deviations between the transfer functions grow nearly linearly with temperature, the 43 °C shows the most significant results for the given temperature range. From its characteristics one can then indicate the temperature dependent behaviour of the transfer function over the whole temperature range, or at least up the the reference temperature 23 °C. The transfer functions are then analysed as before and can be seen in figure 37 for a total of 5 Isels.
In comparison to figure 36 one immediately sees that the parameters for CTC evaluationboard SN0001 were chosen poorly in terms of temperature dependency. For the most Isels, the deviations are in the magnitude of the TARGET C generation, excluding the one with an Isel of 2550 DAC counts, which was already problematic with its low voltage range and non linearities. These non linearities also seem to change with temperature leading to the observed peak at 700 mV by shifting it.

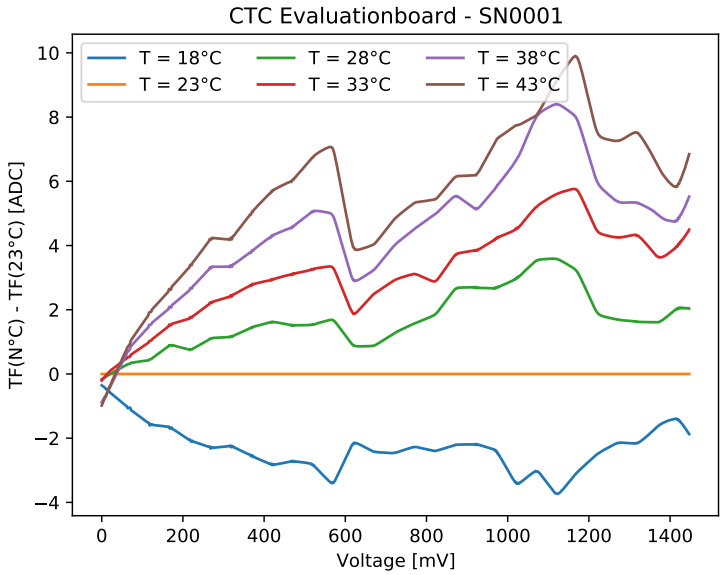

Figure 38: Temperature inducted differences of the DC transfer functions of SN0001 with a Wilkinson clock of 208 MHz and a Isel of 2300 DAC counts

It is interesting that the temperature dependency changes "direction" dependent on the Isel. Lower Isels lead to an increasing ADC count with higher temperatures while higher Isel do the opposite. This leads to a natural minimum temperature dependency for the DC transfer functions with an Isel around 2300 DAC counts. For future applications

this could now be fine tuned to maybe archive a temperature independent DC transfer function. As the current proposed calibration method allows determination of the DC transfer function while operating, this is not further investigated. Although a low temperature dependency is favorable.
Nevertheless, based upon the results of the temperature dependency scan with different Isel and the used ADC range scan in chapter 3.2.4, a fully temperature dependency analysis for SN0001 with an Isel of 2300 DAC counts and a Wilkinson clock of 208 MHz was done and can be seen in figure 38. Upon all DC transfer function across TARGET C and CTC with different parameters, it looks the most promising. For amplitudes greater than 200 mV the relative error always stays below 1% for a temperature range of 18 °C to 33 °C and for the whole voltage and tested temperature range it always stays under 1.5%.
For future operating of the CTC ASICs a clock of 208 MHz and a Isel of 2300 DAC counts is therefore favorable in terms of temperature dependency. As this was one of the last things tested for this work, a Wilkinson clock of 104 MHz and a Isel of 2550 DAC counts are used for the evaluationboards for further analysis as the AC correction, plus a cross check with SN0001 at 208 MHz and Isel of 2300 DAC counts. But as the AC correction is sole sampling cell correction, it should be independent of the Wilkinson ramp parameters. More to that in chapter 4.3.4.

4.3. AC Correction

In contrast to the DC transfer function and the pedestal dependent ASIC temperature, such behaviour could not be observed for different sized pulses. Consequently a pedestal of 802 mV for TARGET C and 700 mV for CTC is used. For most of the underlying DC transfer functions an Isel of 2550 DAC counts and a Wilkinson clock of 104 MHz were used. These parameters where not optimized at this point and could been chosen better. But as the AC Correction will be applied by a data set that is DC corrected at the same temperature, the temperature dependency of the AC Correction and characterisation of the sampling cells should not change as the AC effects do not depend on the digitisation. A cross check with different ramp parameters was performed with the CTC evaluationboard SN0001.
Additionally to the set up now the splitterboard is also in the temperature chamber. Therefore the temperature dependency of it has to be tested first for a consistent result.

4.3.1. Splitterboard Transfer Function

As CHEC-0002 and SSTCAM-0002 have the same components besides the connectors, only CHEC-0002 will be looked at, as the Arduino will also be placed in the temperature chamber. In total, transfer functions of 16 channels in steps of four were taken at five different temperatures. Then a mean transfer function of these 16 channels were made of each temperatures, just as described in chapter 3.3.3.
For comparison the mean transfer functions of each temperature are subtracted by the reference transfer function at 23 °C. This can be seen in figure 39. As previously men-

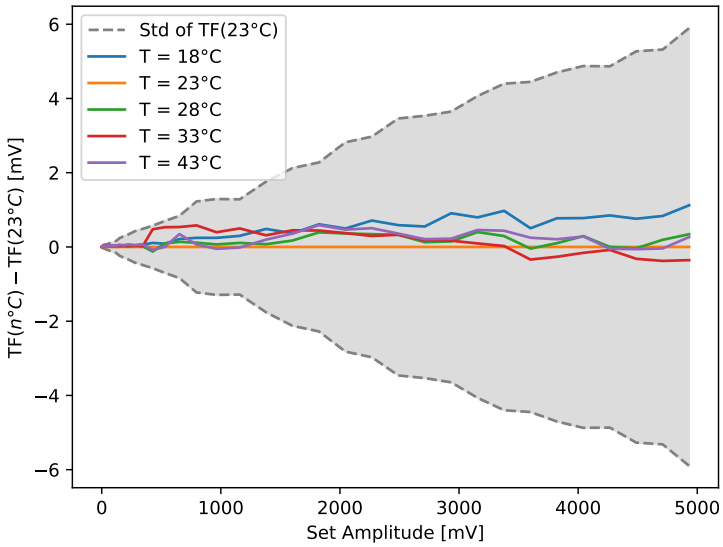

Figure 39: Deviation between splitterboard transfer function dependent of different temperature.s In grey the standard deviation of the reference transfer function at 23 °C

tioned, the amplitude loss due to the triggering issue is not observable as it is cancelled by the subtraction. Only the temperature deviations are left. In grey is the standard deviation of the reference transfer function at 23 °C due to the channel deviations. The difference between the transfer functions is smaller than 1 mV across all amplitudes and always smaller than the channel to channel deviations of a single transfer function. Therefore one can say that the output of the splitterboard is temperature independent. Hence for the AC correction only transfer functions at 23 °C are used, a mean of 16 channels for the whole 64 channels TARGET C module or the 16 individual for these channels and 16 individual ones for the CTC evaluationboard.

4.3.2. TARGET C AC Correction

As this work is a proof of principle for the calibration methods of TARGET and only a limited number of modules/ASICs plus one pair of splitterboards are used, one is primarily interested in the best possible characterisation of the transfer functions and then in a practical solution for calibrating 32 modules per camera. Therefore, only the twelve channels of the 48 channels of the TARGET C module SN0037 are used, where a individual transfer function is available. Also will the TARGET C modules not be used in the SST cam. Nevertheless, there are components in the signal chain before the ASICs that can only be tested on the module and for CTC only the evaluationboards are available at the moment.
Again, five transfer functions at different temperatures were taken, pedestal and DC calibrated on the same temperature, averaged over the used channels and cells, and

then subtracted by the reference one at 23 °C. The result can be seen in figure 40. Obviously something went wrong for the data set of the 33 °C transfer function at about 400 mV and 1750 mV. Sometimes the measurement process is not stable and such errors happen. But the measurement of each set amplitude is an individual process, so this error can be isolated. For an applied AC correction transfer function this must of course be corrected, but for a temperature dependent analysis this can be ignored.

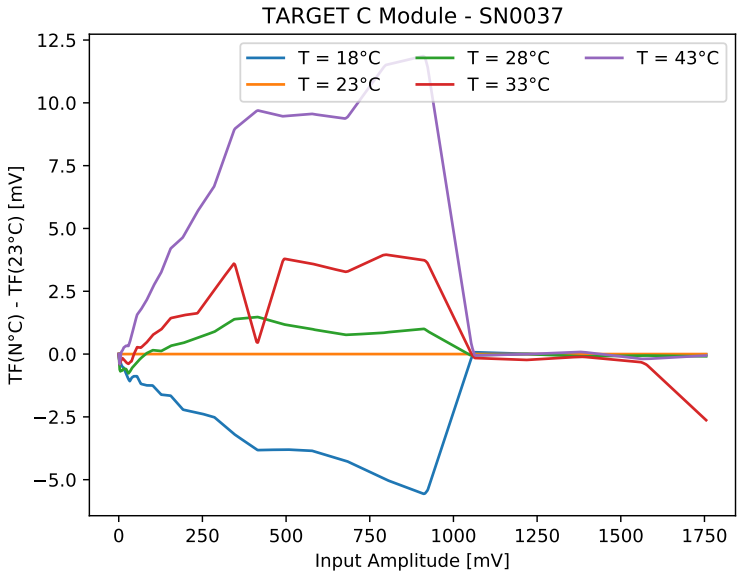

Figure 40: AC correction transfer functions difference due to temperature for the TARGET C module SN0037

Another feature is the saturation of the transfer functions, which sets in at 1V and seems to be temperature independent. Nevertheless, this part is not useable, since multiple input amplitudes are assigned to the same measured amplitude due to the limited DC transfer function.
For the main part of the transfer functions, a temperature dependency can be seen. Slightly worse for lower temperatures as 18 °C than to the opposed 28 °C and 33 °C, maximising at 43 °C. But a closer look reveals that for the temperature span of 18 °C to 33 °C, the difference between the transfer function stays below 1% for input amplitudes greater than 50 mV. For lower amplitudes the relative error diverges due to the small input. Therefore one could approximate the AC transfer function to be temperature stable for a temperature range of about ±7.5 °C around the calibrated temperature. For higher temperatures this is not sufficient. Still one must find out if this temperature dependency is a product of the ASIC or a different component of the module. A pure dependency of the ASIC for example could be counteracted with a Peltier element on top of it. The only circuit remaining in the signal chain of the TARGET C module is the shaper circuit, which is not characterised at this point and could contribute to the dependency.

4.3.3. Shaper as Cause?

For the characterisation of the shaper circuit, in principle the set up of the AC correction is used. The same amplitude as for the splitterboard transfer functions are tapped in the shapers via the splitterboard and are then probed by the oscilloscope Tektronix MSO54 before reaching the ASIC. 500 waveforms are averaged to one and 16 channels (4·n) are measured. The board must be initialized for the shapers to run.

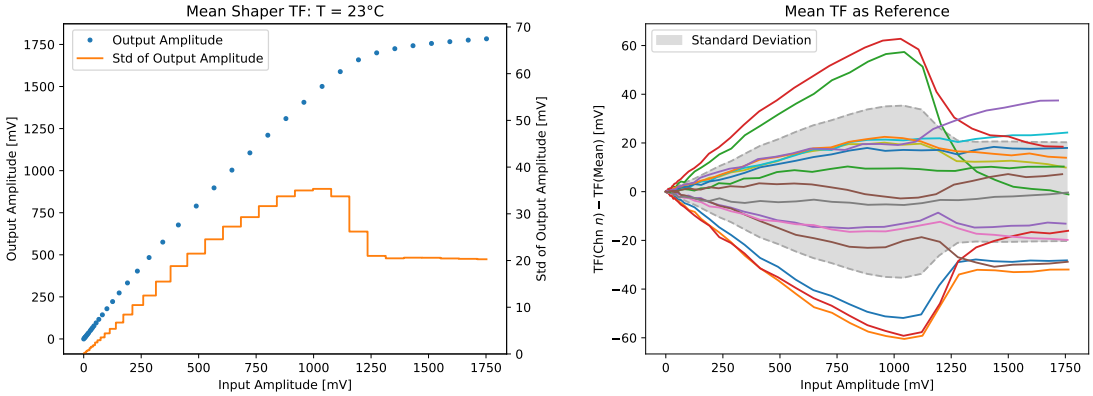

Figure 41: *left:* Mean transfer function of the shapers over 16 channels, *right:* Mean deviation from the mean transfer function

The mean transfer function of the shapers can be seen in figure 41 on the left and the deviation of each channel from the mean on the right. Here, a mean transfer function is not expedient for use as the channel differ up to 6% on the output for the same input. This is indeed a problem, as different channel/pixel will have different trigger rates for the same input due to the higher or lower gain of the shaper. For a future operation and analysis of the camera data, this must be taken into account. Nevertheless, due to the SiPM change, a fully new shaper topology is designed for the CTC generation modules, making this case obsolete. Still this must be checked for the new generation of shapers as this problem emerged for the TARGET C shapers, this may also be the case for CTC. The response of the shapers is approximately linear up to the saturation around 1250 mV with a slightly negative curvature. A pole zero shaper can and does not saturate, but in front and after the shapers are buffers, which saturate due to the op-amp and its limited output range. With the emerging edge, high frequencies are needed for a proper depiction of the cut off pulses which are not available with the bandwidth of the op-amps. Therefore the saturated pulses overshoot. This overshoot grows with rising edge steepness and hence with the amplitude of the input pulse. Thus the saturation is rather soft and grows with amplitude until no more extra current can be drawn from the voltage supply.

Then the mean transfer function is compared for different temperature in the range from 18 °C to 43 °C. In figure 42 the mean transfer function of each temperature is subtracted by the reference one at 23 °C and in grey the standard deviation of it due to the channel differences. Excluding the 28 °C transfer function, the difference for a fixed input

amplitude grows linearly with the temperature. Compared to the temperature induced differences in the AC correction transfer function (see figure 40), the deviations are also in the same magnitude. This suggests that a big part of the temperature dependency of the AC correction comes from the shapers.

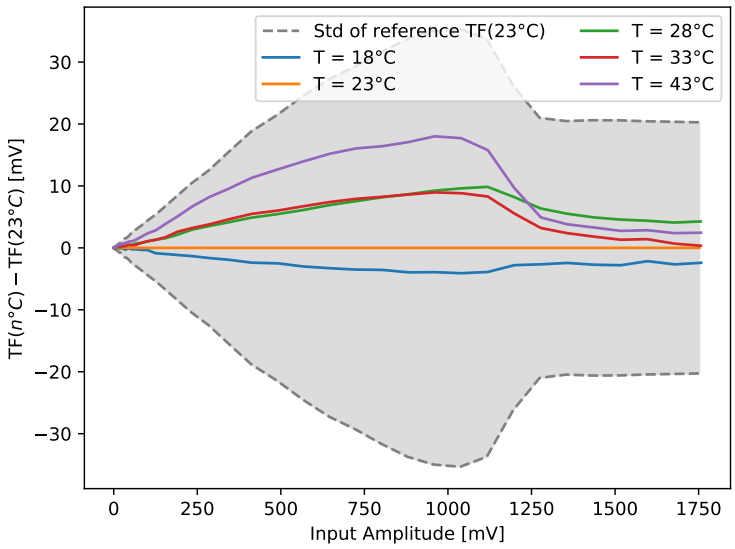

Figure 42: Temperature differences of the shaper transfer functions of TARGET C SN0037. Standard deviation in grey due to the channel spread of reference transfer function at 23 °C

To investigate this further, the shaper transfer functions gets applied upfront of the AC correction, so the AC correction is then a function of the real input into the ASIC and not the input of the module as until now. Keep in mind that the shapers have a gain greater than one leading to bigger input amplitudes. If the shapers are the root of the temperature dependency of the AC correction, then no temperature dependency should be left on the AC correction transfer function with applied shaper transfer function of the correct temperature.
The shaper corrected AC corrections can be seen in figure 43 for channel 8, 12, 16. All shaper transfer functions have the same characteristics as one of these three. Due to these distinctive differences between the channels, a mean transfer function is not expedient.
For channels such as channel 8, the temperature dependency is cancelled out as intended. The transfer function never exceeds the aspired 1% mark. But this does not apply to all channels, as seen in the other two figures in figure 43. For channels such as channel 12 the shaper correction even amplified the temperature dependency. However this is somewhat misleading. By cross checking the transfer functions with the pedestal and DC corrected data, it could be found that the 43 °C shaper transfer functions are quite off from the remaining ones. This could be explained by the tedious measurement pro-

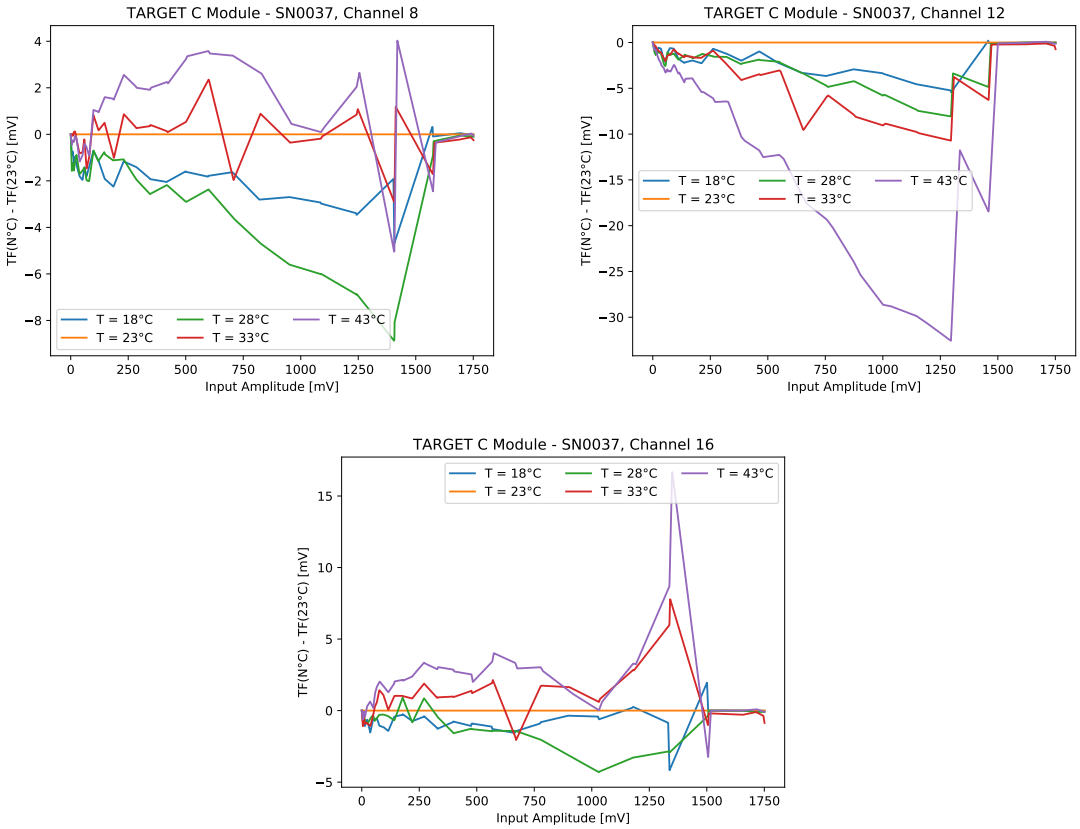

Figure 43: Exemplary characteristics of shaper corrected AC transfer functions in reference to the temperature

cess of the transfer functions. Each channel of the 16 channels has to be single handily probed for five different temperatures. For the last measurement series at 43 °C the probe could be aimlessly set up, leading to a different contact resistance.
By rejecting the 43 °C transfer functions, the deviation between the temperatures drops to the level of channels such as channel 8 even if the illustration in reference to 23 °C make it seem worse. Due to the fact that these transfer functions were directly probed and not plugged in with a coax cable into the oscilloscope, these transfer functions are much more vulnerable to noise, set up differences and therefore contact resistance changes, and temperature dependencies of the probe. Also the total deviation between all transfer function is way more significant than the relative difference to one arbitrary reference transfer function.
Last but not least come channels such as channel 16. In principle do they behave like channel 8 with a spike around 1750 mV. This is in the account of the saturation of the transfer function where it steppens. With the data points of the transfer function being further apart for larger input amplitudes, only two to three data points are there to describe the non linearity. With a linear interpolation, the curvature can only be approximated leading to these deviation, which are nevertheless in the 1% range.

To quantitatively describe the deviation between the transfer function due to temperature differences, the mean standard deviation between each transfer function was calculated and assigned to its channel. This can be seen in figure 44 in blue for the AC correction and in orange for the shaper corrected AC correction. The 43 °C transfer function was dismissed due to the earlier illustrated difficulties. Also for the shaper corrected AC correction channel 0 is discarded with the same cross check. Apparently the pin to probe the signal after the shaper is the problem.

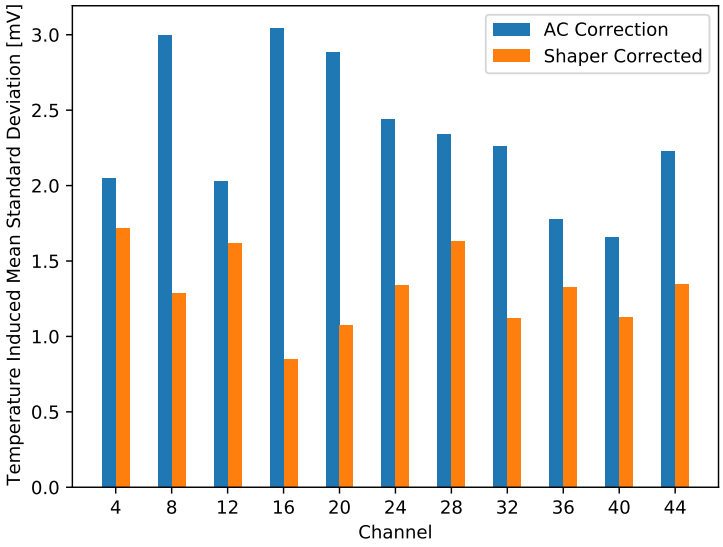

Figure 44: Mean temperature spread of transfer functions per channel for temperatures in the range of 18 °C to 33 °C

One can definitely see an improvement in the temperature induced deviation between the transfer functions with the shaper correction as the standard deviation could be nearly halfed in the mean. This is clearly a indicator that the temperature dependency of the AC correction is a result of the temperature dependency of the shaper. There is still much room for misapprehension because of the way the transfer functions were probed and the given adjustments, which can also be seen in the variety of improvement. The decisive test will then be the AC correction of the CTC evaluationboard where the properties of the ASIC can be probed directly without the shapers in the signal chain.

4.3.4. CTC AC Correction

For the CTC evaluationboards, the same measurement routine as for the TARGET C module is applied, but with an individual splitterboard transfer function for each channel. The corresponding temperature dependency plot for SN0001 can be seen in figure 45. On the left for the suboptimal Wilkinson ramp parameters of 104 MHz and 2550 DAC counts and on the right for the least temperature dependency using parameters 208 MHz

and 2300 DAC counts. Up to small differences, they are both equally temperature independent, maintaining a relative error always below 1% across the whole voltage and temperature range, which even converges below 0.5% for voltages over 100 mV. This demonstrates two important features of the TARGET ASIC. The first one is, that the temperature dependency of the AC correction does not change with the ramp parameters as assumed. AC effects are frequency dependent and with sampling, only the pure voltage value remains in the cells. Therefore, the AC effects are independent to the digitisation process. The absolute values of the AC correction whereas changes, as the input voltage is opposed to the read-out voltage, which changes with different parameters for the Wilkinson ADC.

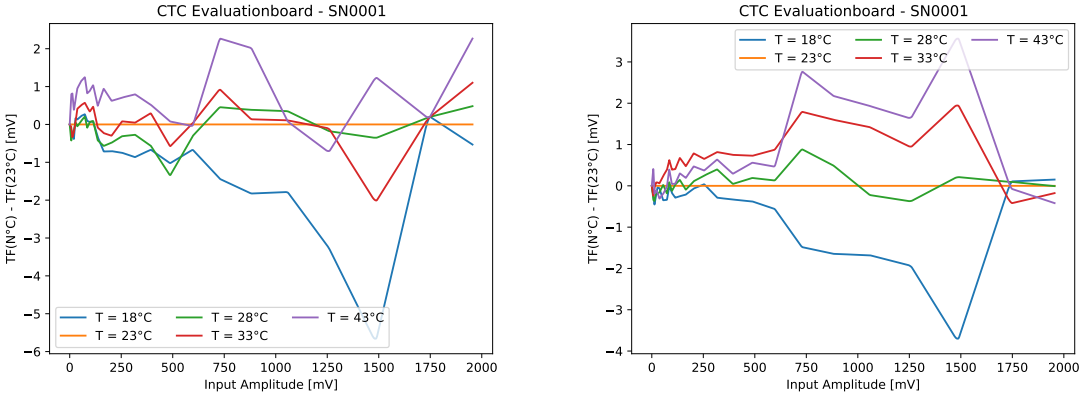

Figure 45: *left:* Wilkinson clock at 104 MHz and Isel at 2550 DAC counts, *right:* Wilkinson clock at 208 MHz and Isel at 2300 DAC counts

The second and more important one is that the AC correction of the CTC ASIC is temperature independent. With a precise look, one can still identify a temperature dependency in figure 45, especially for the one with a Wilkinson clock of 208 MHz and a Isel of 2300. But these changes are so small that they can therefore be overlooked. In conclusion with the results of chapter 4.3.3 this strongly suggest, that the shaping circuit in front of the ASIC contributes the majority of the temperature dependency of a whole TARGET module. Comparing that with the TARGET C module AC correction and its TARGET C shapers in figure 40, one could still argue that the AC correction for a whole CTC module with TARGET C shapers in front could be temperature independent for a small given temperature range. Nevertheless, the CTC shapers will be a new topology with its own characteristics, so this is purely speculative and needs further investigations in the future.

5. Intensity Resolution

To this point, the TARGET module/CTC evaluationboard was looked at in an isolated setting, characterising its transfer functions and their temperature dependencies in terms of different input amplitudes. But in the end one wants measure photons at certain resolution and accuracy with the whole telescope and how the temperature dependency of the transfer functions affect it. Therefore CTA set an intensity resolution requirement to assure the scientific goals of CTA. To describe the quality of the photon reconstruction of the telescope under a realistic setting, different effects need to be added to the known fractional voltage resolution of TARGET. This includes several assumptions as the SiPM is not a part of this work and its properties have to be approximated by the requirements of it. In additions to that come several different properties due to the physical process of detecting photons such as its Poisson statistics and the abundance of a night sky background.
All in all, this can be described with equation 3. A quantum efficiency of 25% for the SiPM tile is used and the amplification is set that one photo electron corresponds to 4 mV of pulse amplitude. This gain is still adjustable, but realistic for the current set up [14, 18]. The gain manifests itself as 4 and 16 (4^2) in equation 3.

$$\frac{\Delta I}{I} = \sqrt{\sigma^2_{\mathrm{TARGET}} + \frac{(1+ENF)^2}{4I} + \frac{\mathrm{NSB}_{\mathrm{rate}} \cdot T}{16I^2} + \sigma^2_{\mathrm{Sys}}} + \sigma_{\mathrm{BIAS}} \tag{3}$$

In total, five different terms contribute to the intensity resolution. The first one is the fractional resolution of the whole TARGET module including amplification noise, digitasation noise, thermal noise and differences in sampling and storage cells. This is the spread of the measured amplitude corresponding to a certain photon pulse and one of two terms which can be tackled with the proposed calibration methods.
The second one is a combination term of the Poisson error and the excess noise factor (ENF) of the SiPM. While the intensity resolution is limited by the Poisson statistics of photons and can not fall below it, the excess noise factor is related to the SIPM. It gives a measure for the crosstalk and unwanted after pulses of the SiPM [19] that restrict its resolution. Following the advice from the previous work on the TARGET 7 generation [18], the ENF will be set to 0.1.
The third term describes the photon background due to the night sky background (NSB). For standard conditioned nights a stray photon rate of $\mathrm{NSB}_{\mathrm{rate}} = 125\,\mathrm{MHz}$ is assumed and adopted by the CTA requirement. These photons create additional pulses in the read-out waveform at random. Most of them can be ignored, as they do not concidence with the real signal. Therefore, only a time frame of T = 5ns is used that contributes to the resolution, which is about the peak width of the pulse that is used to measure the amplitude. For a small photon count it is difficult to distinguish between stray photons and Cherenkov photons, therefore the night sky background induced uncertainty in resolution will be underestimated for small amplitudes with such a short time frame.
The fourth term is the systematic uncertainty, which is a 5% buffer for all unaccounted errors of the camera module, such as crosstalk, calibration uncertainties and uncorrected temperature dependencies.

All these effects are independent of each other and can therefore be added in quadrature to form the overall intensity resolution of the whole FEE. On top of that comes the fractional bias σ_{BIAS} between the input pulse amplitude of the SiPM and the reconstructed pulse amplitude of the TARGET module.

To test the intensity resolution under different circumstances, an extra set of data has been taken at all temperatures, where a DC transfer function and AC correction is available. This was done at a trigger rate of 600Hz to simulate conditions as in the operating camera. In total, about 6000 events were written down for each of the 31 input amplitude for the TARGET C module and 25 for the CTC evaluationboard. The steps between amplitude were chosen in the style of the AC correction, to minimize the error for small amplitudes. But the amplitudes for the intensity resolution and the AC correction are never the same to reduce the potential systematics
For the analysis, the data set for a certain temperature gets calibrated with its corresponding pedestal and DC transfer function. An AC correction for the extracted maxima is applied. Then, the fractional deviation of the amplitude σ_{TARGET} and bias σ_{BIAS} for each amplitude can be extracted from the data set. To simulate how temperature changes in the camera affect the calibration accuracy of the TARGET module, the data of certain temperature can be changed while the transfer function stay the same for example. In total the following configurations in table 1 were tested, which account the limited options in the camera of not being able to redo the AC correction at a different temperatures. The pedestal and the DC transfer function can nevertheless be adjusted.

Table 1: All combinations of data and calibrations, where a intensity resolution is made

	Data	DC TF	AC Correction
a)	23 °C	23 °C	None
b)	43 °C	23 °C	None
c)	23 °C	23 °C	23 °C
d)	43 °C	43 °C	23 °C

As testing all temperature combinations would only be time intensive without giving further insight, only the reference temperature of 23 °C and the one with the highest difference to it are chosen (namely 43 °C) as the highest temperature difference shows the most significant results of what can go wrong due to temperature induced effects.
Option a) is a reference test to control how the AC correction potentially can impact the performance of the TARGET module. To test the influence of the temperature dependency of the DC transfer function alone, option b) is also looked at. For a TARGET module, the AC correction must have a even more significant impact on the intensity resolution, solely due to the uncorrected gain of the shapers. Therefore tests option c) the best possible combination of all calibrations at the right temperature. This should theoretically show the best results possible, as all calibrations are on point with the data temperature. Then again to test the temperature stability of this construct, option d) is looked at. The DC transfer function gets also adjusted to the data temperature as this is possible while camera operation.

5.1. TARGET C

Starting with TARGET C module SN0037 and option a), one sees the corresponding intensity resolution without AC correction in figure 46, in orange the Poisson limit and in blue the CTA requirement limiting the range of possible intensity resolutions to a narrow gab. As addressed in chapter 3.3, the bias due to shapers is the leading error, overshooting the requirements for the whole range. This again emphasises how important the AC correction is for the whole module in terms of accuracy. Without bias, the requirements can be archived (red dotted line), but a precise amplitude reconstruction is worth nothing if the accuracy is not given. Therefore, option b) is not even needed for the TARGET C module as the temperature difference between data and DC transfer function will make it only worse.

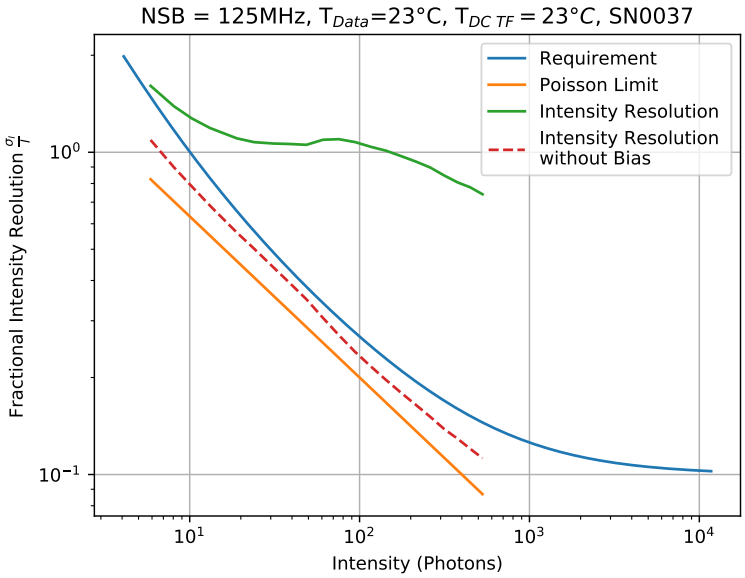

Figure 46: Intensity resolution of option a)

With option c) it is tested how good the AC correction compensates the bias and improves the precision of the intensity resolution. The corresponding intensity resolution can be seen in figure 47 on the left and on the right the contribution of each term stacked onto each other, divided by the requirement. It also shows how little the TARGET module can contribute to the error as most budget is already spent on photon related processes as the inevitable Poisson limit and the SiPM properties. Furthermore, as the requirement gets stricter with photon number, the influence of the 5% systematic error buffer grows from insignificant to a major influence, surpassing the contributions of the TARGET C module for large photon numbers. With the perfect matched calibration, the contributions of the TARGET module are marginal even neglectable for a photon number above 100. Only beneath that photon number has the bias a contribution over 3%.

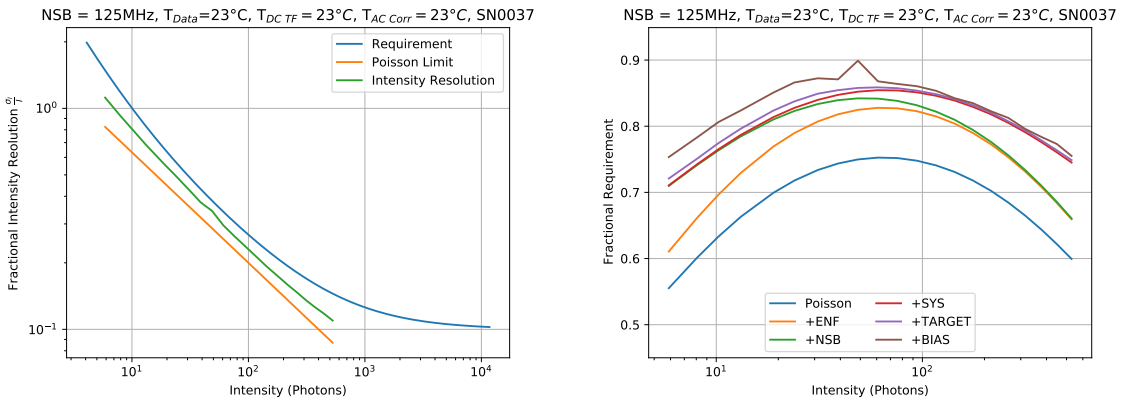

Figure 47: Option c), *left:* Intensity resolution, *right:* Stacked contributions to the intensity resolution divided by the requirement

By changing the temperature of the data and adjusting the DC transfer function according to it (option d)), one can see the behaviour of a non adjusted AC correction (see figure 48). For a small photon number, the bias is nearly unchanged while the precision of the TARGET module slightly drops in resolution. But these are only minor effects and the intensity resolution is still far from the requirement. Whereas for large photon numbers, the precision is still given at the same order, while the bias of the shapers can not be rightly compensated by the AC correction anymore, leading to a deterioration of the intensity resolution. Nevertheless, the resolution is still within the required limits for a very high temperature deviation of 20 °C. This highly supports the proposed calibration method of one AC correction at fixed temperature on the bench and temperature adjustable pedestal and DC calibrations while operating the camera.

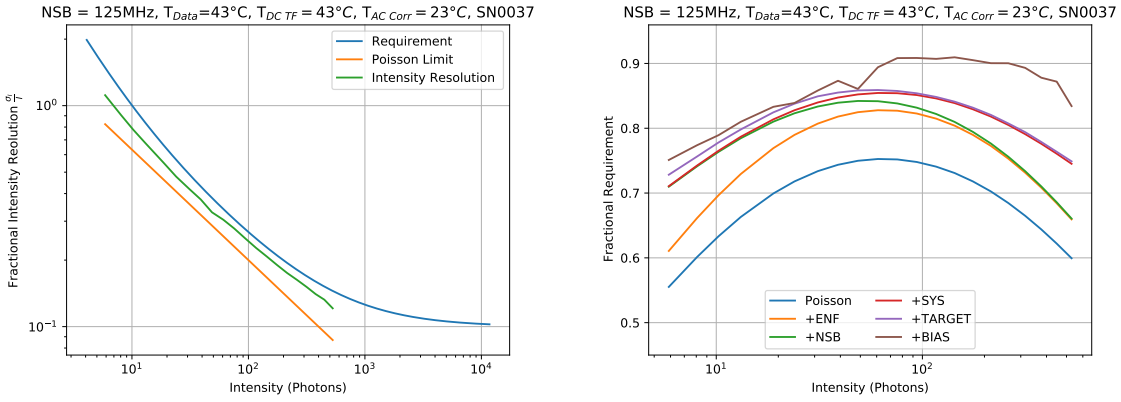

Figure 48: Option d), *left:* Intensity resolution, *right:* Stacked contributions to the intensity resolution divided by the requirement

5.2. CTC

Exemplary for all CTC evaluationboards, SN0001 will be examined at a Wilkinson clock of 104 MHz for comparability with the other modules. The plots for the remaining boards can be seen in appendix C.5. Starting again with option a) without the AC correction, the intensity resolution for the CTC evaluationboard never satisfies the requirements as seen in figure 49 on the left. Taking a look at the contribution plot right beside it, it becomes clear that again the bias is the leading problem. Without the shaper and additional gain, this seems a bit strange at first glimpse. A further look into the bias reveals that the measured amplitudes are always smaller then the input amplitude. As no additional circuit components are between the splitterboard and the sampling ASIC, it seems that the ASIC also has a limited bandwidth. The sharp edges of the narrow 10ns FWHM Gaussian pulses would also support this claim. Nevertheless, this would not explain the high fractional bias at low amplitudes. The further analysis of option c) and d) revealed some additional problems which could possibly explain this behaviour. More on that later.

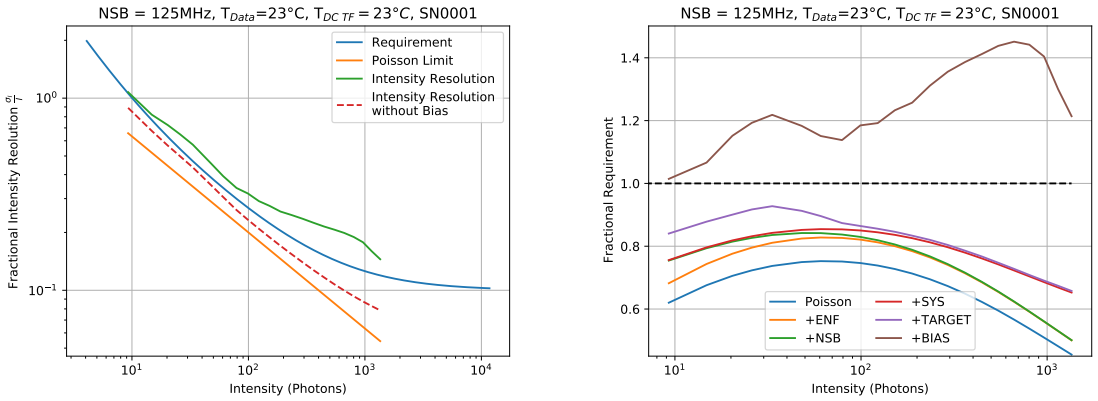

Figure 49: Option a), *left:* Intensity resolution, *right:* Stacked contributions to the intensity resolution divided by the requirement

Option b) can again be left out as the intensity resolution without AC correction does not even meet the requirements at optimal circumstances. Still it must be acknowledged that the different temperature characteristics of the DC transfer function due to the different ramp settings will lead to different results in option b).
For option c), the requirement is nearly matched except for a small range from about 20 to 40 photons (see figure 50). The contribution plot reveals a disproportionately large bias and TARGET addition to the resolution for a photon number below 100. For the rest of the intensity resolutions, the errors are kept at a minimum. A comparison with figure 49 also reveals that the TARGET contribution is even larger with the AC correction than without for a photon number below 100. Therefore one must conclude that the AC correction does not work at the moment, besides the bias reducion and even that does not work that good below 100 photons.

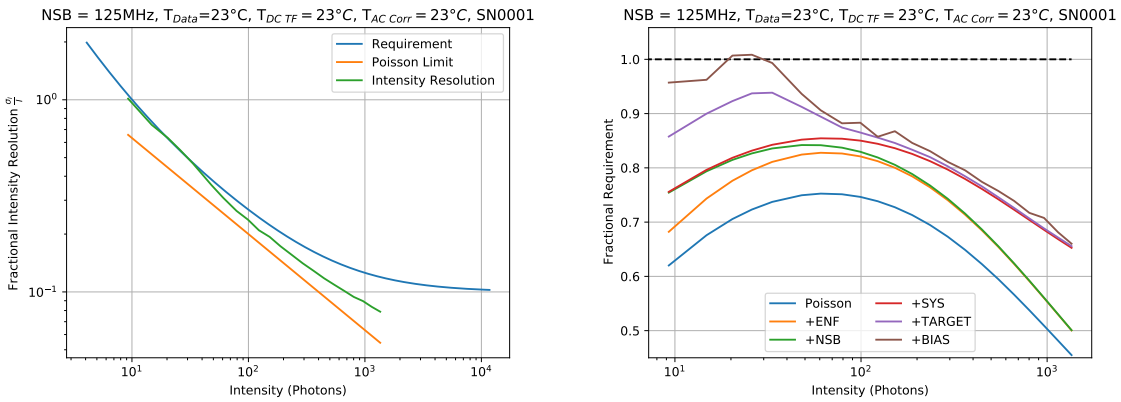

Figure 50: Option c), *left:* Intensity resolution, *right:* Stacked contributions to the intensity resolution divided by the requirement

Further parameters scans for the CTC board revealed that pulses below 100 mV and therefore 100 photons are not rightly digitized and are kind of "spiky" [14]. A example can be seen in figure 51 on the left. Different Wilkinson clocks diminished the problem but the main reason was a suboptimal set CMPBias2. The CMPBias2 determines the transition speed through the linear region of the comparator in the Wilkinson ADC. At the moment it is assumed that the used setting of 726 DAC counts leads to a too fast switching in the ADC for certain cells, which then leads to cross talk between them. As this error occurs in the read-out section of TARGET, it also restrains the precision of the sampling cell corrections as the pulses for calibrating are also affected. Therefore, the precision of the CTC gets worse with AC correction due to the uncertain calibration. For the storage correction (DC transfer function) this can be neglected as only DC signals are used.

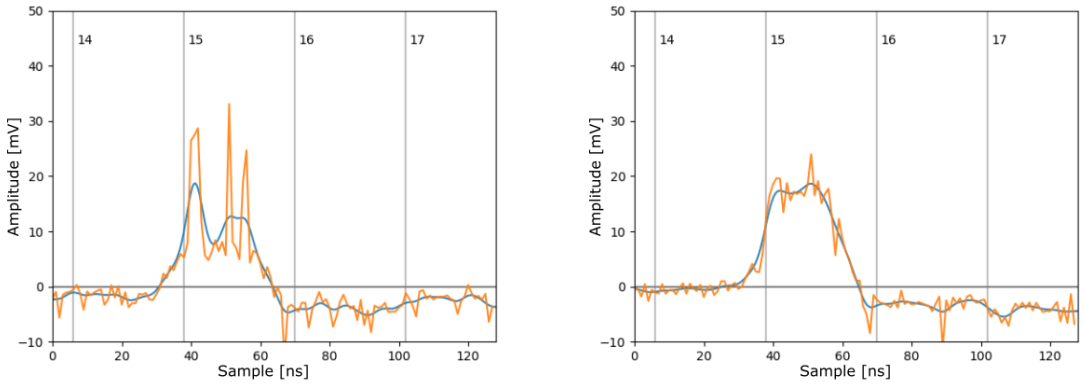

Figure 51: Exemplary Gaussian pulses of 20 mV input amplitude for a CMPBias of 726 DAC counts as used on the left and 1200 ADC counts on the right. The pulses have a FWHM of 25ns for better illustration of the spikes. Additional are also the storage blocks marked. [14] (modified by the author)

With an adjustment of CMPBias2, the pulses are digitised right, dropping the variance of up to ±20 mV in the peak to a normal noise level (see figure 51 on the right). Still is a whole analysis of DC transfer function and AC correction with adjusted CMPBias2 pending. With that in mind, a intensity resolution matching the requirement with the proposed calibrations is still possible. The differences in TARGET C and CTC are not that great in terms of sampling and digitisation. For the evaluationboards SN0002 and SN0004 the requirement is actually archived, even with the moderate AC corrections (see appendix C.5.3).

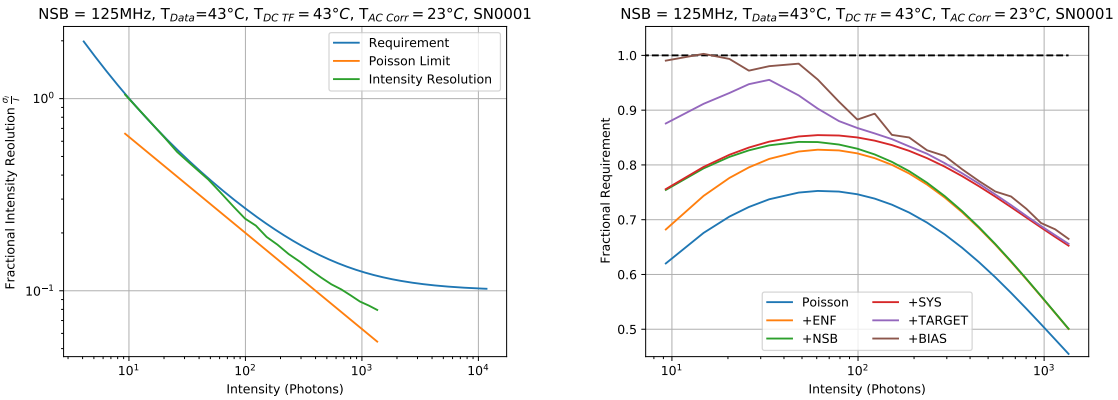

Figure 52: Option d), *left:* Intensity resolution, *right:* Stacked contributions to the intensity resolution divided by the requirement

Also does the temperature independency of the AC correction hold even with these uncertainties as discussed in chaper 4.3.4 and tested with option d). In figure 52, the intensity resolution behaves just like in figure 50. The only difference is the small change in bias in the range of 10 to 12 photons.

6. Conclusion

For the proposed calibration method of an intrinsic DC transfer function at the correct temperature and an one-off AC correction on the bench, several assumptions had to be checked. The Vped transfer function to enable the intrinsic DC transfer functions had to be temperature stable. A temperature dependency would mean a non justifiable extra afford. This was certainly not the case as it remains under 1% as reported in chapter 4.1.
Ongoing with the DC transfer function, a temperature dependency was found as assumed, but since the DC transfer function can be redone at any time and temperature, this is no problem. Dependent on the different ramp parameters, the deviations varied from 110 to 15 ADC counts at maximum for a 20 °C difference. For a Wilkinson clock of 208 MHz and a Isel of 2300 DAC counts, the most stable parameters were found with the maximal deviation of 15 ADC counts at 20 °C difference. The method of taking DC transfer function data itself was not temperature stable as different set pedestals caused different working temperatures for the sampling ASIC. As this was in a range of ± 0.75 °C and ± 3 ADC counts, it is not significant and in the the error budget.
In order to reduce calibration steps and worthwhile lab time, the AC correction has to be temperature independent. For the TARGET C module SN0037 this was certainly not the case. The cause for this could be traced down to the shapers in front of the sampling ASIC. Intrinsically, the sampling cell correction of the ASIC is not temperature dependent as a cross check with the CTC generation ASICs on the evaluationboard showed. The attempt of eliminating the influence of the TARGET C shapers by measuring and applying a transfer functions of them also verified this and showed that the AC correction is unavoidable in terms of correcting the shaper gain. The previously tested AC transfer function of a whole module accomplished that automatically [15].
Nevertheless, the TARGET C module could archive the desired CTA intensity resolution requirement, with a DC transfer function on the same temperature as the data and a temperature fixed AC correction with a temperature different up to 20 °C. Still is it worthwhile to reduce the temperature dependency of the shapers to elevate the accuracy of the AC correction. Furthermore, this has to be check for the new CTC shaper topology.
For the CTC evaluationboard, the intensity resolution requirement was not fully reached probably due to the unadjusted CMPBias2 parameter, which lead to spiky pulses for amplitude below 100 mV. Therefore, also the calibration in itself is not dependable for these amplitudes, producing a poor correction of the data. Above this mark, the unadjusted CMPBias2 did not matter, the pulses behaved normally and the requirement was archived, just as with the TARGET C module. Therefore, it is probable that with a corrected CMPBias2, the proposed calibration method will work fine. Also the intensity resolution in chapter 5 was extended with the bias, aggravating the requirement. Nevertheless is this justified with the internal DC transfer function being responsible for the translation between ADC counts and mV, as it ignores the shaper gain. Though has this to be tested for a adjusted CMPBias2.

References

[1] M. P. Alessandro De Angelis, *Introduction to Particle and Astroparticl Physics*. Springer Verlag Italia, 2015.

[2] R. White and H. Schoorlemmer, "A compact high energy camera (chec) for the gamma-ray cherenkov telescope of the cherenkov telescope array," 2017.

[3] T. C. Consortium, "Cherenkov telescope array: The next generation gamma-ray observatory," 2017.

[4] L. Tibaldo, J. A. Vandenbroucke, A. M. Albert, S. Funk, T. Kawashima, M. Kraus, A. Okumura, L. Sapozhnikov, H. Tajima, G. S. Varner, T. Wu, and A. Zink, "Target: toward a solution for the readout electronics of the cherenkov telescope array," 2015.

[5] M. de Naurois and D. Mazin, "Ground-based detectors in very-high-energy gamma-ray astronomy," *Comptes Rendus Physique*, vol. 16, p. 610–627, Aug 2015.

[6] H. J. Völk and K. Bernlöhr, "Imaging very high energy gamma-ray telescopes," *Experimental Astronomy*, vol. 25, p. 173–191, Mar 2009.

[7] N. W. Hermann Kolanoski, *Teilchendetektoren*. Springer Spektrum, 1 ed., 2016.

[8] `https://www.cta-observatory.org/`. Accessed: 2021-03-01.

[9] I. Gabriel Pérez Diaz, "Cta technology." `https://www.cta-observatory.org/project/technology/`. Accessed: 2021-02-25.

[10] W. Wild. `https://www.cta-observatory.org/small-sized-telescope-harmonization-process-and-status/`, October 2019. Accessed: 2021-06-25.

[11] J. J. Watson and J. Zorn, "Commissioning and performance of chec-s – a compact high-energy camera for the cherenkov telescope array," 2019.

[12] S. Funk, D. Jankowsky, H. Katagiri, M. Kraus, A. Okumura, H. Schoorlemmer, A. Shigenaka, H. Tajima, L. Tibaldo, G. Varner, A. Zink, J. Zorn, and the CTA consortium, "Target: A digitizing and trigger asic for the cherenkov telescope array," 2016.

[13] A. Albert, S. Funk, H. Katagiri, T. Kawashima, M. Murphy, A. Okumura, R. Quagliani, L. Sapozhnikov, A. Shigenaka, H. Tajima, and et al., "Target 5: A new multi-channel digitizer with triggering capabilities for gamma-ray atmospheric cherenkov telescopes," *Astroparticle Physics*, vol. 92, p. 49–61, Jun 2017.

[14] A. Zink. Personal information.

[15] J. Schäfer, "Temperature dependent aspects of the compact high energy camera (chec-s) front-end electronic (fee) calibration," Master's thesis, 2019.

[16] `https://www.testequity.com/1007C-specs`. Accessed: 2021-01-23.

[17] J. J. Watson. Personal information.

[18] M. Kraus, *The Cosmic-Ray Electron Anisotropy Measured with H.E.S.S. and Characterization of a Readout System for the SST Cameras of CTA*. PhD thesis, 2018.

[19] S. Vinogradov, "Analytical models of probability distribution and excess noise factor of solid state photomultiplier signals with crosstalk," *Nuclear Instruments and Methods in Physics Research Section A: Accelerators, Spectrometers, Detectors and Associated Equipment*, vol. 695, pp. 247–251, 2012. New Developments in Photodetection NDIP11.

A. Oscilloscope Characterisation

For the transfer functions of the splitterboard and the shapers, the Tektronix MSO54 was used. Due to some internal errors of the oscilloscope, the measured amplitude of a pulse changed with the used mV/Div for high amplitudes. Therefore only two different mV/Div were used, namely 40 mV/Div and 500 mV/Div, which were investigated to measure the same amplitude.
To fasten up the data acquisition, an average of 500 waveforms were acquired and its mean read-out and analysed as stated in chapter 3.3.3. Hence, statistical information as deviation and corresponding standard error are lost in translation. To offset this dispute, one transfer function was made, were each of the 500 acquisitions for each mV/Div is read-out independently, allowing statistical estimations for all other transfer functions. This can exemplary be seen for the splitterboard transfer function in figure 53, resulting in a average standard error of about 17μV for 40 mV/Div and 0.2 mV for 500 mV/Div for every data point and thus a relative error always below 0.2%.

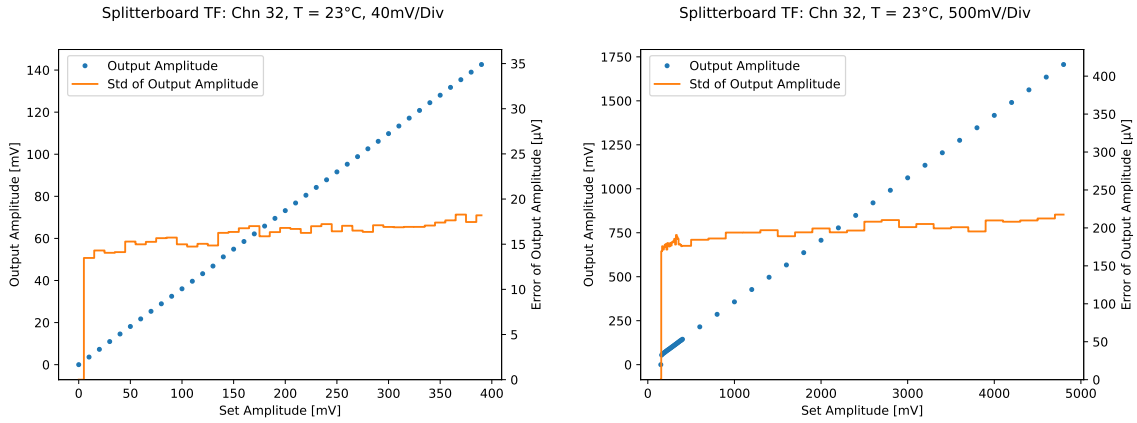

Figure 53: Mean transfer function and error for different mV/Div

B. Splitterboard Resistor Change

To see, if the follow up resistor or the IC of the splitterboard is the cause for the deviation between the channels, the two resistors of the channels with some of the highest deviation where changed. Namely channel 4 with an original resistance of $R_4 = 50.12\Omega$ and channel 48 with $R_{48} = 49.97\Omega$, both measured with a standard handheld multimeter. If the resistors are the sole cause, the deviation of the transfer functions to mean should directly be reversed after the switch. If nothing changes, the ICs are the cause and the resistors do not play a significant role.
In figure 54 one can see the transfer function of each channel subtracted from the mean of all 16 channels and the corresponding standard deviation of the mean transfer function as the grey area. As additional cross check, the transfer functions of channel 4 and 48 of an old data set are also plotted, both matching the data of the new transfer function with the original resistors. After the resistor swap, channel 4's deviation reverses while the deviation of channel 48 approaches the mean. This implies that the deviation of channel 4 mainly comes from the resistor, while the one from channel 48 is adjustable with resistor but the main contribution comes from the IC. Compared to all other channels, channel 48's high deviation remains a mere exception. Therefore it seems reasonable to minimize the resistors tolerances to decrease the deviations between the channels.

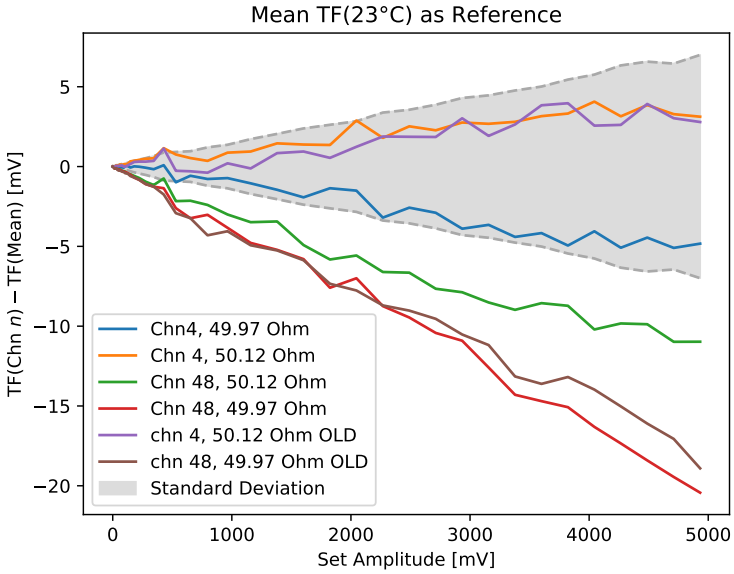

Figure 54: splitterboard transfer functions subtracted by mean transfer function of selected channels with different follow up resistor

C. Module Specific Plots

Here are all analytic plots for the remaining evaluationboards of the temperature dependency chapter 4. The already discussed plots of CTC evaluationboard SN0001 are also displayed for better comparability.

C.1. Temperature Translation Plots

After all, one is interested in the temperatures on board not in the one of the chamber. But as different set ups and fan placements between runs can change the temperature quite drastically even for the same module, it is cumbersome to write and repeat all different temperatures of each sensor for each run. Therefore only the temperature of the chamber is used to account for a run in the main work. For consistency a translation plot for each run between the chamber temperature and sensor temperature is needed. In the end, a run for each module consists of a pedestal, data for the DC transfer function, data for the AC correction and a data set under operating settings. Of course additional measurements are done, but these are either in the same run or only a proof of principle, only needing the approximately temperature which is about the same for each module. Additionally the temperature changes in the DC transfer function, as mentioned in chapter 4.2, can be seen in the following chapter C.3 for the additional modules.

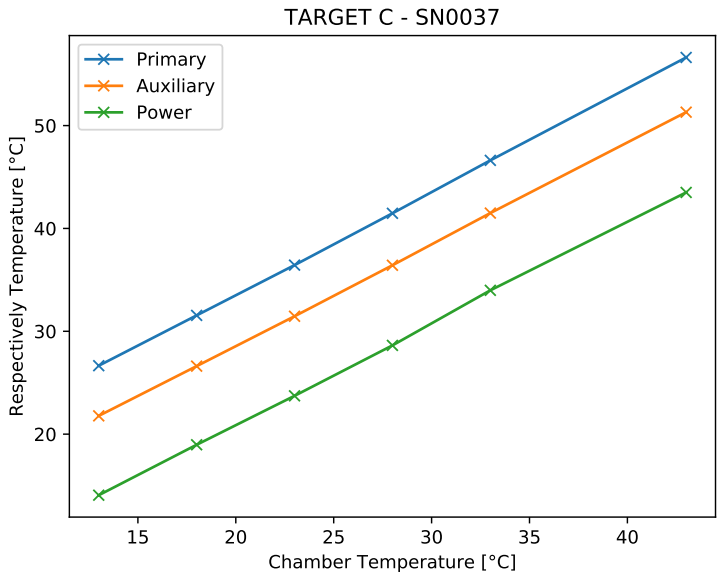

Figure 55: Temperature translation for the three sensors on the TARGET C module SN0037

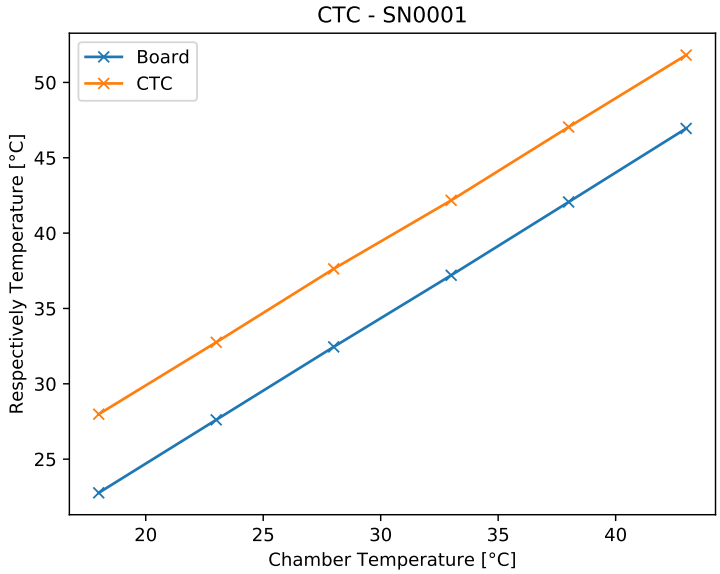

Figure 56: Temperature translation for the PT100 on top of the CTC ASIC and the sensor on the PCB (Board) for evaluationboard SN0001

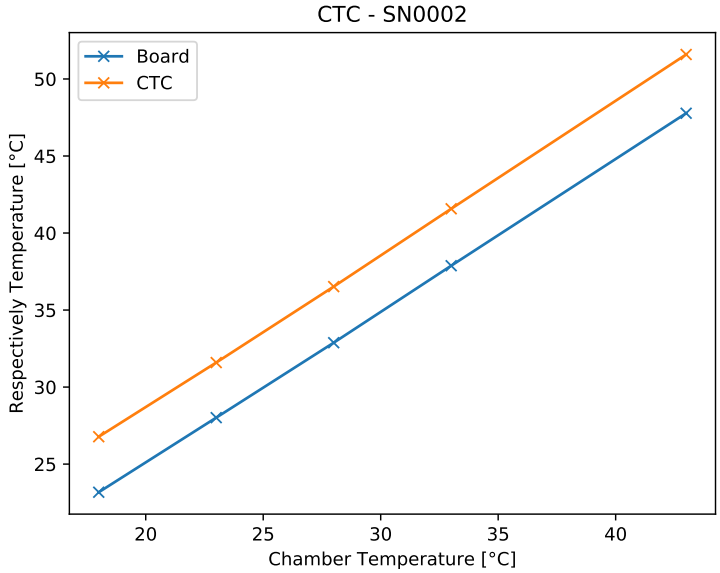

Figure 57: Temperature translation for the PT100 on top of the CTC ASIC and the sensor on the PCB (Board) for evaluationboard SN0002

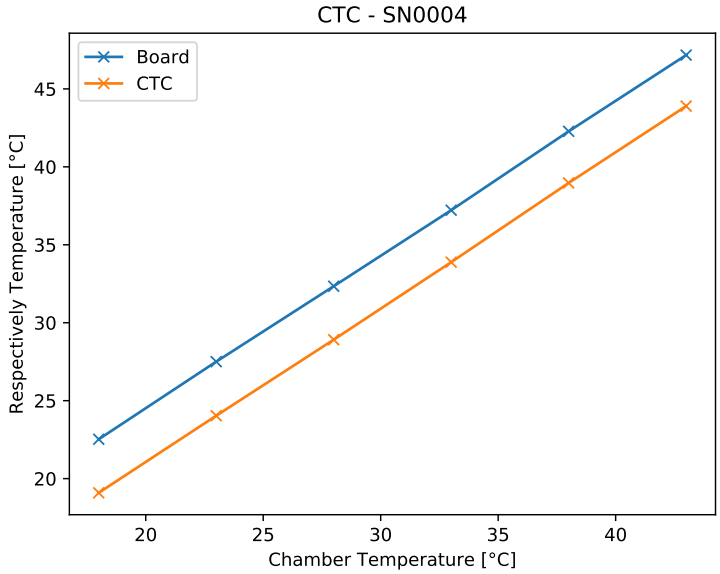

Figure 58: Temperature translation for the PT100 on top of the CTC ASIC and the sensor on the PCB (Board) for evaluationboard SN0004

As these lookup tables are all linear, the respectively board temperature can be calculated with following fit parameters if wanted:

$$f(x) = m \cdot x + t$$

Parameter	m	t
TARGET C SN0037		
Primary	1.00	13.53
Auxiliary	0.99	8.87
Power	0.99	1.21
Evaluationboard CTC SN0001		
Board	0.97	5.38
CTC	0.95	10.87
Evaluationboard CTC SN0002		
Board	0.99	5.38
CTC	0.99	8.77
Evaluationboard CTC SN0004		
Board	0.99	4.79
CTC	0.99	11.17

C.2. Temperature per Set Vped

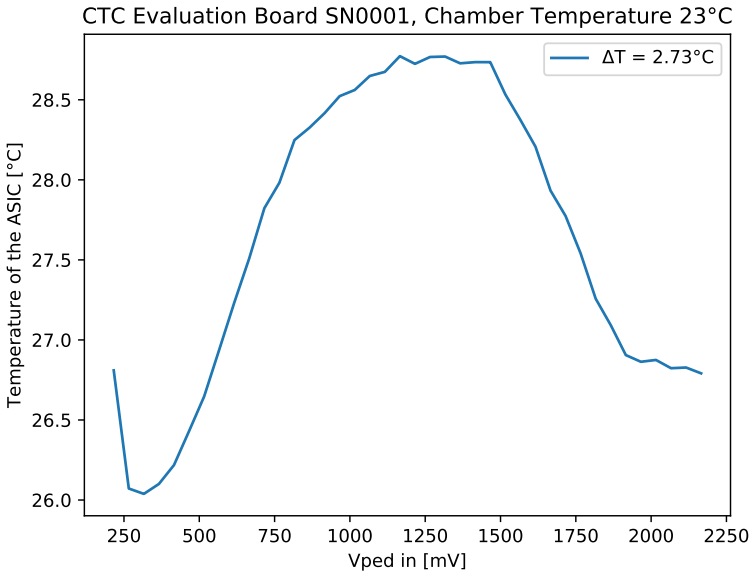

Figure 59: SN0001, Wilkinson clock at 104 MHz, Isel at 2550 DAC counts, on TARGET module fitting heatsink

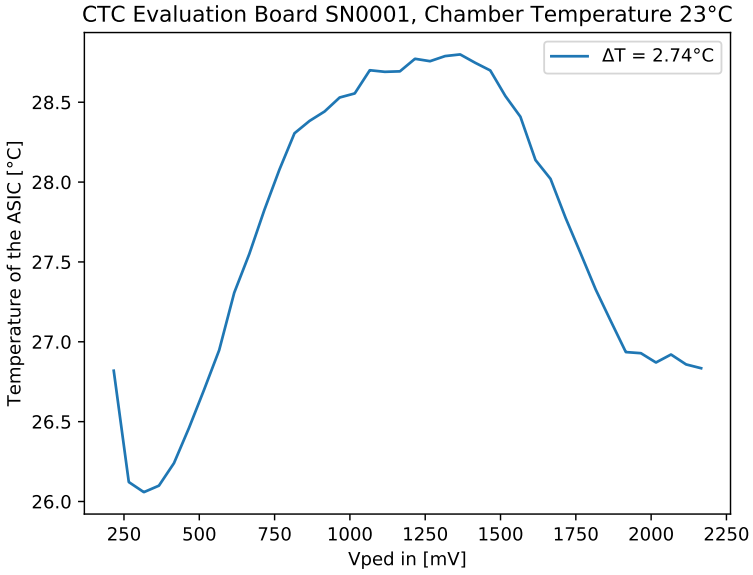

Figure 60: SN0001, Wilkinson clock at 208 MHz, Isel at 2300 DAC counts, on TARGET module fitting heatsink

No difference between them as assumed, as the ramp does not interfere with the pedestal settings

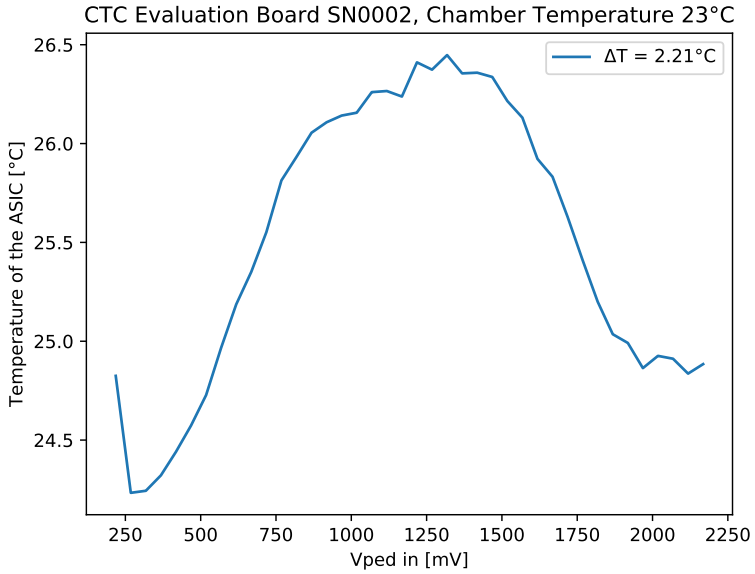

Figure 61: SN0002, Wilkinson clock at 104 MHz, Isel at 2550 DAC counts, too big heat sink for the TARGET module

For SN0004 the data was unfortunately overwritten and therefore lost.

C.3. Temperature Dependency of the DC Transfer Function

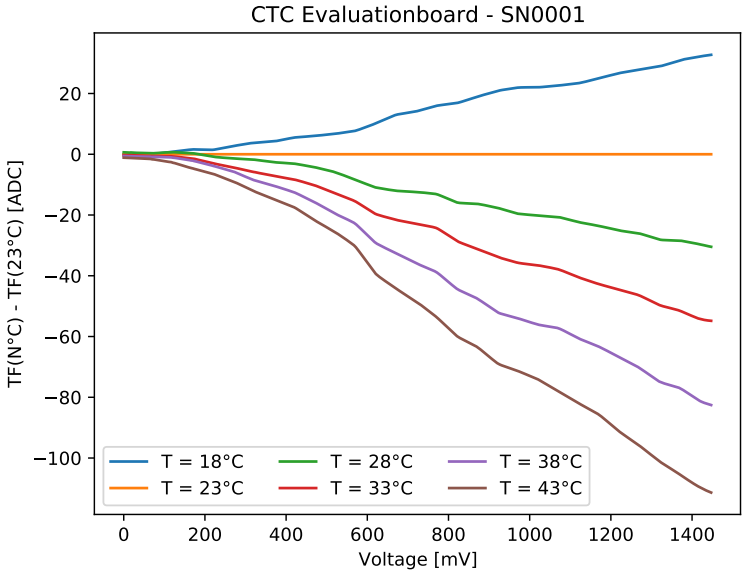

Figure 62: SN0001, Wilkinson clock at 104 MHz, Isel at 2550 DAC counts

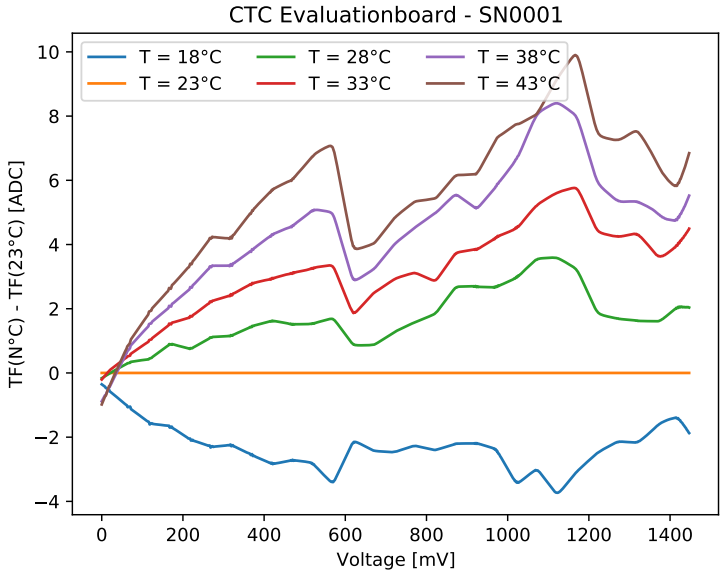

Figure 63: SN0001, Wilkinson clock at 208 MHz, Isel at 2300 DAC counts

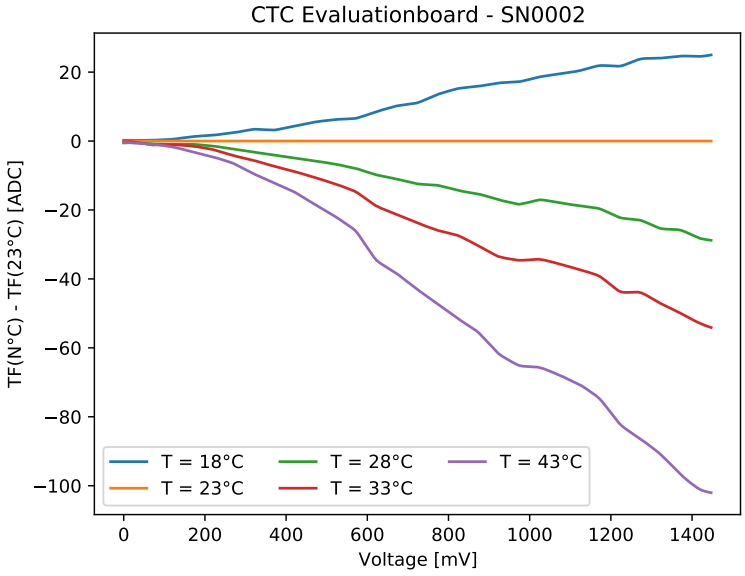

Figure 64: SN0002,Wilkinson clock at 104 MHz, Isel at 2550 DAC counts

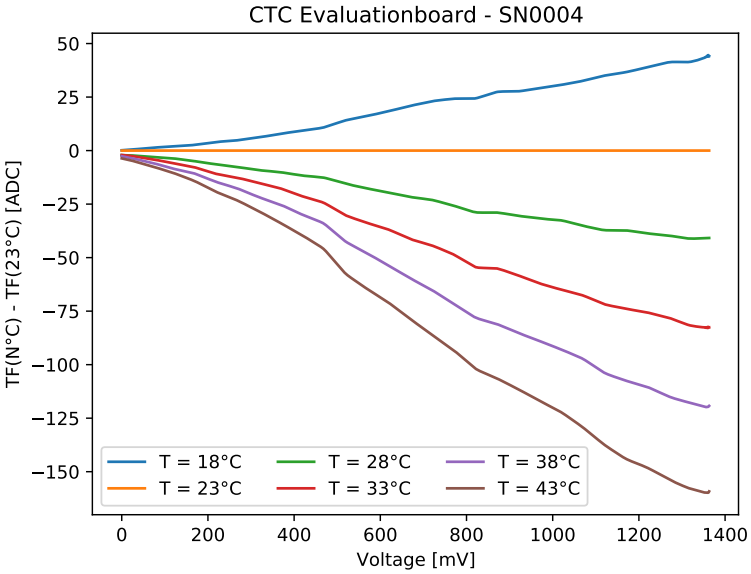

Figure 65: SN0004, Wilkinson clock at 104 MHz, Isel at 2550 DAC counts

C.4. Temperature Dependency of the AC Correction

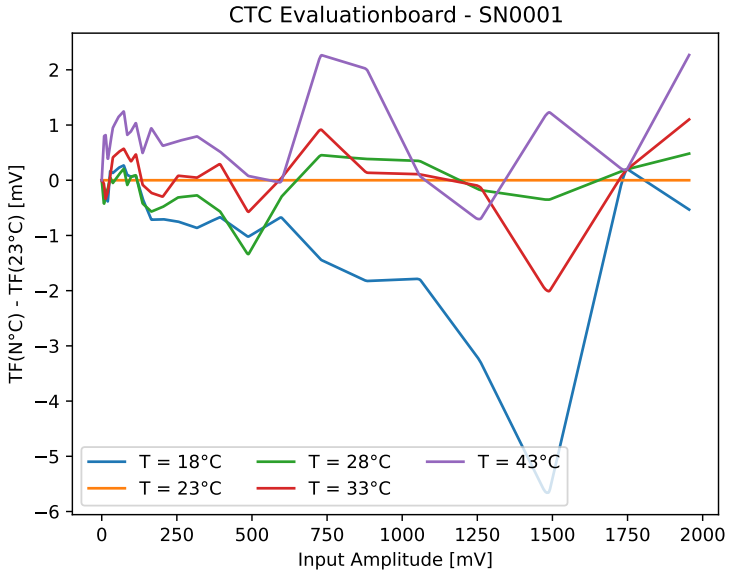

Figure 66: SN0001, Wilkinson clock at 104 MHz, Isel at 2550 DAC counts

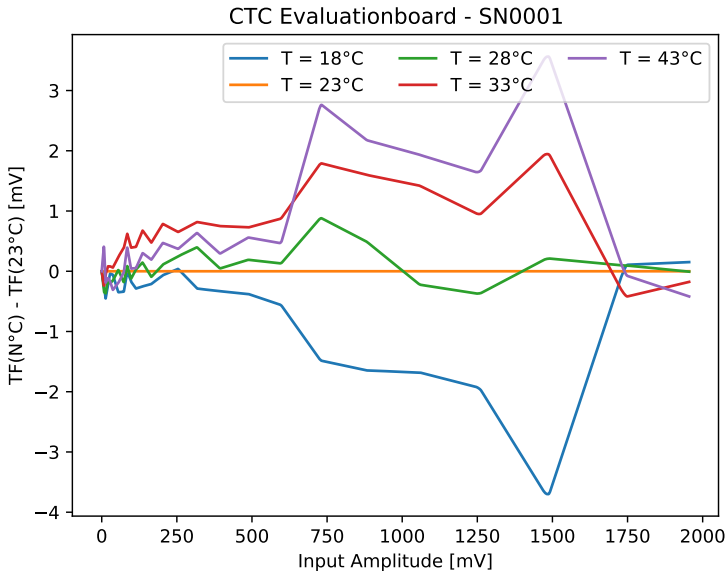

Figure 67: SN0001, Wilkinson clock at 208 MHz, Isel at 2300 DAC counts

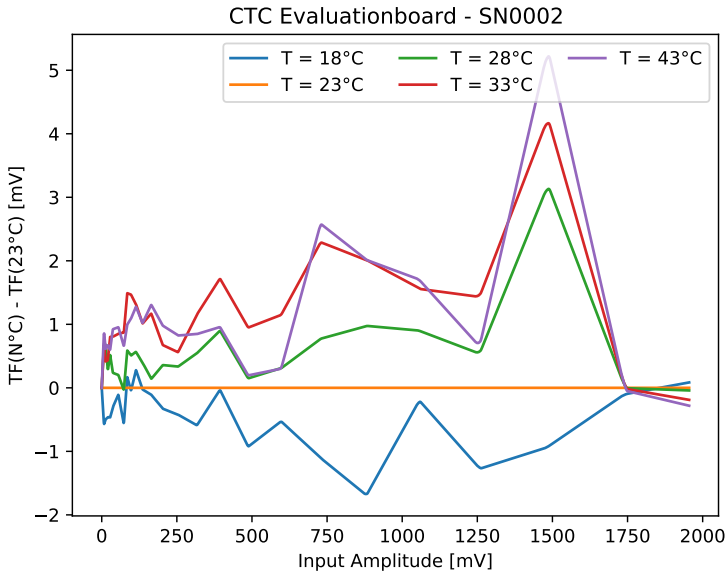

Figure 68: SN0002, Wilkinson clock at 104 MHz, Isel at 2550 DAC counts

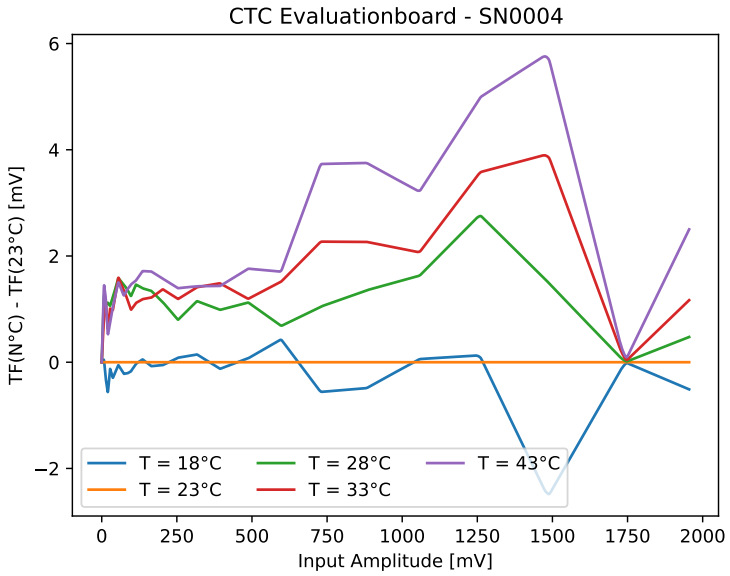

Figure 69: SN0004, Wilkinson clock at 104 MHz, Isel at 2550 DAC counts

C.5. Intensity Resolution

For the evaluationboards SN0002 and SN0004, the respective data set at 43 °C is broken. While SN0004 is now at the University of Leicester for further testings, evading a revision of measurements, the stumble of SN0002 did only stuck out at the last minute. Therefore option b) and d) is spared out for both boards in this thesis.

C.5.1. Option a)

Data at 23 °C, DC transfer function at 23 °C, no AC correction.

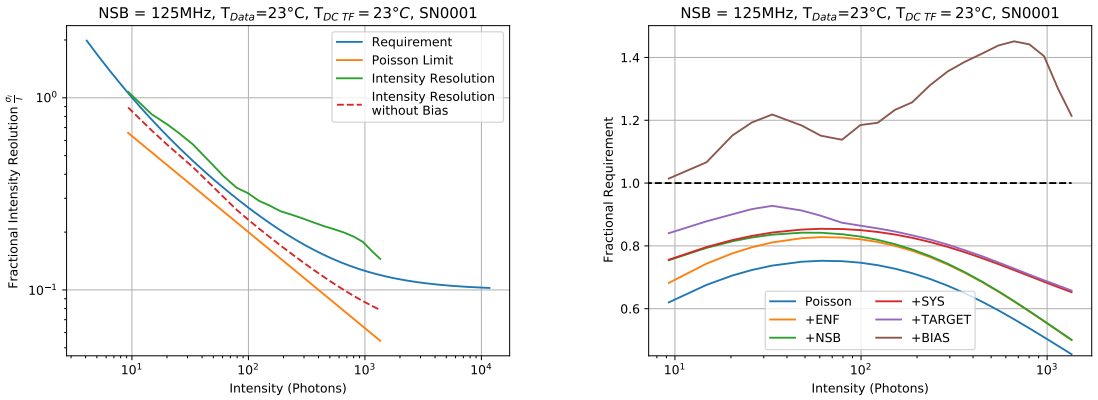

Figure 70: SN0001, Wilkinson clock at 104 MHz, Isel at 2550 DAC counts. *Left:* Intensity resolution; *right:* Stacked contributions to the intensity resolution divided by the requirement

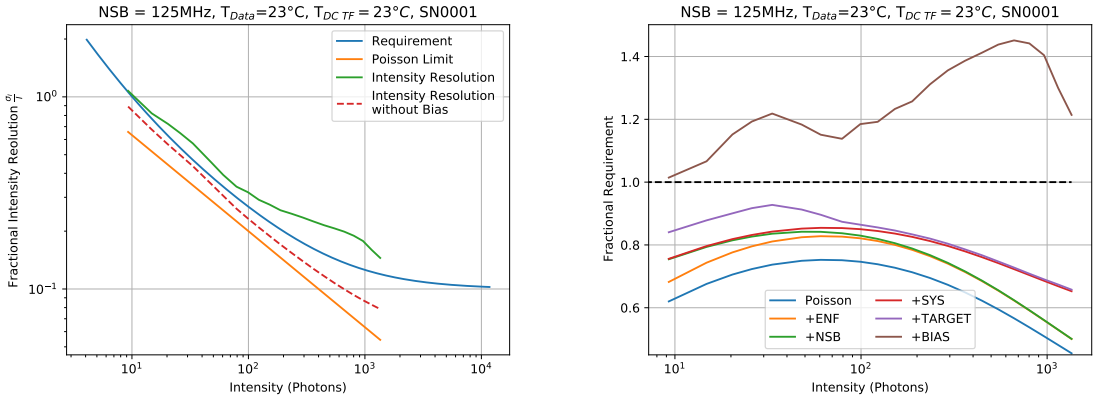

Figure 71: SN0001, Wilkinson clock at 208 MHz, Isel at 2300 DAC counts. *Left:* Intensity resolution; *right:* Stacked contributions to the intensity resolution divided by the requirement

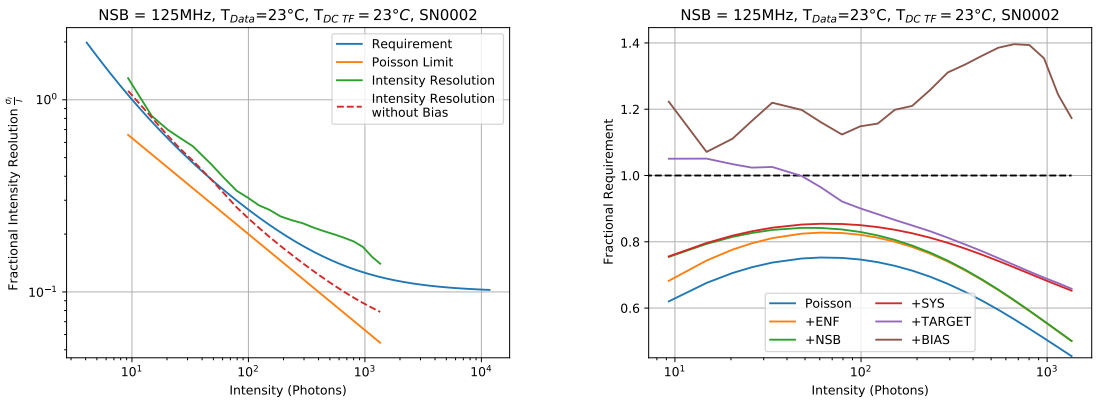

Figure 72: SN0002, Wilkinson clock at 104 MHz, Isel at 2550 DAC counts. *Left:* Intensity resolution; *right:* Stacked contributions to the intensity resolution divided by the requirement

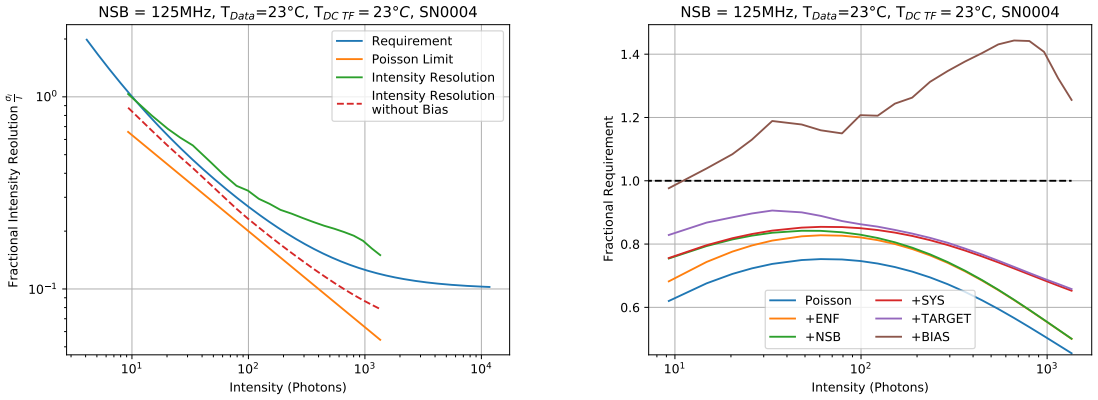

Figure 73: SN0004, Wilkinson clock at 104 MHz, Isel at 2550 DAC counts. *Left:* Intensity resolution; *right:* Stacked contributions to the intensity resolution divided by the requirement

C.5.2. Option b)

Data at 43 °C, DC transfer function at 23 °C, no AC correction.

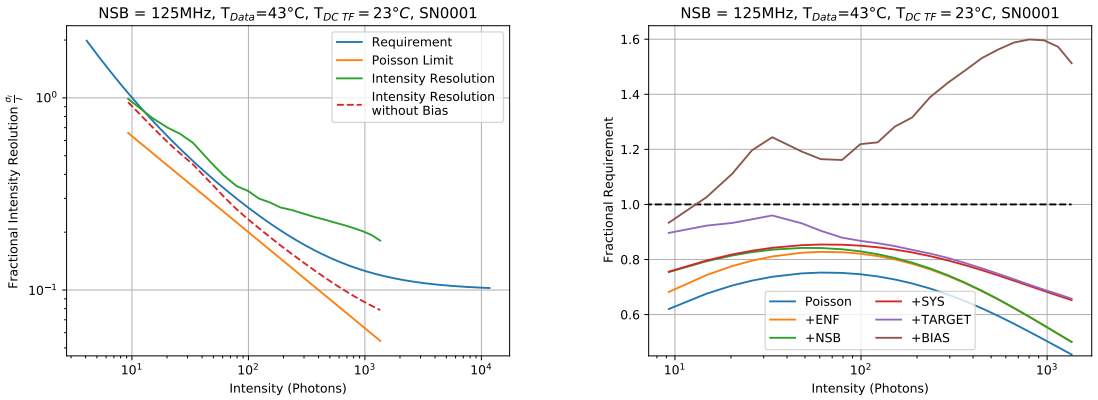

Figure 74: SN0001, Wilkinson clock at 104 MHz, Isel at 2550 DAC counts. *Left:* Intensity resolution; *right:* Stacked contributions to the intensity resolution divided by the requirement

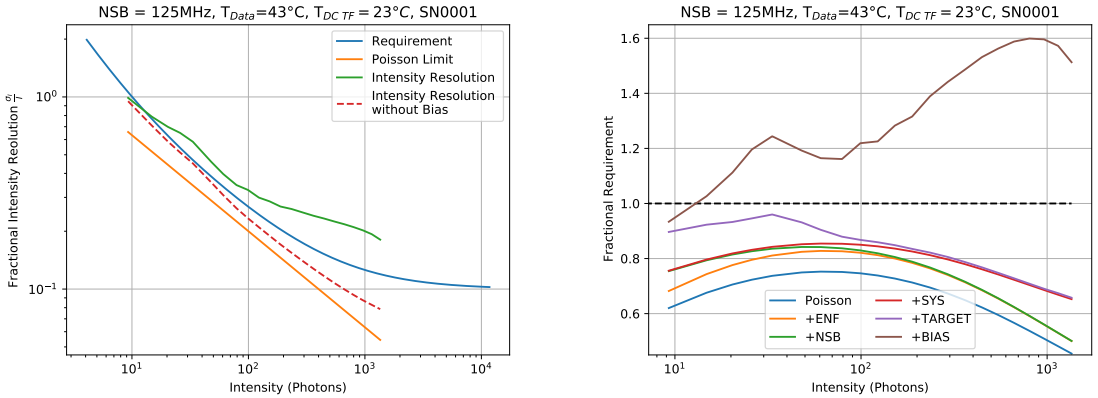

Figure 75: SN0001, Wilkinson clock at 208 MHz, Isel at 2300 DAC counts. *Left:* Intensity resolution; *right:* Stacked contributions to the intensity resolution divided by the requirement

C.5.3. Option c)

Data at 23 °C, DC transfer function at 23 °C, AC correction transfer function at 23 °C.

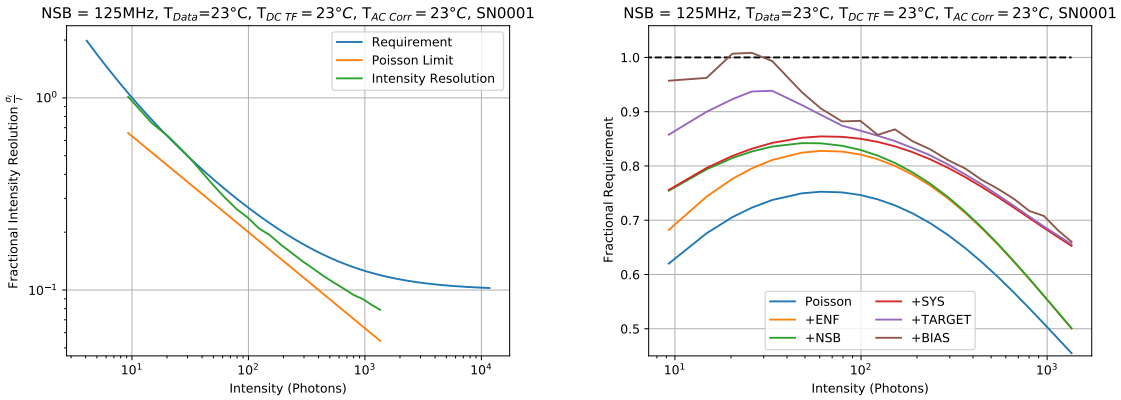

Figure 76: SN0001, Wilkinson clock at 104 MHz, Isel at 2550 DAC counts. *Left:* Intensity resolution; *right:* Stacked contributions to the intensity resolution divided by the requirement

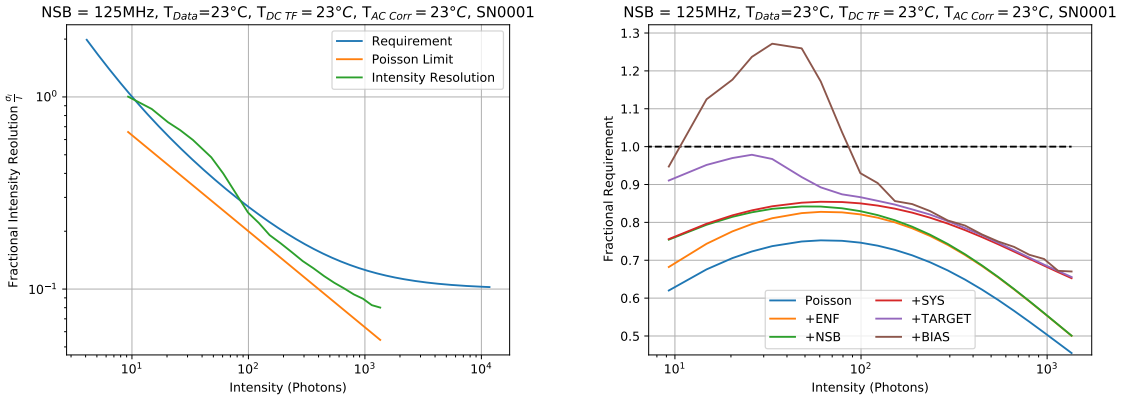

Figure 77: SN0001, Wilkinson clock at 208 MHz, Isel at 2300 DAC counts. *Left:* Intensity resolution; *right:* Stacked contributions to the intensity resolution divided by the requirement

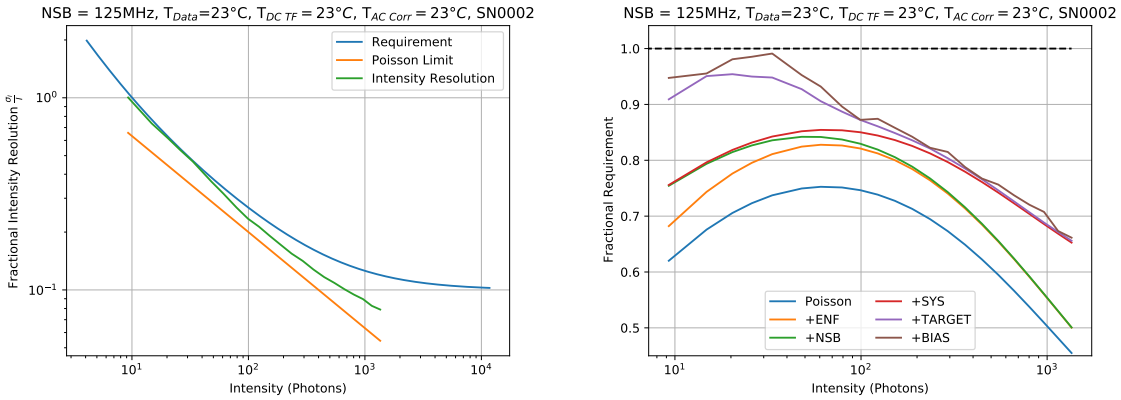

Figure 78: SN0002, Wilkinson clock at 104 MHz, Isel at 2550 DAC counts. *Left:* Intensity resolution; *right:* Stacked contributions to the intensity resolution divided by the requirement

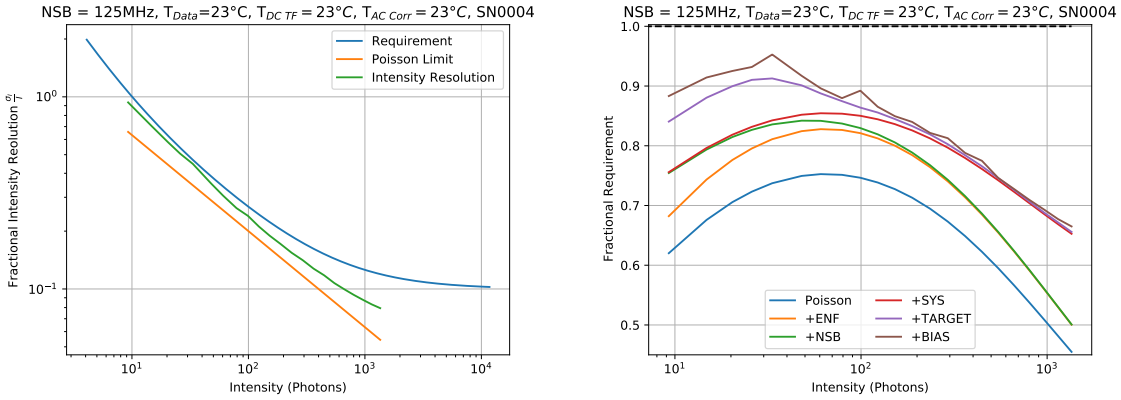

Figure 79: SN0004, Wilkinson clock at 104 MHz, Isel at 2550 DAC counts. *Left:* Intensity resolution; *right:* Stacked contributions to the intensity resolution divided by the requirement

C.5.4. Option d)

Data at 43 °C, DC transfer function at 43 °C, AC correction transfer function at 23 °C.

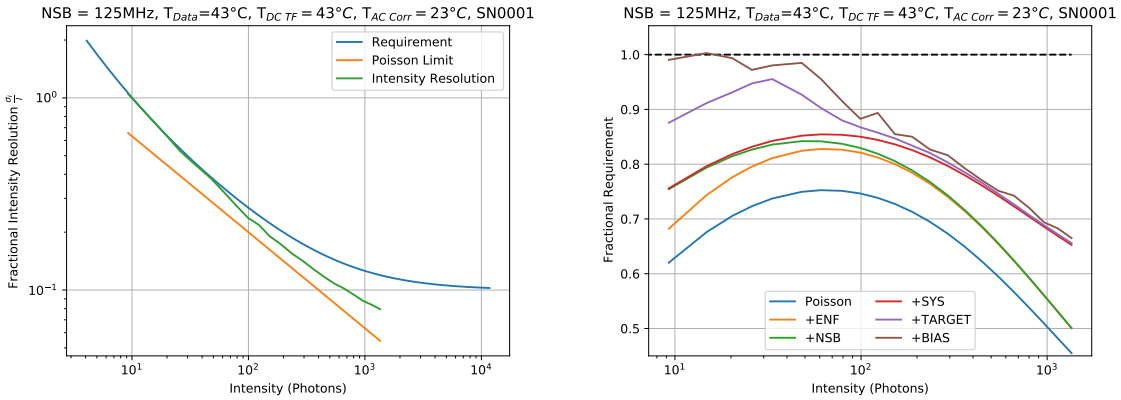

Figure 80: SN0001, Wilkinson clock at 104 MHz, Isel at 2550 DAC counts. *Left:* Intensity resolution; *right:* Stacked contributions to the intensity resolution divided by the requirement

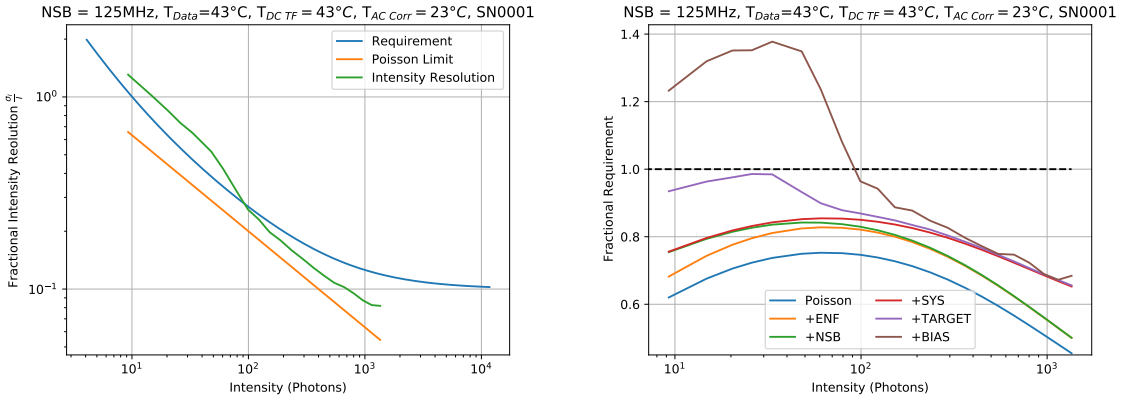

Figure 81: SN0001, Wilkinson clock at 208 MHz, Isel at 2300 DAC counts. *Left:* Intensity resolution; *right:* Stacked contributions to the intensity resolution divided by the requirement

Statement of Authorship

I hereby certify that this thesis has been composed by me and is based on my own work, unless stated otherwise. No other persons work has been used without due acknowledgement in this thesis. All references and verbatim extracts have been quoted, and all sources of information, including graphs and data sets, have been specifically acknowledged.

Place, date

Signature

Ackownledgements

I would like to thank everyone who has supported me during my master's thesis. Special thanks to:

- My wife Stefanie Schwab for her never ending support.
- Prof. Dr. Stefan Funk for giving me the opportunity to work in this exciting field of astroparticle physics.
- Dr. Adrian Zink for his unlimited knowledge and patience with me. This work would not be the same without him.
- Johannes Schäfer and Jelena Celic for the nice office time and help on all sorts of programming issues.
- The whole gamma-ray group for the pleasant and encouraging atmosphere.
- My family for the everlong support.